

Energy Advances

Accepted Manuscript

This article can be cited before page numbers have been issued, to do this please use: S. S. Mani, R. Sivaraj, T. Mathew and G. S. Chinnakonda, *Energy Adv.*, 2024, DOI: 10.1039/D4YA00249K.



This is an Accepted Manuscript, which has been through the Royal Society of Chemistry peer review process and has been accepted for publication.

Accepted Manuscripts are published online shortly after acceptance, before technical editing, formatting and proof reading. Using this free service, authors can make their results available to the community, in citable form, before we publish the edited article. We will replace this Accepted Manuscript with the edited and formatted Advance Article as soon as it is available.

You can find more information about Accepted Manuscripts in the [Information for Authors](#).

Please note that technical editing may introduce minor changes to the text and/or graphics, which may alter content. The journal's standard [Terms & Conditions](#) and the [Ethical guidelines](#) still apply. In no event shall the Royal Society of Chemistry be held responsible for any errors or omissions in this Accepted Manuscript or any consequences arising from the use of any information it contains.

A review on recent advances in the design and structure-activity correlation of TiO₂-based photocatalysts for solar hydrogen production

Sunesh S Mani,^a Sivaraj Rajendran,^a Thomas Mathew,^{a,*} and Chinnakonda S Gopinath^{b,c,*}

^[a]Department of Chemistry, St. John's College (Affiliated to University of Kerala), Anchal, Kerala – 691306, India, E-Mail: thomasm74@gmail.com

^[b]Catalysis and Inorganic Chemistry Division, CSIR - National Chemical Laboratory, Dr. HomiBhabha Road, Pune 411 008, India. E-mail: cs.gopinath@ncl.res.in

^[c]Academy of Scientific and Innovative Research (AcSIR), Ghaziabad 201002, India.

Abstract

The major issues that determine the efficiency of photocatalyst composite materials for solar hydrogen production, with or without sacrificial agent, are efficient visible light harvesting properties, efficient separation of charge carriers and their utilization at redox sites, and stability. Significant efforts have been made in the past few decades to modify the above characteristics by integrating the constituent components of composite with different approaches. The present review attempts to enumerate the recent advances, predominantly, in the area TiO₂-based photocatalyst composites for solar hydrogen production. First we provide the recent progress in the material integration aspects by describing the integration of TiO₂ with different category of materials, including noble/3d metals, metal oxides/sulphides/selenides, other low bandgap semiconductors, C-based materials, dye sensitization. How the material integration helps in tailoring the electronic and optical properties for activity tuning in solar H₂ production is also presented. The critical changes in the physico-chemical and electronic properties of composites with respect to preparation methods, morphology, crystallographic facet, particle size, dopant, calcination temperature, and its structure-activity relation to solar hydrogen production were addressed in detail. We also discuss the importance of fabrication of photocatalyst in thin film form and performing solar hydrogen production in different reactor set up for enhancing the photocatalytic performance, while addressing the device scalability. Despite significant advancements has been made in this field, the solar-to-hydrogen conversion efficiency is still need to be improved to implement it for practical applications. Direct conversion of water into hydrogen by overall water splitting, renewable H₂ production with waste water or by using a biomass component by employing suitable photocatalyst are some possible ways to improve the energy efficiency and continuous research in the above directions are highly desired.

Keywords: Energy Conversion, Energy Storage, Visible Light, Photocatalysis



1. Introduction

View Article Online
DOI: 10.1039/D4YA00249K

The steadily increasing demand for energy due to population growth and industrialisation, poses a serious concern on the depletion of fossil fuels (oil, gas and coal), which account >85% of energy production and currently the major sources of energy.^{1,2} Besides, the general consensus on the limited reservoir of fossil fuels, the combustion of fossil fuels leading to the emission of CO₂ and other harmful gases is also a major issue, which brings an almost irreversible change in the atmosphere leading to drastic climate changes. Carbon-free hydrogen production by water splitting, with and without any sacrificial agent, in the presence of a semiconductor by utilizing solar energy is a renewable process and is considered to be a promising alternative for an economically and socially sustainable future to meet the increasing energy demand.³ Since the overall water splitting reaction to H₂ production is an uphill reaction with a positive Gibbs free energy of 238 kJ mol⁻¹, a photocatalyst that can efficiently harvest solar radiation is essential to make the reaction process energetically and economically feasible.² Different semiconductor materials, such as, TiO₂, Cu₂O, Co₃O₄, CdS, ZnIn₂S₄ has been examined to evaluate their potential as a photocatalytic material in water splitting reaction to produce hydrogen.⁴ Poly(heptazine imide) ionic carbon nitrides are another emerging class of photocatalytic system recently applied for hydrogen evolution.⁵ Among various photocatalytic materials, TiO₂ has been the extensively studied semiconductor material due to several advantageous aspects, such as, availability, low cost, interesting physico-chemical properties, non-toxic and environmental friendly, feasible synthesis at low temperatures, amenability to integrate with different materials, and high chemical and photostability.⁶

Ever since the potential of TiO₂ for photolysis of water was revealed by Fujishima and Honda for the first time in 1972,⁶ its performance has been largely explored for a variety of applications, such as, photocatalytic pollutant degradation,⁷ supercapacitors,⁸ solar cells,⁹ carbon dioxide reduction,¹⁰ lithium-ion batteries,¹¹ biomedical devices,¹² self cleaning,¹³ water splitting.¹⁴ However, the wide bandgap (3.2 eV) of TiO₂ restrict its light-harvesting ability mainly under UV region (which is ~5% in sunlight), and the fast recombination of the photo-generated electron-hole pair in bare TiO₂ limit its photocatalytic functionality.⁶ To overcome the above mentioned inherent drawbacks of TiO₂ and to enhance its photocatalytic performance for solar H₂ production, significant efforts have been made on the catalyst design, such as, doping with metals and non metals,^{15,16} dye sensitization,¹⁷ use of noble metals (Pt, Pd, Au and Ag) as co-catalyst,¹⁸ engineering the band structure to match particular energy levels,¹⁹ fabrication of semiconductor heterojunction and/or Schottky junctions.²⁰

For the past few years, number of excellent review articles have been published on photocatalytic water splitting to hydrogen production, which are based on different catalyst systems including semiconductor-based catalyst systems,^{21,22} metal-free photocatalysts,²³ spinel materials,²⁴ ionic carbon nitride,²⁵⁻²⁸ carbon-based materials,²⁹ transition metal complexes,³⁰ and TiO₂-based semiconductor materials.³¹⁻³⁶ Although there are few reviews available for TiO₂-based photocatalysts for solar hydrogen production,³¹⁻³⁶ they emphasize primarily on general aspects of photocatalytic H₂ production. Readers interested in above aspects may refer those references. However, the present review emphasizes on the structure-activity correlation, and how the material integration helps for activity tuning. The various



critical changes in the physico-chemical and electronic properties of TiO₂-based materials fabricated by integrating TiO₂ with variety of dopants and/or materials and its structure-activity relation to solar hydrogen production were addressed in detail. The efficient and concurrent utilization of both photogenerated holes and electrons to improve the photocatalytic efficiency of the material is discussed in this review. We also discuss the importance of fabrication of photocatalyst in thin film form and performing solar hydrogen production in different reactor set up for enhancing the photocatalytic performance of the material and its scalability.

A Scopus based survey was made using the following three sets of key words of the manuscript, to know the number of publications with TiO₂-based photocatalyst for water splitting, namely, (i) TiO₂ photocatalysts and hydrogen production, (ii) TiO₂ photocatalysts and water splitting, and (iii) TiO₂-based photocatalysts, and hydrogen production and water splitting. This survey revealed that the articles published in this area are still steadily increasing for the past ten years and the result is shown in **Figure 1**. As shown in **Figure 1**, an increase in the number of articles on TiO₂-based photocatalysts for H₂ production appears after 2017 underline the importance of sustainable production of hydrogen from renewable sources and the world-wide focus on it.

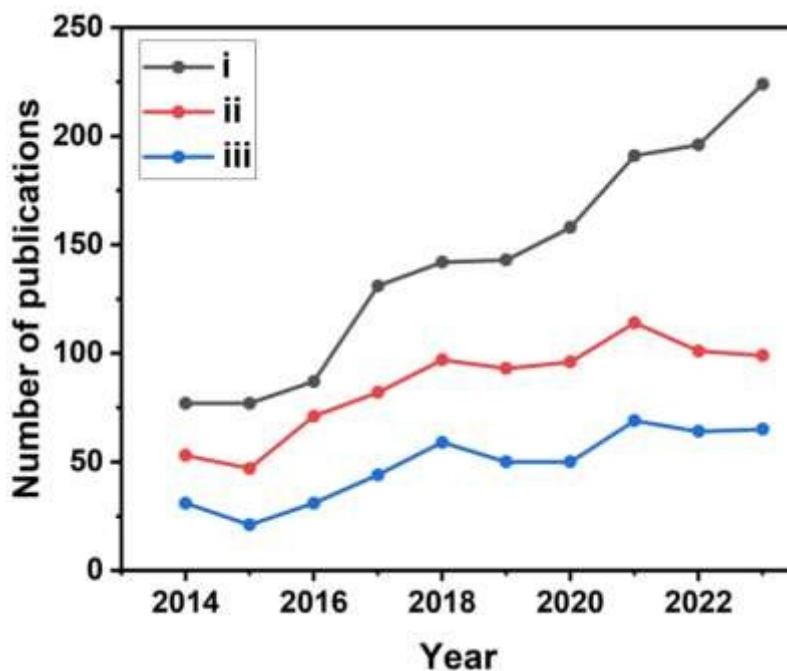


Figure 1. A scopus data-based survey (conducted on Feb. 29, 2024) indicating the number of publications appeared in the area of TiO₂-based photocatalytic water splitting to H₂ production, with three different sets of keywords, as explained in the text. (i) TiO₂ and photocatalyst and hydrogen production; (ii) TiO₂ and photocatalyst and water splitting, and (iii) TiO₂ and photocatalyst and hydrogen production through water splitting.

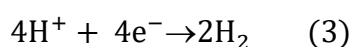
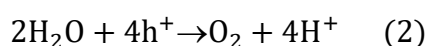
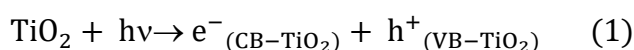
Several variations and advances have been made in the past decade, especially on TiO₂-based semiconductor photocatalysts for solar hydrogen production using water as major hydrogen source. Therefore, in this review, we comprehensively summarize and highlight the recent progress in the design and structure-activity relation of TiO₂-based photocatalysts towards solar hydrogen production with water as main hydrogen source; those works carried out with



sacrificial agents are also included to a significant extent. In the beginning, we provide the fundamental aspects of the material integration aspects with different materials with TiO₂, such as, noble metals, non-noble metals, metal oxide/sulphide/selenide, incorporation of low bandgap semiconductors; structure-activity correlation is given emphasis to understand the mechanistic aspects as well as how the entire photocatalytic hydrogen production area has been progressing. The role of TiO₂-based photocatalysts is also specifically reviewed based on the effects of various factors including preparation methods, morphology, crystallographic facet dependent activity, catalyst amount, dopant concentration. We also discuss the importance of engineering strategies, such as the importance of fabrication of photocatalyst in thin film form to overcome the drawbacks of TiO₂ in powder form for improved photoactivity as well as for scalability. Finally, the major challenges and an outlook on the future strategies in this research field are discussed from the viewpoint of the structure-activity relation of the various TiO₂-based photocatalysts.

2. TiO₂-based photocatalytic water splitting processes

The photocatalytic water splitting to H₂ and O₂ on TiO₂-based semiconductor surface is effected through a redox reaction process as described in equations (1) to (3).³⁷



The above described redox reaction is accomplished through three critical processes²¹ (i) light absorption by photocatalyst forming a free exciton (e⁻ h⁺) pair, (ii) separation of the photogenerated exciton pair into electrons and holes followed by their migration to the catalyst surfaces, and (iii) conversion of water molecules into hydrogen and oxygen on the catalyst surface by utilizing the photogenerated electrons in the conduction band for reducing protons to H₂ molecule and holes in the valence band for oxidizing water to O₂ molecule. A flowchart illustration of the various fundamental and critical steps involved in TiO₂-based photocatalytic water splitting processes is shown in **Figure 2**.

The bandgap and band position of the photocatalyst,³ the ability of the photocatalyst in enhancing the charge (electron-hole pair) separation and charge diffusion to the redox sites,³⁸⁻⁴⁰ presence of sacrificial reagents⁴¹ etc. are crucial factors which determine the efficiency of solar hydrogen production. The conversion efficiency of solar energy into hydrogen can be calculated by apparent quantum yield (AQY) according to the equation (4).⁴²

$$\text{AQY} = \frac{2 \times \text{Number of hydrogen molecules}}{\text{Number of photons}} \times 100 \quad (4)$$



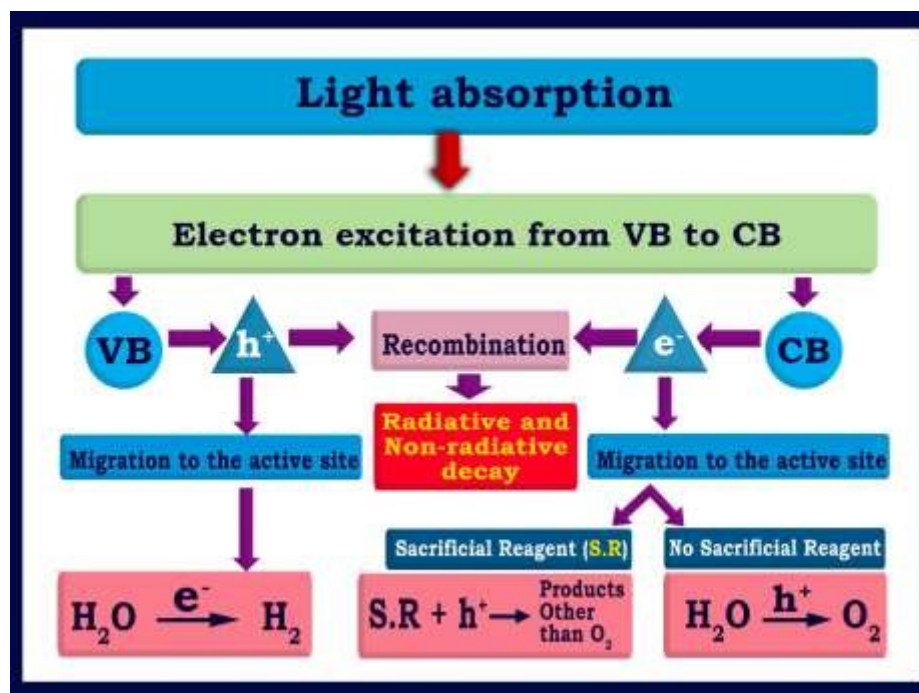


Figure 2. A flowchart illustration of the fundamental and critical processes involved in any semiconductor based photocatalytic water splitting processes.

3. TiO₂-based water splitting photocatalysts

Significant efforts have been made in the past few decades to enhance the activity of the TiO₂-based photocatalysts by modifying the band gap, electron-hole separation and charge transfer characteristics of TiO₂ by integrating it with different components.^{42,44–47} The different kinds of components used to make electronically integrated TiO₂-based photocatalysts are non-metallic dopants (S, N, F, and C),^{15,46,47} metal nanoparticles,^{48–54} low bandgap metallic oxides (Cu₂O, Fe₂O₃, CeO_{2-x}, NiO, Co₂O₃, SiO₂, ZnO),^{6,55–62} metal sulphides (CdS, ZnS, MoS₂, FeS₂, SnS₂ etc.),^{45,63–66} carbonaceous materials (carbon nanotubes, graphene, reduced graphene oxide (rGO)),^{43,67–71} graphitic carbon nitride (g-C₃N₄),^{72,73} and dye sensitization.^{74,75} Integration of above components with TiO₂ in optimum concentration modify the band gap and electronic structure with improved photocatalytic activity for H₂ production than bare TiO₂.^{38,39} A schematic representation of the various components used to improve the photocatalytic efficiency of TiO₂ is provided in **Figure 3**.

3.1. Metal nanoparticles

Integration of TiO₂ with metal nanoparticles is one of the effective strategies to enhance electron-hole separation by forming metal-semiconductor Schottky junctions with improved charge transfer efficiency.⁷⁶ Due to the difference in the Fermi energy levels of metal and TiO₂, when metal and TiO₂ come into contact, photoexcited electrons were transferred from TiO₂ to metal until their Fermi energy levels are equilibrated. The potential of a metal nanoparticle as a co-catalyst relies on ease of electron transfer from the conduction band of TiO₂ to the Fermi level of the metallic surface via the Schottky junction. The Schottky





Figure 3. Schematic representation of different kinds of chemical components used to improve the photocatalytic efficiency of TiO_2 .

junction resulted due to the charge difference between the metal nanoparticles (excess negative charge) and TiO_2 surface (excess positive charge) acts as an effective trap for capturing electrons, which can inhibit the combination of electrons and holes.^{51,77,78}

Noble metals Ru,⁷⁹ Rh,⁸⁰ Pd,^{45,49,81} Au,^{50,82–84} Ag,^{85–87} and Pt^{51,88–90} are widely used as a co-catalyst with TiO_2 in photocatalytic hydrogen production due to their unique properties such as formation of Schottky barrier^{44,91} and efficient interfacial electron transfer, photostability, ability to show surface plasmon resonance,⁹² formation of impurity energy levels,⁷⁹ and oxygen vacancies.⁸⁰ Noble metals are of two types: plasmonic (Ag & Au) and non plasmonic (Pt, Pd, Ru, Rh).^{49,76} Schottky barrier is more critical for non-plasmonic metals like Pt and Pd, which function as an effective electron trap, imparting a high density of states at the Fermi level and facilitate charge separation and utilization. For example The non-plasmonic noble metals are not capable of exhibiting visible light absorption; however, shows very high cocatalyst activity.^{43,76} Noble metals such as Au and Ag at the surface of TiO_2 increases the photon absorption in the visible region through localised surface plasmon resonance (LSPR) effect.^{93,94} Surface plasmon resonance (SPR) effect increases the production of hot electrons at the interface between metal and TiO_2 . Since the SPR level of metal is higher than the conduction band of TiO_2 , electrons are transferred from the SPR level of metal to the conduction band of TiO_2 . At the same time the Schottky barrier could prevent the back transfer of electrons to metal nanoparticles.⁵⁰ The formation of intermediate energy level enables Ru for charge separation and extends light absorption within the visible region,⁷⁹ whereas Rh induce oxygen vacancies in TiO_2 which allows the withdrawal of electrons from the metal, leading to an enhancement of hydrogen production activity.⁸⁰ A schematic illustration of the LSPR effect that occurs on a plasmonic metal nanoparticle surface and H_2 production



augmented by electron transfer via Schottky barrier at the interface between metal semiconductor, such as in the case of Au nanoparticle surface are shown in **Figure 4 (a, b)**.

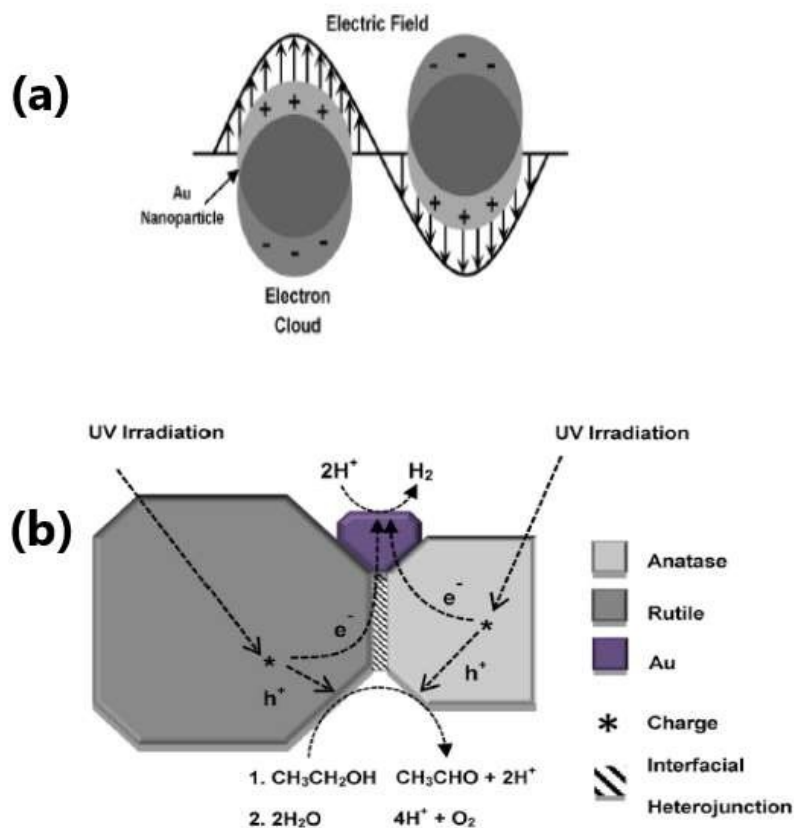


Figure 4. (a) Schematic representation of LSPR effect showing the oscillation of electric field of incident light at the resonance frequency at the surface of Au nanoparticle. (b) Schematic diagram of the proposed mechanism for photocatalytic H₂ production from ethanol/water mixtures over Au/P25 TiO₂. Reproduced with permission from ref.92. Copyright © 2015, Wiley-VCH.

Although noble metals are highly performing as co-catalyst for photocatalytic hydrogen generation, high cost and low abundance of them leads to the investigation of earth abundant and cheap non-noble metals co-catalysts.^{96–98} Non-noble metal nanoparticles, such as, Cu and Ni as co-catalysts with TiO₂ are found to be highly effective in enhancing the rate of hydrogen production in water splitting reaction.^{16,99–103} Heterogeneously surface distributed non-noble metal nanoparticles on TiO₂ increases the charge separation and facilitate the charge transfer.¹⁰⁴ Copper is one of the most studied non-noble metal cocatalyst for solar hydrogen evolution because of its low cost, high conductivity, capability to show SPR effect etc. The presence of metallic copper substantially changes the electronic structure of TiO₂ because of the formation of structural defects or due to the formation of energetic electron trap centres which prevents electron-hole recombination.^{96,99,105} Nickel is another attractive non-noble metal co-catalyst because of its high work function, availability and low cost. The high work function of Ni is favourable in preventing the migration of electrons back into the conduction band of TiO₂ in Ni/TiO₂.¹⁰⁶ Metallic Ni nanoparticles dispersed on TiO₂ as small-sized clusters resulted in an improved rate of photocatalytic hydrogen evolution.¹⁰⁶ A schematic description of the



properties related to various metal nanoparticles employed for fabricating metal integrated TiO_2 photocatalyst system for photocatalytic H_2 production is provided in **Figure 5**.

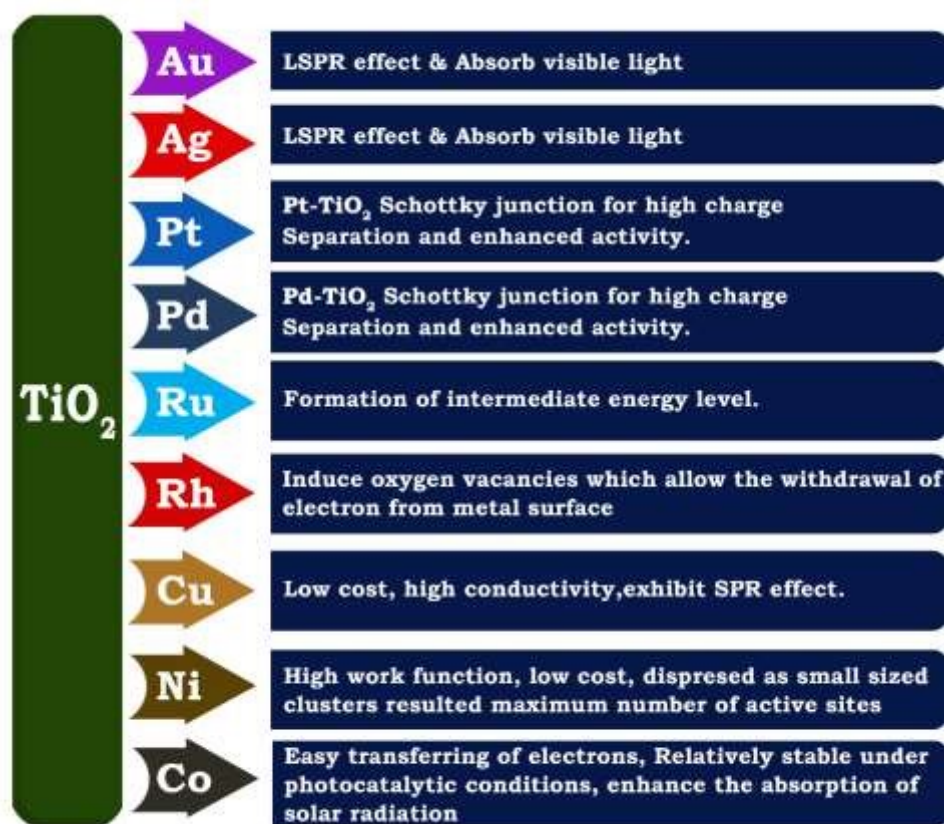


Figure 5. Schematic representation of various noble metals used for improving the photocatalytic hydrogen evolution activity of TiO_2 .

3.2. Bimetallic co-catalyst

Compared to single metallic component, bimetallic cocatalysts provide more active sites for H_2 production. The combined effect and the possible synergetic interaction between the two components of bimetallic system effectively improves the charge separation and charge transfer; when one of the bimetallic component is SPR active, it enhances the light absorption capability too.^{18,100} For example, Cu/Ag bimetallic quantum dots on TiO_2 nanotube is beneficial for solar hydrogen generation which take advantage of the SPR effect of Cu and Ag as well as co-catalyst capability of Cu.¹⁰⁰ A schematic representation of the synthesis of bimetallic Cu/Ag@ TiO_2 nanocomposite and the charge transfer mechanism involved in it is provided in **Figure 6**.



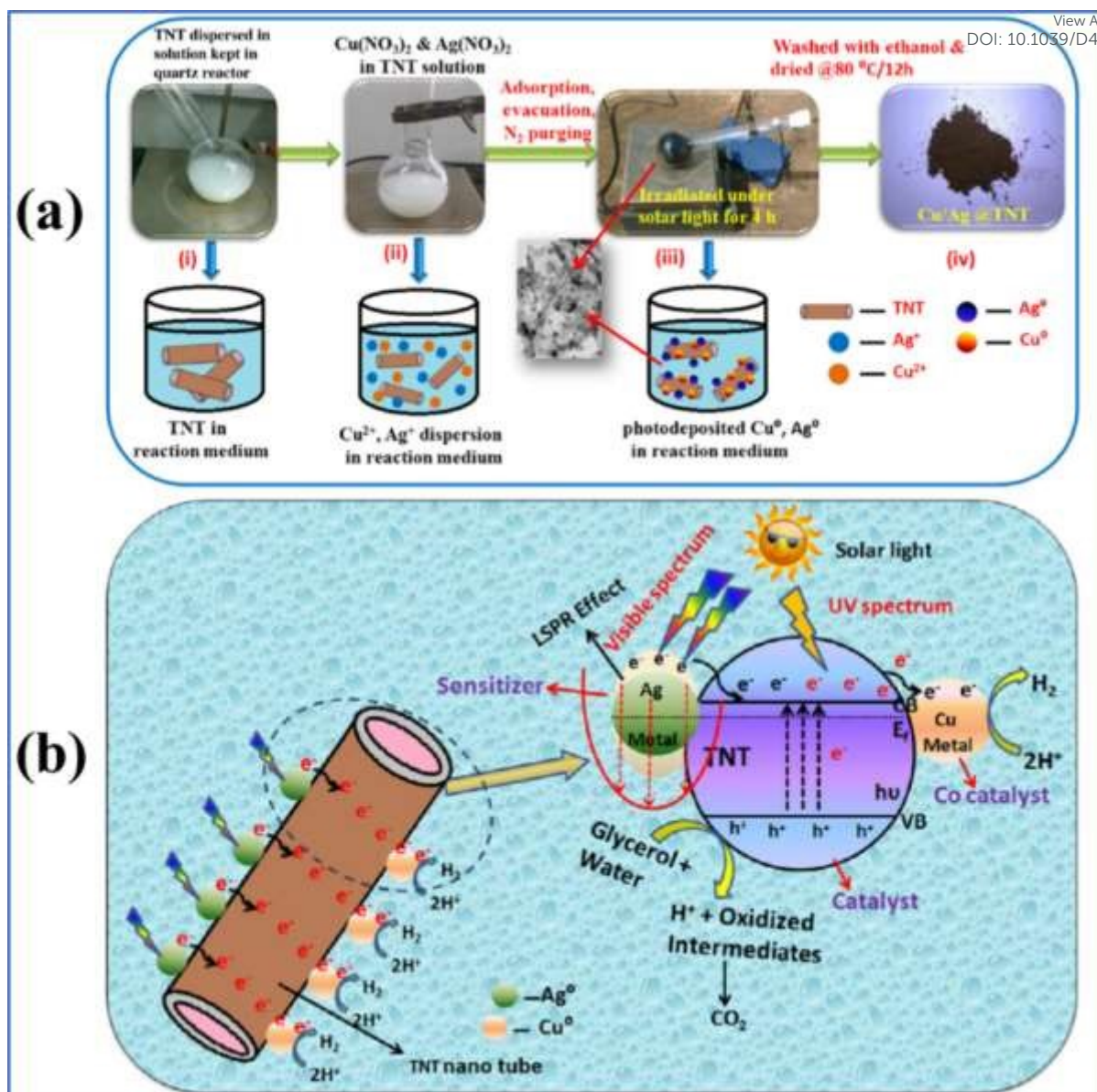


Figure 6. (a) Synthesis scheme of Cu/Ag bimetallic deposition on Titanium Nano Tube (TNT), (b) charge separation and hydrogen evolution mechanism of as synthesized Cu/Ag@TiO₂. Reproduced with permission from ref.100. Copyright ©2017, Elsevier Ltd.

Similarly, NiCu alloy is also found to enhance the solar hydrogen production with a quasi-artificial leaf device (QuAL) made with Mn-doped CdS integrated with mesoporous TiO₂.¹⁰⁷ Mn-doping in CdS was shown to enhance the visible light absorption to longer wavelength, compared to virgin CdS. With NiCu-alloy co-catalyst, the QuAL device of 1 cm² area was demonstrated to produce 10.5 ml/h of H₂ with power conversion efficiency of 4.8%. Another interesting aspect of this QuAL work is an increase in the visible light absorption efficiency, due to different size Mn-CdS integrated, which exhibits significantly wide range of band-gap values due to different QD sizes. Even the fluorescence is emitted from smaller QDs apparently absorbed by the significantly bigger size QDs or nanoparticles of the same Mn-CdS.



3.3. Non metal doping

View Article Online
DOI: 10.1039/D4YA00249K

Doping in TiO₂ using non metals, such as S,⁴⁶ C,¹⁵ F,⁴⁷ N,¹⁰⁸ etc. leads to the lowering of bandgap and it is an effective approach to enhance the visible light absorption capability and to improve solar hydrogen evolution.^{15,109} The addition of non metal dopants in TiO₂ matrix may results structural defects in the material, impurity energy level formation and hence narrowing of band gap, and als ohelpful in overcoming disadvantages like carrier trapping and thermal instability that are often met with metal nanoparticles.^{110–113} Nitrogen is one of the most studied anion dopant, because of several advantageous aspects, such as, its similar atomic size with oxygen, formation of metastable energy states and considerable overlapping of N2p states and the O 2p states resulting in the narrowing of bandgap and smooth excitation of electrons between the valence band and conduction band.^{114,115} **Figure 7** demonstrates that, in comparison to pure TiO₂, the optical properties, valence band characteristics, and band positions of N-doped TiO₂ samples were modified.¹¹⁶ Further, N doped samples exhibited an increased in charge separation and charge carrier desity compared to pure TiO₂.

3.4. Integration with Low band gap semiconductors

Formation of TiO₂-based composite with semiconductors having low band gap is another efficient strategy for enhancing the rate of photocatalytic hydrogen production. Low band gap semiconductors include both metal oxides and metal chalcogenides. Based on the band position of TiO₂, semiconductors can be classified into two: semiconductor having CB position more negative than TiO₂ (e.g., Cu₂O,^{6,117} CuO,^{118–120} CeO₂,⁵⁶ ZnO,⁶⁰ CuInS₂,¹²¹ CdS,^{63,122,123} SnS₂,⁶⁶ etc.), and semiconductor having CB positions less negative than TiO₂ (e.g., NiSe,²⁰ FeS₂,⁶⁵ Cu₂S,⁶ MoS₂,⁶⁴ etc.). A plot between the band positions of TiO₂ and various semiconductors against redox potentials is depicted in **Figure 8**.

The electron hole separation and the electron transfer process through the formation of heterojunction with low band gap semiconductor depend on the band position of both TiO₂ and supporting semiconductor. If the CB edge potential of supporting semiconductor is more negative than that of TiO₂, thephotogenerated electrons in the conduction band of semiconductor usually transfer to the lower-lying conduction band of TiO₂.^{55,56,124} Whereas, the CB edge potential of supporting semiconductor is less negative than that of TiO₂, the electrons from the conduction band of TiO₂ will be transferred to the lower-lying conduction band of supporting semiconductor.^{20,64,125,126}

3.4.1. Metal oxide semiconductors

A large number of semiconductor metal oxides like ZnO,⁶⁰ CeO₂,⁵⁶ WO₃,¹²⁷ SrTiO₃,¹²⁸ Y₂O₃,¹²⁵ CoO,^{129,130} NiO,^{57,124,129} Cu_xO,^{6,118,131} Ag₂O,^{132,133} and Fe₂O₃⁵⁵ are used for making stable and low costheterojunction structures with TiO₂. These composites with reduced band gaps are found to be be very effective for electron-hole separation and charge transfer^{64,132,134} and hence a promising alternative to the highly expensive noble metal-based photocatalyst systems.The p-n junction formed at the interface between the n-type TiO₂ semiconductor and



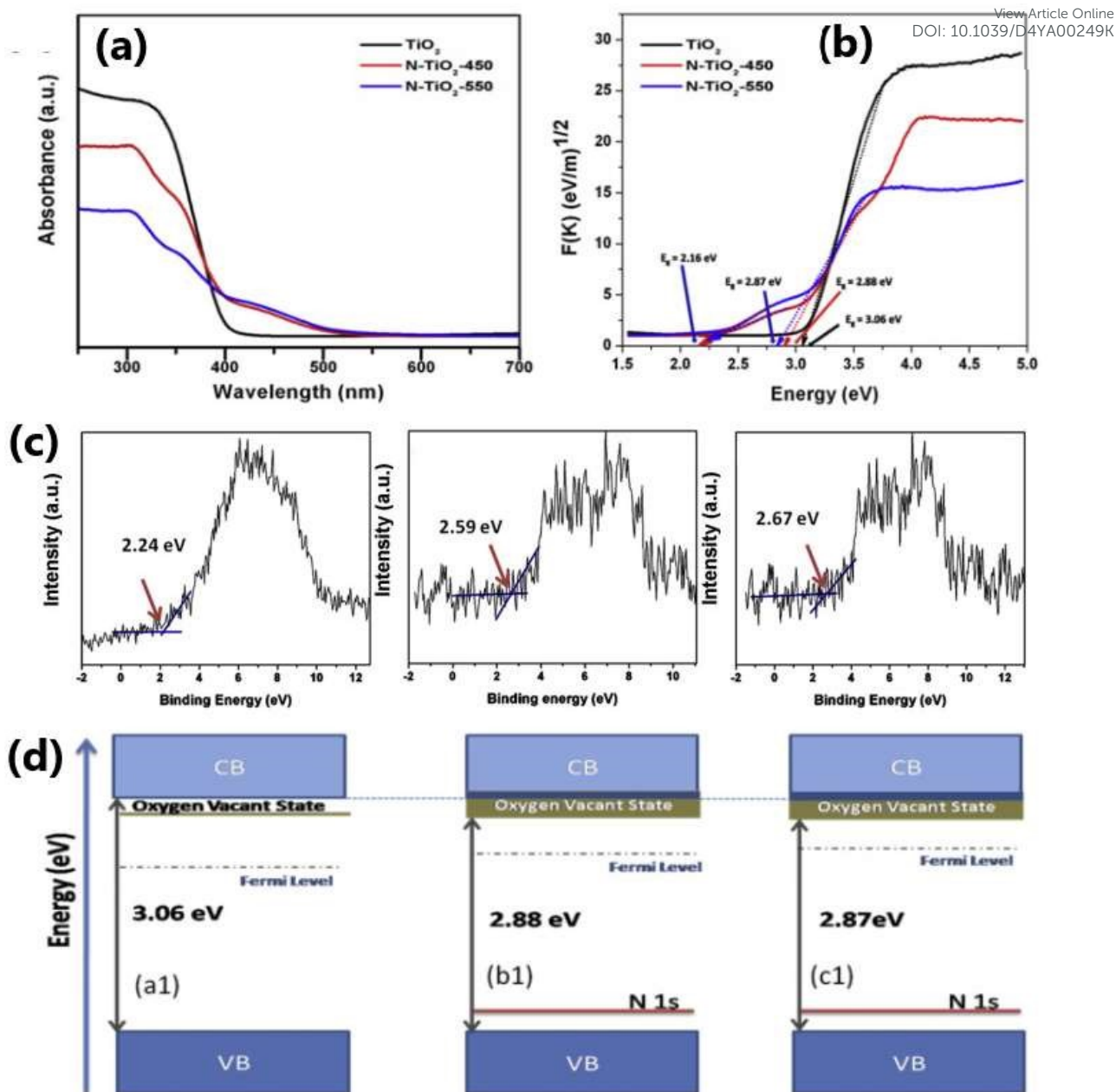


Figure.7 (a) UV-Vis absorbance spectra and (b) Tauc plot obtained from the reflectance spectra and (c) Valence band edge analysis of TiO₂, N-TiO₂-450, N-TiO₂-550. (d) Proposed band diagrams of the TiO₂ and N-doped TiO₂ catalysts. Reproduced with permission from ref.116. Copyright© 2016, ElsevierLtd.

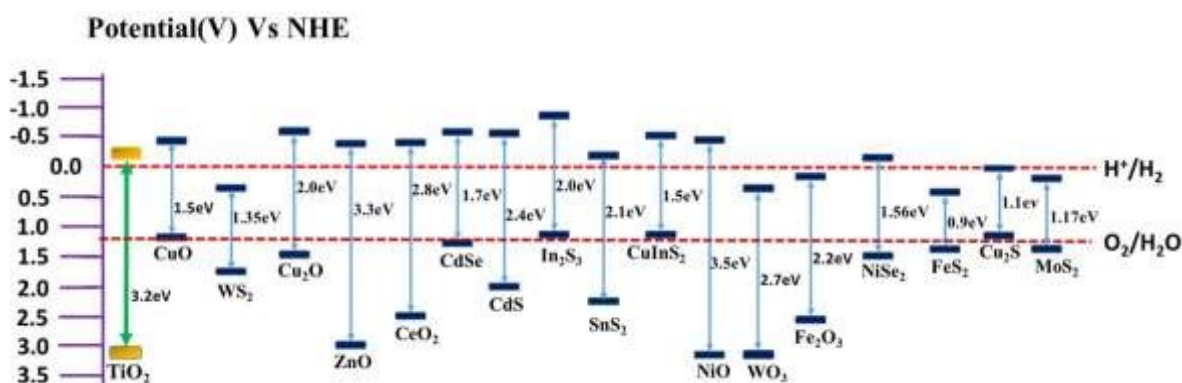


Figure 8. A plot between band positions of semiconductors against redox potential at pH=7 View Article Online
DOI: 10.1039/D4YA00249K

the p-type semiconductors such as α -Fe₂O₃, CoO, NiO and Cu_xO enhance the rate of photocatalytic H₂ production due to the appropriate band position for water reduction, enhanced lifetime of charge carriers and rate of charge transfer, and ability to expand its absorption in the visible region.^{55,57,124,131,135} A schematic description of the properties related to various metal oxide nanoparticles employed for the fabrication of stable heterojunction with TiO₂ photocatalyst system for photocatalytic H₂ production is provided in **Figure 9**.

The activity of TiO₂ can be further improved by surface modification of it with Ni (metal) and P (nonmetal) by making heterojunctions more effective.⁵⁶ For example, CeO₂-TiO₂ photocatalyst after surface decoration with Ni-P has become an effective photocatalyst for hydrogen evolution due to the lowering of the bandgap to 2.4 eV and powerful electron-hole separation.⁵⁶ In this photocatalyst, Ni-P acts as a bridge for electron transportation. SiO₂ is an interesting substrate used for dispersing and maintaining the active phase, imparting thermal



Figure 9. Schematic representation of various metal oxides used for improving the photocatalytic hydrogen evolution activity of TiO₂.

stability and improving surface area to the TiO₂-based photocatalyst.⁵⁹ For example, the pore channels of SiO₂ has been successfully utilized for anchoring TiO₂ quantum dots (TiO₂-QDs) in a highly dispersed state on the silica surface via in-situ hydrolysis of Ti-alkoxide.⁵⁹ The anchoring effect between TiO₂-QDs and the pore-wall of SiO₂ foam provide extra stability to



TiO₂-QDs, which helps in maintaining TiO₂-QDs in anatase phase without undergoing any phase transformation and particle growth even after high temperature up to 1000°C.

NiO is a p-type semiconductor with a bandgap of 3.5 eV, and it possesses high charge carrier concentration and high mobility of charge carriers. It can make efficient p-n heterojunction with anatase TiO₂ which facilitates the red shifting of the bandgap energy of NiO/TiO₂ heterostructure.¹²⁴ The internal electric field developed at the interface of the NiO/anatase TiO₂ p-n heterojunctions facilitates the dissociation efficiency of photogenerated electron-hole pairs and enhances the photocatalytic efficiency. For example, mesoporous heterostructure of 1 wt% NiO on anatase TiO₂ nanoparticulate photocatalyst showed a H₂ production rate of 2693 μmolh⁻¹g⁻¹ by methanol photoreforming, which is higher than pure anatase TiO₂ and commercial P25.

3.4.2. Transition metal chalcogenides

The potential of low band gap transition metal chalcogenides, such as, molybdenum sulphide (MoS₂),⁶⁴ cadmium sulphide (CdS),¹²² tungsten sulphide (WS),¹²⁶ nickel sulphide (NiS),¹³⁶ copper sulphide (Cu₂S),⁶ cadmium selenide (CdSe),¹³⁷ CuInS₂¹²¹ etc. in heterojunction with TiO₂ has been explored in H₂ production by water splitting reaction. The favourable photocatalytic properties of these composite structures, such as, remarkable light absorption in the visible region (e.g., TiO₂/MoS₂)¹³⁸ excellent charge carrier separation and charge transfer due to intimate and large contact interface, large surface area with increased number of active sites (e.g., TiO₂/CdS), feasible reduction potential (TiO₂/Cu₂S)⁶, large optical absorption coefficient (e.g., TiO₂/FeS₂),⁶⁵ excellent chemical stability in acid or neutral solution and thermal stability in air (e.g., TiO₂/SnS₂)⁶⁶ makes these materials to offer high photocatalytic activity and H₂ production rate.^{6,65,66,139,140} Guo et al. demonstrated that nonmetal plasmonic MoS₂@TiO₂ heterostructures with broad spectral response ranging from near UV-visible to near IR region exhibited an enhanced H₂ production activity.¹⁴⁰ The MoS₂@TiO₂ system was fabricated by a series of reactions involving anodization, physical vapor deposition (VD), and chemical vapor deposition (CVD) processes (**Figure 10a**). In order to get deep insight about this nonmetal plasmonic system structural and textural analyses, FEM simulation and DFT calculations were also performed (**Figure 10b-i**) and it was found that the uniform heterostructure with surface plasmon resonance is responsible for charge transfer and charge carrier separation process. In another example, the HRTEM images of in FeS₂-TiO₂ composite (**Figure 11b**) demonstrates the intimate junction between (210) facet of FeS₂ and abundantly available (101) facet of TiO₂; as a result of it, the photocatalytic H₂ production rate shown by FeS₂-TiO₂ is much higher than that of both FeS₂ and TiO₂ (**Figure 11c**) due to the efficient electron-hole separation mechanism of the composite material as illustrated in **Figure 11b**.⁶⁵ There are some novel chalcogenides, which act as excellent photocatalytic system.⁴ For example, excellent photocatalytic activity of ZnIn₂S₄ is reported in the literature.⁴ The layered structure provides sufficient active sites for photocatalytic reactions, thus enhancing its overall catalytic performance. Additionally, the long-term durability study of this catalyst in repeated catalytic cycles of operations reveals that ZnIn₂S₄ exhibits strong photochemical stability.⁴



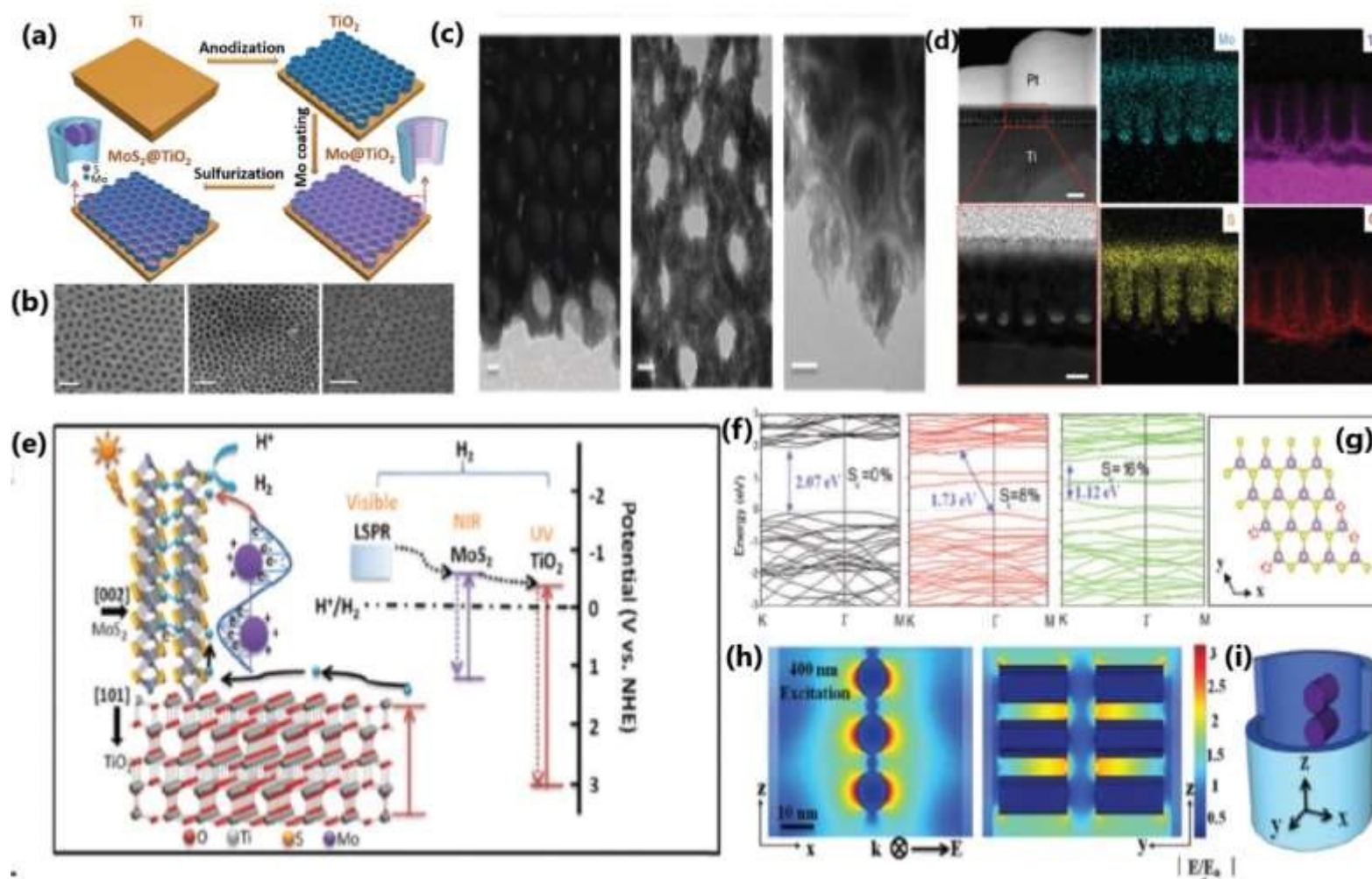


Figure 10. (a) Schematic illustration of the assembly process of the $\text{MoS}_2@\text{TiO}_2$ heterostructure. (b) SEM pictures of $\text{MoS}_2(10)@\text{TiO}_2$, $\text{MoS}_2(20)@\text{TiO}_2$ and $\text{MoS}_2(30)@\text{TiO}_2$, respectively (scale bar: 100 nm). (c) TEM and HRTEM images of $\text{MoS}_2(10)@\text{TiO}_2$, and $\text{MoS}_2(20)@\text{TiO}_2$ (scale bar: 20 nm). (d) Cross-sectional HAADF-STEM images and EDS elemental mapping of the $\text{MoS}_2@\text{TiO}_2$ heterostructure (First row, scale bar: 200 nm, and second row, scale bar: 50 nm). (e) Schematic diagram of the energy band structure, plasmonic resonance and electron transfer pathway in the $\text{MoS}_2@\text{TiO}_2$ heterojunction. (f) Band structure of monolayer 2H- MoS_2 with 0%, 8% and 16% S-vacancies, with the valence band maximum and conduction band minimum both at the K point. (g) The model used for band gap computation by DFT. (h) FEM simulation of the near-field electric field distribution inside $\text{MoS}_2@\text{TiO}_2$ heterostructures excited by a 400 nm laser and (i) a 3D-simplified model used for FEM simulation. Reproduced with permission from ref. 140. Copyright ©2018, Royal Society of Chemistry.



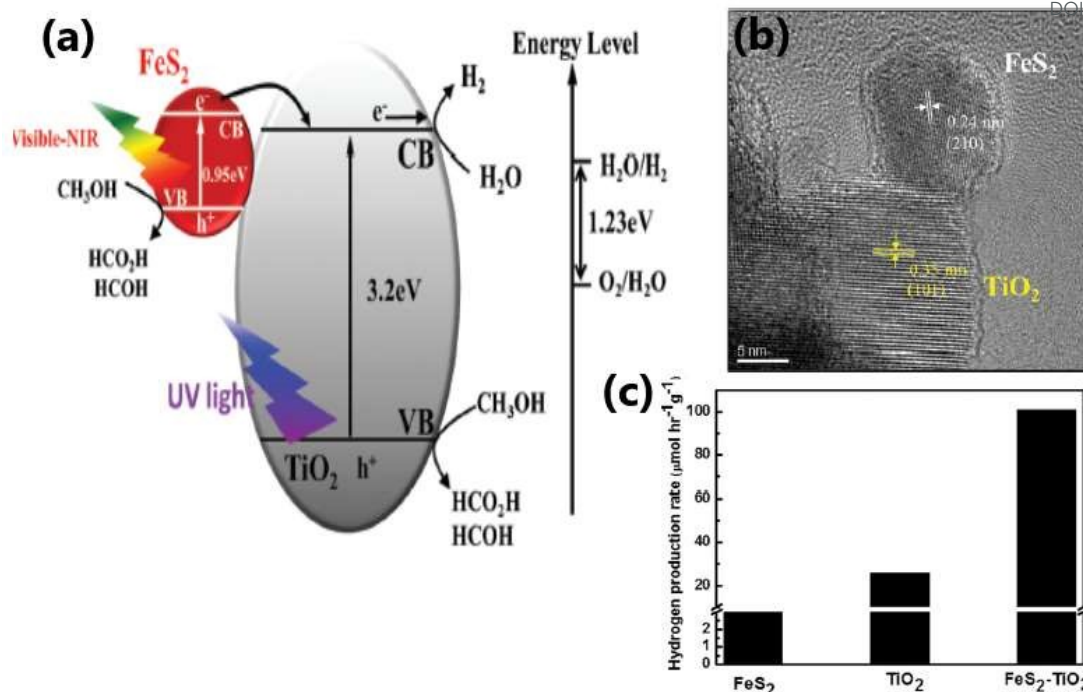


Figure 11. (a) Schematic illustration of the interfacial charge transfer process in FeS₂-TiO₂ catalyst under UV, visible and near-IR light irradiation. (b) HRTEM image showing the intimate contact between the (210) plane of FeS₂ and the (101) plane of TiO₂ in FeS₂-TiO₂, and (c) shows the rate of hydrogen evolution from TiO₂, FeS₂ and the FeS₂-TiO₂ nanocomposite under a 300 W xenon lamp. Reproduced with permission from ref. 65. Copyright ©2018, Royal Society of Chemistry.

3.5. Carbon-based Photocatalytic materials

Combination of TiO₂ with carbonaceous materials like graphene^{70,141} graphene oxide^{43,142,143} carbon nanotube (CNT)⁶⁷ and graphitic carbon nitride (g-C₃N₄)^{144–147} leads to highly promising hetero structures for photocatalytic hydrogen generation, in addition to mechanical strength. One of the study⁷⁰ indicates a rough estimate of the weight ratio of TiO₂ to RGO to be around 10⁵–10⁶; nonetheless, the RGO layers seem to be intact without any tear. These composite materials are effective to prevent the agglomeration of metal nanoparticles and display good light absorption capacity and electron-hole separation.¹⁴⁸ The enhanced rate of photocatalytic H₂ production displayed by nanocomposite of TiO₂ with two-dimensional (2D) carbonaceous materials reported in the literature include graphene¹⁴⁹ reduced graphene oxide¹⁵⁰ and g-C₃N₄^{68,145,151,152}. The excellent physical, chemical and photocatalytic properties of these TiO₂-2D carbonaceous materials, such as, high specific surface area, high mechanical and chemical stability, outstanding visible light absorption ability, high electrical conductivity and mobility of charge carriers, ability to shuttle charges between the composite material and regain its sp² hybridised structure, spatial charge separation of electron-hole pairs, reduced band gap and good charge separation make them highly performing.^{67,68} The enhanced photocatalytic activity and H₂ production ability of CNT/TiO₂ composite materials are due to the incredible electron transport and optical properties of CNT, and creation of intermediate energy level,



that helps to improve the visible light absorption capacity of the material.^{67,68,153} **Figure 12** illustrates the synthesis protocol for fabricating the TiO₂/g-C₃N₄ nanosheet composites, detailing its optical absorption properties, morphology, photocatalytic hydrogen evolution mechanism, and valence band characteristics.

3.6. Dye sensitization

Dye sensitization is a simple and effective technique to improve the visible light-harvesting capacity^{17,154} and thereby enhances the photocatalytic hydrogen production activity. Amongst different dye sensitizers, organometallic complexes¹⁷ and metal-free organic dyes¹⁵⁵ are most widely used and TiO₂ in combination with them displayed enhanced photocatalytic hydrogen production.¹⁵⁶ During photocatalysis the electrons from the lowest unoccupied molecular orbital of sensitized dye are injected into the conduction band of TiO₂ leading to efficient separation of electrons and holes. In comparison with dye sensitized TiO₂, bare TiO₂ shows poor solar light conversion efficiency.¹⁰¹ Dyes used for sensitization, especially the organic dyes, may degrade with time as a result of exposure to light, changes in the temperature, or chemical interactions with the environment. As a result of this deterioration, the overall stability and effectiveness of the photocatalytic system may be lowered. In certain cases, the photochemical stability of dyes may be enhanced if the dye and semiconductor are connected by a covalent bond rather than a weak interaction.¹⁵⁷ A diagrammatic illustration of the dye sensitization and the hydrogen evolution mechanism of Eosin Y-sensitized C-TiO₂ hollow nanoshells system is given in **Figure 13**.¹⁵⁶

3.7. TiO₂-based Ternary composite material

Construction of structurally organized ternary nanocomposites with efficient heterojunction through intimate contact between them is a versatile approach to improve the photocatalytic performance and hydrogen yield in water splitting reaction. Different kind of ternary composite systems with superior catalytic performance than the corresponding binary composites have been reported in the literature, which include Au-Pd/rGO/TiO₂,⁴³ Au/(TiO₂-g-C₃N₄),^{158,159} Pt/Cu/TiO₂,¹¹⁸ GO/TiO₂/ZnIn₂S₄,¹⁴³ CuInS₂/TiO₂/MoS₂,¹²¹ CuO-CO₃O₄/TiO₂,¹⁶⁰ Pd-SrIn₂O₄-TiO₂,¹⁶¹ CuS-TiO₂/Pt,¹⁶² Cu₂O/TiO₂/Bi₂O₃,¹⁶³ etc. Different hydrogen generation activity reported for same/similar catalysts from the above references suggests the quality of heterojunctions are different, which could be one of the main reasons for efficient charge separation and migration to the redox sites. For example, the superior activity of Au/(TiO₂-g-C₃N₄) ternary composite is due to the efficient charge separation and enhanced visible light absorption in a wide range of wavelength resulted from the SPR effect of Au nanoparticle and the potential to shuttle electrons by using g-C₃N₄.^{158,164} The photocatalytic performance of TiO₂ can be enormously improved by creating a triple composite CuInS₂/TiO₂/MoS₂ which exhibit a huge range of absorption from the UV region to the near-infrared region.¹²¹ On irradiation, the excited electron from CuInS₂ is smoothly transferred via TiO₂ to MoS₂ where



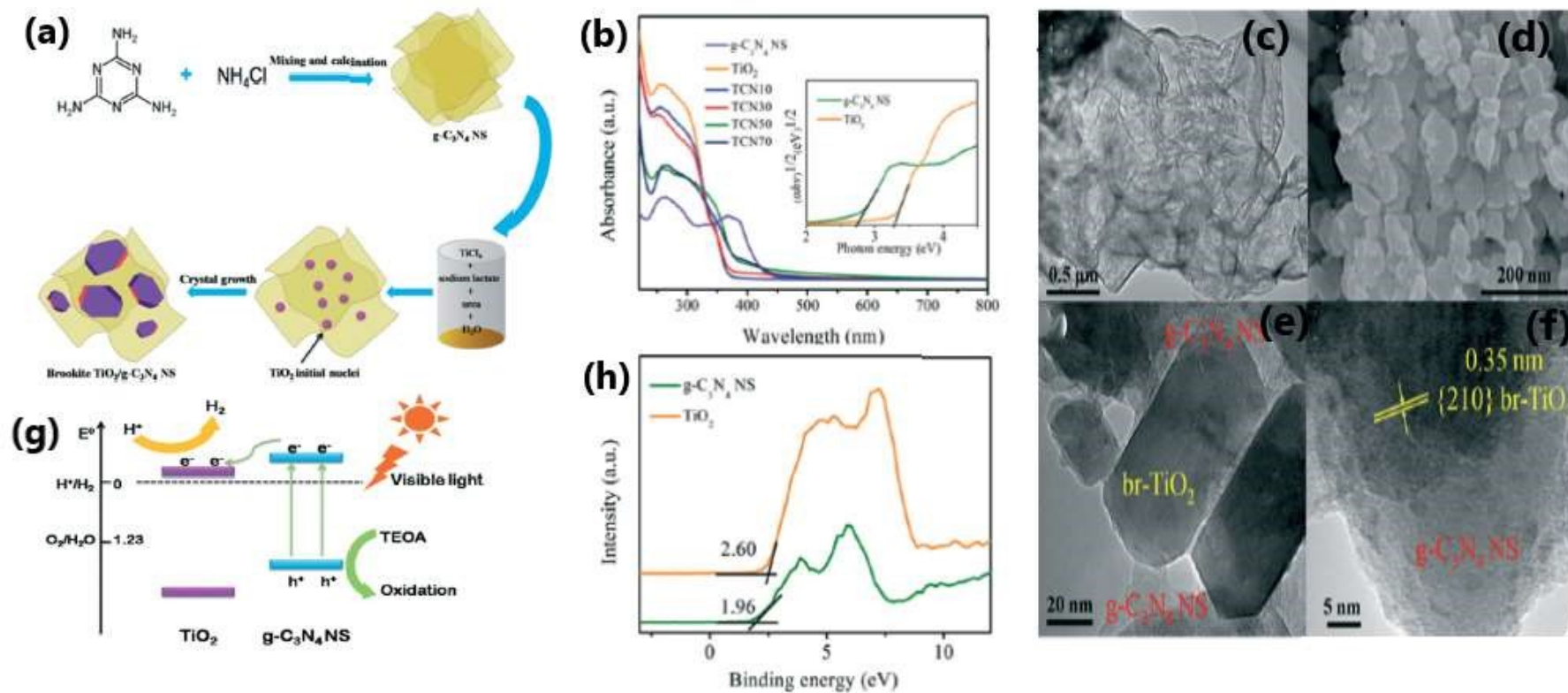
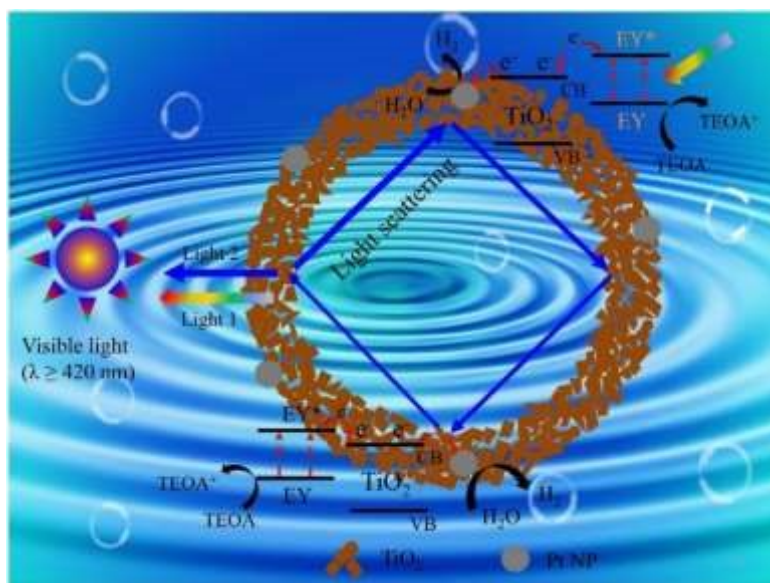


Figure 12. (a) Schematic illustration of the synthesis of TCNx composites. (b) UV-vis absorption spectra of TiO₂ and TCNx composites. SEM images of (c) g-C₃N₄ NS and (d) TCN50. (e) and (f) represent HRTEM images of TCN50. (g) Proposed mechanism for visible light photocatalytic activities of TCNx composites. (h) VB XPS of TiO₂ and g-C₃N₄ NS. Reproduced with permission from ref. 152. Copyright © 2017, Royal Society of Chemistry.



View Article Online
DOI: 10.1039/D4YA00249K

Figure 13. Mechanism for photocatalytic H_2 evolution over Eosin Y-sensitized C-TiO₂ hollow nanoshells with Mie resonance. Reproduced with permission from ref.74. Copyright ©2021, Elsevier LTD.

the adsorbed proton is reduced to H_2 .¹²¹ The metal nanoparticles in ternary composites act as an effective co-catalyst and further enhances the rate of hydrogen generation by supplying electrons and active sites for hydrogen generation.^{43,158,161} **Figure 14** shows a schematic illustration of the electron transfer mechanism and photocatalytic H_2 production over Au-Pd/rGO/TiO₂ triple composite wherein the SPR induced electron is directly transferred from Au to the CB of TiO₂ via rGO.⁴³ **Table 1** lists a detailed comparison of the H_2 yield and the corresponding experimental conditions for selected TiO₂-based photocatalysts.

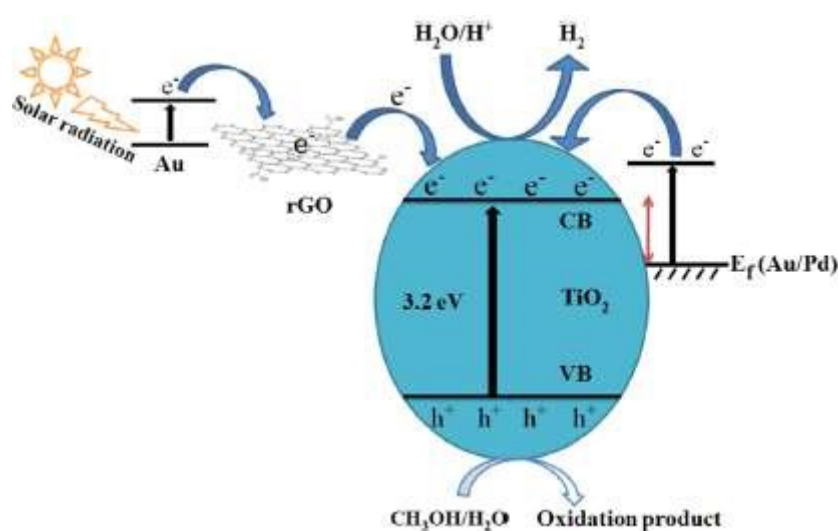


Figure 14. A schematic illustration of the mechanism of photocatalytic hydrogen evolution from Au-Pd/rGO/TiO₂ triple composite in which SPR electron from Au is transferred to TiO₂ via rGO. Reproduced with permission from ref.43. Copyright ©2019, ACS.



Table 1: Hydrogen yield and experimental conditions associated with various TiO₂-based photocatalytic systems reported in the literature.

Metal integrated TiO ₂				
No.	Material	Experimental condition	H ₂ yield / mmol/h.g	Ref
1	0.5Rh/TSG (TiO ₂ Sol-Gel)	50 mg of 0.5Rh/ TSG photocatalyst in aqueous solution of ethanol (50% v/v, water), A UV pen ray Hg lamp ($\lambda = 365$ nm)	7.2246	52
2	Ru 8.0 /TiO ₂ NBs-400	10 mg of photocatalyst was suspended in 10 mL of water containing 0.1 g of ethylenediamine tetra acetic acid disodium salt (EDTA-2Na), 300 W xenon lamp	25.34	48
3	TiO ₂ Ag-F	200mg catalyst in 200 ml of distilled water, 4 ml of methanol, A mercury lamp of 250 W	0.180 in 4h	38
4	TiO ₂ -Au-1%Pt	10 mg of TiO ₂ -Au photocatalyst into an aqueousmethanol solution (120mL, 25 vol%), 300 W XeLamp UVcut-420 nm filter	0.0924	50
5	3 wt% Au/P25 TiO ₂	(6.5 mg) was placed in Ethanol (15 mL) and milli-Q water (3.75 mL), 200 W, 365 nmwith6.5 mWcm ²	31.5	92
6	Ag@TiO ₂	0.05 g catalyst were suspended in deionized water and methanol mixed solutions (40 mL, 3 : 1), 300 W xenon lamp	0.5319	165
7	Pd/P25 1 wt% of Pd	Thin film forms of photocatalysts(1mg) with 25% v/v aqueous methanol solution, Direct Sunlight 50.2 mW cm ²	104	166
8	Au(2%)@TiO ₂	15mg of photocatalyst was dispersed in 25ml total volume containing 20% methanol (v/v) in aqueous solution, Natural sunlight	3.99 μ mol/h with 100 mg	167
9	The TiO ₂ -Pd NSs	15 mg photocatalysts were dispersed in50 mL of methanol/H ₂ O mixture (20 vol% methanol), 300 W Xe lampUV and vis-NIR light were used as illumination source400 nm cutofffilter 2.7 and 100 mW cm ²	2.80	168
10	Au@TNT	50 mg of photocatalysts were added to100 mL of methanol-deionized water mixed solution(V _{MeOH} /V _{H2O} = 1:10), Xe lamp ($\lambda > 400$ nm) intensity of incident visible light (k[400 nm) was 0.1 W/cm ²	0.482	169
11	1.5% Ag/TiO ₂	20%(v/v)aqueous solution of Na ₂ S+Na ₂ SO ₃ , 254 nm wavelength of UV light intensity of light was 4.40 mWcm ²	23.496	113
12	TiO ₂ -Au 9 wt%,	30 mg of catalysts was dispersed in 150 mL of water/methanol mixture with the volume ratio of 9 : 1, 300 W xenon arc lamp Intensity was 380 mW cm ² .	12.440	170
13	Pd/TiO ₂ nanosheets (0.18 At.% Pd NPs)	50 mg of photocatalyst in 50 mL of an aqueous solution containing 20% methanol in volume, 300 W Xe lamp equipped with an cut-off filter i ($\lambda > 420$ nm). light intensity (50mW cm ²)	3.096	171
14	0.1mol%Ru-TiO ₂	0.5 g of fine powder photocatalysts was suspended in 550 mL water and 50 mL methanol, 500 W Hg mid-pressure immersion lamp $\lambda > 320$ nm	3.400	79
15	1wt%Ag/TiO ₂ (TiAg -1)	1 mg photocatalyst was dispersed in 1 ml ethanol dropcasted on a thin film, 25 % (v/v) methanol/water mixture, Direct sunlight	4.59	44
16	TiO ₂ /Cu	20 mg of TiO ₂ and a given amount of metal particle were added to 30 mL, A 15W black light emission of ~352 nm; 1.0 mW/cm ²	0.850 mmol/g in 3h	172
17	Cu/Ag@TNT 0.1 M Cu and 0.1 M Ag	5 mg of catalyst was dispersed in 50 mL of 5 vol.% glycerol aqueous solution, 300W Xe lamp with an UV cutoff filter with wavelength >400 nm	56.167	100
18	TiO ₂ -Ni-1%	50 mg photocatalyst was added into methanol solution (20 vol %), A 300 W Xe lamp	1.433	16
19	Cu(3%)-TiO ₂ /ErB	5 mg of catalyst in 70 mL water containing 10 vol% triethanolamine, 300 W Xe lamp 0.15 W cm ²	13.4	105
20	0.5 wt% Ni/P25 TiO ₂	Photocatalyst (6.5 mg) was placed in the reactor and 20 mL of an aqueous glycerol mixture (10 vol%), 100 W, 365 nm) at a distance of 10 cm from the reactor. The photon flux at the sample	26.0	102
21	Ni-a/TiO ₂ 0.46 wt.%	50mg of the sample disperses in 100 ml of 10 vol.% methanol aqueous solution, 300 W Xe lamp	0.0945 mmol/h with 50 mg	173
22	TiO ₂ -NT/Pd-ND	1 mg catalyst in H ₂ O/MeOH solution (2:1), 300 W Xe lamp, maximum intensity of 203.3 mW/cm ² at wavelength of 365 nm	0.143 mmol/h with 1 mg	174
TiO ₂ with non-metals				
23	15 wt % S modified TiO ₂ /β-SiC	0.05 g of catalyst was suspended in 50 mL of an aqueous solution containing 10 vol % of methanol solution, 125 W medium pressure Hg visiblethe lamp was used, 1M NaNO ₂ solution as a UV filter under visible light irradiation ($\lambda \geq 400$ nm)	1.254	46
24	N-doped hollow TiO ₂ fibres nitrogen up to 5 at% (N-TiO ₂)	photocatalyst sample (0.02 g) was immersed into an aqueous methanol solution (5 ml methanol and 20 ml deionized water), 150 W Xe lamp optical filter, which allowed only wavelengths higher than 420 nm	0.185 μ mol/g in 6h	109
25	TiO ₂ /C	5 mg catalyst powder in aqueous solution (10 mL) consist of triethanolamine (10 vol%), 300 W Xe lamp, cut-off filter ($\lambda > 400$ nm).	57.2 μ mol/h with 5 mg	175
TiO ₂ with metal oxide semiconductor				



26	5Wt% Fe ₂ O ₃ /TiO ₂	50 mg Fe ₂ O ₃ /TiO ₂ nanocomposite was suspended with magnetic stirring in 200 mL aqueous solution 10 vol% glycerol, A 500 W Xenon lamp with UV cutoff filter ($\lambda > 420$ nm)	1.0 mmol/h.g DOI: 10.1039/D4YA00249K	55 Article Online
27	Ni-P/CeO ₂ -TiO ₂	0.5 g of the prepared catalysts were directly dispersed in 20 mL deionized water, 1 Sun (1000 mW/cm ²) was applied by the solar simulator	1.30 mmol in 5 h with 0.5 g	56
28	Pt/NiO-TiO ₂	0.1 g of catalyst was suspended in water + methanol mixtures (33% v/v, 15 ml), 400 nm, $\lambda_{max} = 536$ nm (medium-pressure Hglamp, 400 W) and UV-vis light source (Hg lamp, , 400 W)	0.537 mmol/g.h	57
29	TiO ₂ -QDs/SiO ₂	50.0 mg of TiO ₂ /SiO ₂ composite photocatalyst was suspended in 80.0 mL of aqueous solution containing methanol (25.0 V%), UV-LEDs (3 W, 365 nm)	10.399 mmol/g.h	59
30	TiO ₂ -ZO-(0.6%)	30 mg catalyst powders were ultrasonically dispersed into 80 mL H ₂ O, and then 20 mL methanol, 300 W Xe lamp the light intensity was kept at around 244mW cm ⁻²	0.3135 mmol/h with 30 mg	60
31	2.82wt.% Ag ₂ O.TiO ₂	0.2 g catalyst was suspended in 100 mL glycerolan aqueous solution (with 7 vol.% of glycerol), 300W Xe arc lamp (320-780 nm)	336.7 $\mu\text{mol h}^{-1} \text{g}^{-1}$	132
32	1wt% NiO /anatase TiO ₂	(50 mg) and the mixture of methanol/H ₂ O (1:1 v:v, 10 mL), UV-light (Hg vapor light source(LUMATEC SUPERLITE 400)	2.693	124
33	25 wt% of Y ₂ O ₃ in TiO ₂	Photocatalysts (10 mg) were dispersed in a 7.5 mL aqueous solution. After sonication, 2.5 mLethanol was added as asacrificial reagent, 300 W Xenon/Mercury lamp	1.380 in 2.5h	125
34	1 wt% Cu/TiO ₂	photocatalyst (2.5 mg) was loaded in the reactor containing 25 mL of a glycerol-water mixture (5 vol% glycerol), 100 W, 365 nm UV light excitation $\sim 6.5 \text{ mW cm}^{-2}$	15.32	176
35	2.5-Cu ₂ O/TiO ₂	450 mL aqueous solution, ethylene glycol as scavenger of10 vol.% in reaction solution, 500 W Xe arc lampbandpassfilter ($\lambda = 365$ nm with the photon flux of 3.6 mW cm ⁻²)	2.048	177
36	TiO ₂ -(0.1wt%)CuO	0.1 g of the the sample was suspended in 1 M KOH, 300 W xenon lamp	2.715 in 5h	178
37	Cu ₂ O/TiO ₂	0.1 g of the Cu ₂ O/TiO ₂ photocatalyst was dispersed in 100 mL 10 vol % aqueous methanol, 300 W xenon lamp with or without a band pass filter ($\lambda > 420$ nm)	24.83	179
TiO₂ with metal chalcogenides				
38	S-doped hetero nanostructured TiO ₂ /Cu ₂ S	Aqueous solution containing0.35 M Na ₂ SO ₃ and 0.35 M Na ₂ S, visible light irradiation conditions ($\lambda > 420$ nm)	1.280 with 50mg	6
39	NiSe/TiO ₂	50 mg of the as-prepared photocatalyst powderinto 100 ml aqueous solution containing 10 vol % Methanol	55.4 $\mu\text{mol h}^{-1}$	20
40	FeS ₂ -TiO ₂	1 g catalyst (50% aqueous methanol solution), mercury arc lamp (400W)	0.331	65
41	MoS ₂ /TiO ₂ (0.14 wt%)	50 mg photocatalyst was suspended in an 80 mL solution containing 20 mL methanol, Four low-power LEDs (3.5 W cm ⁻² , $\lambda = 365$ nm,)	2.443	126
42	10 mmol NiS/TiO ₂ nanosheet films	80 mL 10% ethanol/H ₂ O (v/v) solution, 500 W Xe lamp	4.31 $\mu\text{mol/cm}^2$ in 3 h	136
43	MoS ₂ /TiO ₂	MoS ₂ @TiO ₂ films with a size 7×7 mm were submerged in 15 ml of the mixed solution made of DI water (Seawater) and methanol (8:2 by volume), solar light simulator (AM 1.5, 300 W Xe, 100 mW cm ⁻²)	580	140
44	0.50 wt% MoS ₂ , the 2D-2D MoS ₂ /TiO ₂	100 mg photocatalyst in 100 ml aqueoussolutioncontaining 10% methanol in volume, 300 W Xe-arc lamp	2.145	138
45	2D/1DTiO ₂ nanosheet/CdS nanorods	50 mg photocatalyst was suspended in aqueous solution (20 mL lactic acid, 210 mL water), 300 W Xenon arc light source after filtering the UV light with circulating cooling NaNO ₂ aqueous solution (1 M) to pass only visible light ($\lambda > 400$ nm).	128.3	180
TiO₂ with carbonaceous material				
46	g-C ₃ N ₄ -TiO ₂ (1:4)	75 mg of photocatalyst was dispersed in 75 ml of aqueous solution containing 10% triethanolamine, 250W visible light source	1.041	68
47	TiO ₂ -100-G	Photocatalyst (100 mg) was dispersed in an aqueous solution containing H ₂ O (80 mL) and CH ₃ OH (20 mL), 300 W Hg lamp witha wavelength of approximately 365 nm	1.93	181
48	TiO ₂ /g-C ₃ N ₄	15 mg sample dispersed in 8 mL ethanoland 72 mL H ₂ O, A 150 W Xenon lamp with a cutoff filter($\lambda > 420$ nm)	0.35	182
TiO₂ with dye sensitization				
49	C-TiO ₂ hollow nanoshells with Eosin Y sensitization	Under visible light irradiation ($\lambda > 420$ nm).	0.468	74
50	Ru(dcbpy) ₃ /TiO ₂	50 mL of solution containing 20 mg of photocatalyst and EDTA (2 mmol L ⁻¹), Irradiated by a xenon lamp (150 W) with a UV cutoff filter ($\lambda > 400$ nm).	94 $\mu\text{mol/g}$ in 5h	17
51	carbazole based organic dye sensitized Nafion	20 mL aqueous suspension containing 10 mg of the photocatalyst and 10 vol% of TEOA as SED. The Xenon arc lamp (400 W) was used as a light source	67.9 $\mu\text{mol h}^{-1}$	155



	coated Pt/TiO ₂ system (D1 @NPT)		DOI: 10.1039/D4YA00249K	View Article Online
52	BE-Au(1wt%)-TiO ₂ (modified poly(benzothiadiazole) flake denoted as BE	30 mg catalyst was dispersed in 30 mL 10% vol TEOA aqueous solution, filters ($\lambda=420, 500$ nm etc.) are used	781.2 $\mu\text{mol/h-30mg}$	183
TiO₂-Ternary composite material				
53	Au-Pd/rGO/TiO ₂	25 mg of the catalyst was suspended in 40 mL of an aqueous methanol solution (25% v/v), (300 W xenon arc lamp) with AM 1.5 filter under 1 sun conditions (100 mW/cm ²)	21.50	43
54	Pt0.5-Au1/TiO ₂	(20 mg) of catalyst was added to a 30 ml of distilled water and 10 ml methanol, 300 W power AM1.5 (100mW/cm ²) or >400 nm (92 mW/cm ²) filter	1.275	76
55	0.5 wt.% Pt /0.1 wt.% Cu/TiO ₂	20 vol.% methanol-water, The photocatalyst powder (14 mg) was mixed with distilled water (1.2 mL), deposited on 0.85–0.42 mm quartz beads (3 g), xenon arc lamp, 300 W, 40.0 mW·cm ⁻² irradiation intensity	27.2	118
56	CuInS ₂ /TiO ₂ /MoS ₂ photocatalyst with 0.6 mmol·g ⁻¹ CuInS ₂ and 0.5 wt% MoS ₂	50 mg photocatalyst was suspended in 250 ml of an aqueous solution contains 0.1 M Na ₂ S and 0.1 M Na ₂ SO ₃ , 300 W Xenon lamp equipped with a UV cutoff filter ($\lambda > 420$ nm)	1.034	121
57	rGO/TiO ₂ /ZIS (2.0 wt% rGO and 50 wt% ZIS)	0.01 g of sample is added into 10 mL of aqueous solution containing 0.35M of Na ₂ S and 0.25M of Na ₂ SO ₃ , with a light source (300W Xe lamp)	0.4623	143
58	0.5 wt% Au/(TiO ₂ -g-C ₃ N ₄) (95/5)	1 L of Milli-Q water and triethanolamine (TEOA) (1 vol%), solar light	1.750	158
59	CuO(1%)-Co ₃ O ₄ (0.05%)/TiO ₂	20 mg photocatalyst was suspended in 100 mL of pure water or methanol aqueous solution (30 vol %), 300 W Xe lamp, light intensity of 600 mW cm ⁻²	0.273 with 20 mg	160
60	2 wt% Cu ₂ O/TiO ₂ /Bi ₂ O ₃	5% glycerol-water solution 0.05 g/L photocatalyst, natural solar light	6.727 with 50 mg	163
61	Pt(0.02%)Co ₃ O ₄ (0.05%)(D)/N-TiO ₂ (PCNT(D))	100 mg of photocatalyst dispersed in 100 mL of an aqueous solution containing methanol (V _{H₂O} : V _{MeOH} = 9: 1), 300 W Xe lamp and a UV light cutoff filter ($\lambda > 400$ nm) with a light intensity of 380 mWcm ⁻² .	197	184

4. Factors influencing solar hydrogen generation activity of TiO₂

The performance of a photocatalyst and its photocatalytic hydrogen evolution activity depends on the extent of photogeneration of electrons and holes, large extent of charge separation followed by charge transfer to the redox sites for redox reactions to occur.¹³⁴ The use of dopants and/or co-catalysts in suitable combination and composition and their synthesis strategy are crucial to obtain efficient photocatalysts; various material properties, such as, morphology, surface area, particle size, band gap etc helps for realizing the maximum performance for solar H₂ production.^{76,124} The critical factors that determine the photocatalytic performance in solar hydrogen evolution activity on TiO₂-based photocatalysts is summarized in **Figure 15**.





Figure 15. Schematic representation of the various factors which determine the photocatalytic hydrogen evolution activity of TiO₂-based photocatalysts.

4.1. Effect of preparation method

Synthesis method largely influence the physical and chemical properties of photocatalyst, which in turn have a huge impact on the rate of solar hydrogen evolution.^{67,135,185} Numerous new synthesis strategies have been developed in recent years for the fabrication of TiO₂-based photocatalysts, which include molten salt method¹⁷³ impregnation method^{67,142} sol-gel (SG) method¹⁴² chemical adsorption decomposition (CAD)¹⁴² composite precipitation (CP)¹⁴² ionic liquid assisted hydrothermal method (ILAHM)¹³⁵ chemical bathtub deposition process (CBD),⁹ electrospinning preparation etc. A schematic representation of some of the most common synthesis strategies of TiO₂-based photocatalytic system reported in the literature is shown in **Figure 16**.

Li et al. reported six distinctive preparation methods for fabricating CuO/TiO₂ photocatalysts and evaluated the relative performance of these differently prepared materials in the photocatalytic hydrogen evolution reaction.¹⁸⁵ As illustrated in **Figure 17**, among the six methods, CAD, CP, impregnation (EI, SWI, and SI) and SG, the CuO/TiO₂ prepared by CAD method showed the highest rate of hydrogen evolution (3155.7 μmol/g.h). The highest activity of CAD prepared material is due to the formation of TiO₂ in anatase/rutile mixed-phase. The advantages of anatase/rutile mixed-phase include the enhanced electron-hole separation and transfer of electrons from rutile to anatase phase, and formation of catalytic hot spots at the interface of anatase and rutile.

An activity comparison of TiO₂/CuO nanocomposites prepared by ILHAM, hydrothermal, sol-gel and ionic liquid co-precipitation methods for photocatalytic H₂ production; this study revealed that ILHAM produced TiO₂/CuO nanocomposite showed the highest hydrogen evolution activity (8.670 mmol/g in a time span of of 2.5 h) under a





Figure 16. Schematic representation of various synthesis strategies of TiO₂-based photocatalyst system reported in the literature.

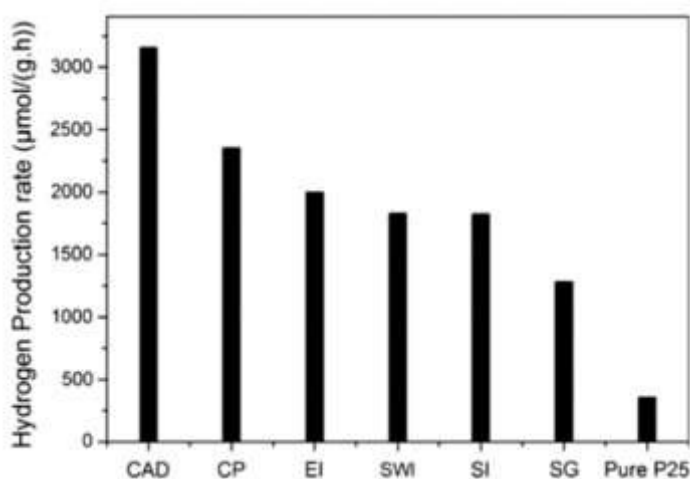


Figure 17. Comparison of the photocatalytic hydrogen evolution rate on pure P25 and CuO/TiO₂ samples produced by different preparation methods, namely chemical adsorption decomposition (CAD), composite precipitation (CP), ethanol impregnation (EI), simple wet impregnation (SWI), stepwise impregnation (SI), and sol-gel (SG). Reproduced with permission from ref.185. Copyright© 2014, Springer.

xenon/mercury lamp using aqueous methanol.¹³⁵ The higher activity of TiO₂/CuO nanocomposite obtained by ILAHM method is attributed to the versatility of the synthesis strategy to control the morphology and other physico-chemical characteristics of the catalyst by utilizing the unique properties of ionic liquids such as its thermal stability, low vapor pressure.¹³⁵

A comparison of the photocatalytic activity of mesostructured Ag@TiO₂ prepared by in situ electrospinning method and electrospinning in combination with photodeposition approach revealed that Ag@TiO₂ nanofiber prepared through the former method displayed the



highest H₂ yield at 531.9 μmol/g.h in one sun conditions with 25% aq. methanol.¹⁶⁵ The high activity of Ag@TiO₂ nanofiber fabricated by in situ electrospinning method is attributed to its relatively large BET surface area (39.8 m²g⁻¹) and smaller particle size (16.5 nm) than the one prepared by the other method.¹⁶⁵

Xiao et al. developed a new molten salt technique to synthesize atomically dispersed Ni species on TiO₂ as illustrated in **Figure 18** a for the application of photocatalytic water splitting to H₂ production, which exhibited a 4 times improvement (94.5 μmol/h for 50mg of the sample) than Ni/TiO₂ prepared by conventional impregnation method.¹⁷³ The experimental and theoretical studies (**Figure 18b-d**) revealed that the higher activity of Ni/TiO₂ produced by molten salt technique is due to the fact that it enabled the atomic distribution of Ni ions on TiO₂, which favoured the formation of strong Ni-O bond and large number of oxygen vacancies; this makes the material highly integrated and helps for efficient charge carrier utilization. Chemical bath deposition process is another versatile synthesis strategy employed in the literature for achieving uniform deposition of metal species on TiO₂ as reported by Chang et al. for the fabrication of Cu₂O on mesoporous TiO₂ beds (MTBs), which facilitate charge separation essential for improved hydrogen generation rate (223 mmolh⁻¹g⁻¹).⁹

The synthesis strategy that leading to the formation of TiO₂ with sufficient amount of Ti⁴⁺ ions in tetrahedral coordination enhances the photocatalytic H₂ production rate due to fact that the photocatalytic activity of a TiO₂-based catalyst depends upon the quantity of Ti⁴⁺ ions present in tetrahedral environment.¹⁸⁶ Kumari et al. reported an impregnation method for the fabrication of functionalized carbon nanotube (FCNTs) integrated with TiO₂ nanotubes (TiNTs), which showed high performance (7476 μmolh⁻¹g⁻¹) for photocatalytic hydrogen evolution reaction due to the strong interaction between FCNTs and TiNT and the well dispersed nature of the catalyst.⁶⁷

A careful control of the synthesis parameters and process variation are essential since even slight variation in the synthesis process may introduce a variety of defects and impurities that could improve or worsen the material's photocatalytic activity and stability. Anatase phase of TiO₂ generally exhibits higher activity than rutile, but the synthesis frequently results in mixed-phase materials, resulting property optimisation more challenging.

4.2. Effect of Surface area

Surface area can be a crucial factor that influences the photocatalytic performance of a catalyst. Since the photocatalytic hydrogen generation is a surface-based phenomenon, a catalyst with high specific surface area can offer more adsorption sites and photocatalytic reaction centers.⁴⁶ Khore et al performed a comparative study of the photocatalytic performance of pristine TiO₂ and Au@TiO₂ photocatalysts for hydrogen generation under natural sunlight and arrived a correlation between surface area and activity.¹⁶⁷ As illustrated in **Figure 19**, among all catalysts studied, 2wt% Au loaded TiO₂ with highest surface area (60 m²/g) showed the highest activity with a H₂ yield of 3.99 mmol/g.h and the activity decreases as the surface area decreases¹⁶⁷.



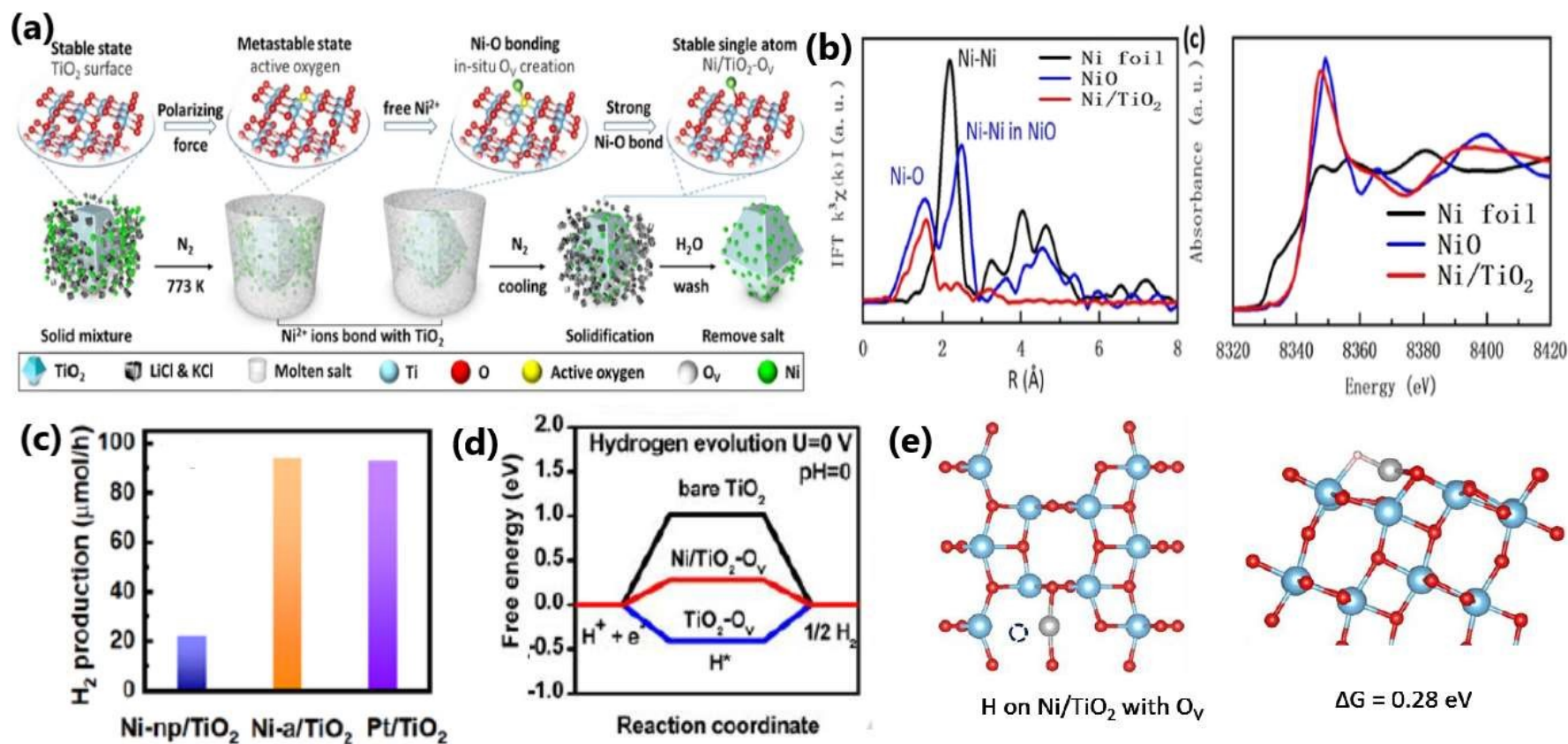


Figure 18. (a) Schematic illustration of molten salt mediated preparation of atomic Ni on TiO₂. For the TiO₂ molecular structure, (b) EXAFS and XANES spectra of Ni/TiO₂, respectively. Ni loading amount: 0.46 wt.%. (c) Comparison of H₂ evolution activity on Ni-np/TiO₂, Ni-a/TiO₂ and Pt/TiO₂ with the same loading amount (~0.5 wt.%). Experimental condition: 50 mg of the sample disperses in 100 ml of 10 vol.% methanol aqueous solution (278 K) under the irradiation of a 300 W Xe lamp (d) Free energy versus the reaction coordinates of different active sites. The simulation is based on the (101) facet of anatase TiO₂ (e) Molecular models of O_v on Ni/TiO₂ and the corresponding formation energy of O_v. Reproduced with permission from ref.173. Copyright© 2020, Wiley-VCH.

In yet another variation, among different TiO₂-NT (nanotube)-based photocatalysts (TiO₂-NT, TiO₂-NT/ZnO-NR (nano rod), TiO₂-NT/ZnO-NR/Ag-NP (Nanoparticle), TiO₂-NT(nanotube)/Pd-NDs(nanodendrites)) attempted for photocatalytic H₂ production under one sun conditions using H₂O/MeOH (1:2) mixture, TiO₂-NT(nanotube)/Pd-NDs catalyst having the highest surface area showed the highest hydrogen generation rate of 143.1 μmol/h.¹⁷⁴ Mishra et al. synthesized 15 wt% S modified TiO₂/β-SiC and showed that the high photocatalytic hydrogen evolution activity of the catalyst is due to its high specific surface area.⁴⁶

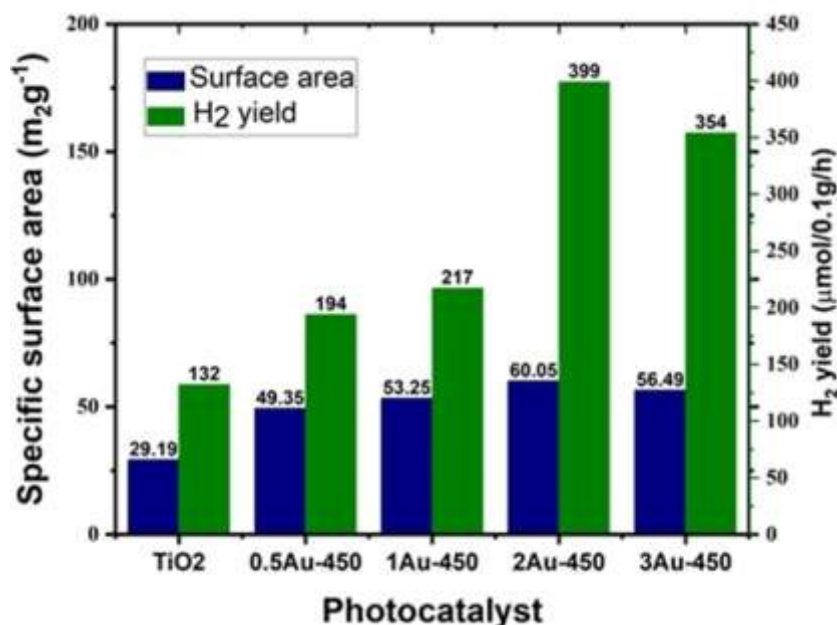


Figure 19. Amount of hydrogen production Vs surface area of photocatalysts for Au@TiO₂: 0.5Au-450, 1Au-450, 2Au-450 and 3A-450 under natural solar light. Adopted from ref.167. Copyright ©2018, Royal Society of Chemistry.

A 2D TiO₂/g-C₃N₄ photocatalyst with 20 wt% TiO₂ having high specific surface area showed 2.4 times higher photocatalytic hydrogen evolution rate than g-C₃N₄ nanosheet having a relatively low specific surface area. The high photocatalytic activity of 2D TiO₂/g-C₃N₄ is due to its high surface area and hence more active sites available for hydrogen production.¹⁸² Another way of utilizing the advantage of the high surface area in improving the photocatalytic H₂ production rate of titania is by modifying it in the form of silica embedded titania and/or titania silica mixed oxide.⁸⁷ Although the correlation between surface area and photocatalytic activity has been demonstrated in the literature, there are some reports which show surface area has hardly any influence on the photocatalytic activity and H₂ production rate in comparison with other favourable factors as illustrated in the case of CuO/TiO₂ heterojunction and pt@CuO/TiO₂ composites synthesized from TiO₂ nanosheet and nanorod precursors.¹⁸⁷ Further, high surface area is invariably associated with high porosity (with micro and mesopores), large number of surface defects and they could act as recombination centers. In view of such contradicting views, caution to be exercised while deriving a proper conclusion and proceeding further in photocatalysis.



4.3. Effect of calcination temperature

In majority of the cases, photocatalytic performance of a catalyst and the hydrogen production rate displayed by it may be influenced by the calcination temperature of the photocatalyst. Calcination temperature may affect the crystallinity,¹³² particle size,¹⁸⁸ phase characteristics,¹³² oxidation state of dopant,¹⁸³ porosity,¹⁰¹ surface area,⁴⁴ number of active sites,¹⁸⁹ and morphology,¹⁹⁰ of the photocatalyst. In general, a photocatalytically active catalyst material show relatively low activity at low calcination temperature due to poor crystallinity and an optimum calcination temperature is required to achieve the desired physico-chemical characteristics for the maximum photocatalytic performance.¹³² The TiO₂ photocatalyst crystallized in pure anatase phase undergo anatase-to-rutile phase transformation starts from a calcination temperature around 500 to 800°C. However, it is worth to note that the calcinations temperature can vary depending on the specific phase requirements of TiO₂.

In general, the photocatalytic activity of TiO₂ is mainly contributed by anatase phase due to the high surface area and small particle size; however, as the calcinations temperature increases the photocatalytically less active rutile phase increases.¹⁹¹ Thus, TiO₂-based photocatalytic material show maximum hydrogen generation at a calcination temperature of 300-500°C.¹⁹¹ Besides that as the calcination temperature increases the probability of charge carrier recombination at the bulk traps also increases.⁵⁴ The contribution of anatase phase in enhancing the photocatalytic H₂ evolution reaction rate is exemplified in the literature.¹⁹² Among the different N doped TiO₂ samples prepared at different calcination temperature ranges from 300 to 800°C, NTP-400 (N-doped TiO₂ calcined at 400 °C) showed the highest rate of photocatalytic hydrogen production due to the formation of highly crystallized anatase phase, and incorporation of N in the crystal lattice.¹⁹⁰

Sun et al. reported that calcination temperature affect the photocatalytic hydrogen evolution activity of TiO₂-based photocatalyst because the anatase-to-rutile ratio in TiO₂ varies with calcination temperature.¹⁹² Camposeco et al. prepared 0.5Rh/TSG (TiO₂) by sol-gel method and studied the photocatalytic performance of this material as a function of calcination temperature (100, 200, 300, 400 and 500°C) for water splitting reaction using 50%(v/v) ethanol-water mixture under UV pen ray Hg lamp ($\lambda = 365\text{nm}$). As illustrated in **Figure 20a**, 0.5Rh/TSG prepared at 400°C (anatase) showed the highest H₂ production rate of 7246 $\mu\text{mol h}^{-1}\text{g}^{-1}$.⁵²

A comparison of the photocatalytic H₂ evolution activity of Ru (wt%=8.0)/TiO₂NBs (nanobelts) non annealed sample and the same catalyst calcined at different calcination temperatures (200, 400, 600, and 800°C) as illustrated in **Figure 20b** revealed that Ru 8.0/TiO₂ NBs calcined at 400°C showed the highest photocatalytic hydrogen production rate of 25.34 $\text{mmol h}^{-1}\text{g}^{-1}$.⁴⁸ The improved activity of Ru 8.0/TiO₂ NBs@400°C is due to the improved crystallinity with the formation of the crystalline phase Ru/RuO₂ crystal phase and an intimate junction formation between Ru/RuO₂ and TiO₂. With further increase of calcination temperature, an increased amount of RuO₂ is formed due to oxidation of Ru, which is a detrimental effect on the rate of hydrogen evolution.⁴⁸



Majority of the researchers tried to maintain more anatase phase content in TiO_2 . The rutile phase, while stable, has poorer photocatalytic activity compared to anatase because of its bigger bandgap and smaller surface area. If this phase transition is not properly managed, photocatalytic efficiency may significantly decline. Furthermore, high calcination temperatures can lead to particle growth and agglomeration, which reduces the surface area and active sites for photocatalytic reactions. On the other hand, inadequate calcination may result in the presence of leftover organic matters or partially broken-down precursors, which can serve as sites of recombination for charge carriers produced during the photocatalytic process and hinder the activity.

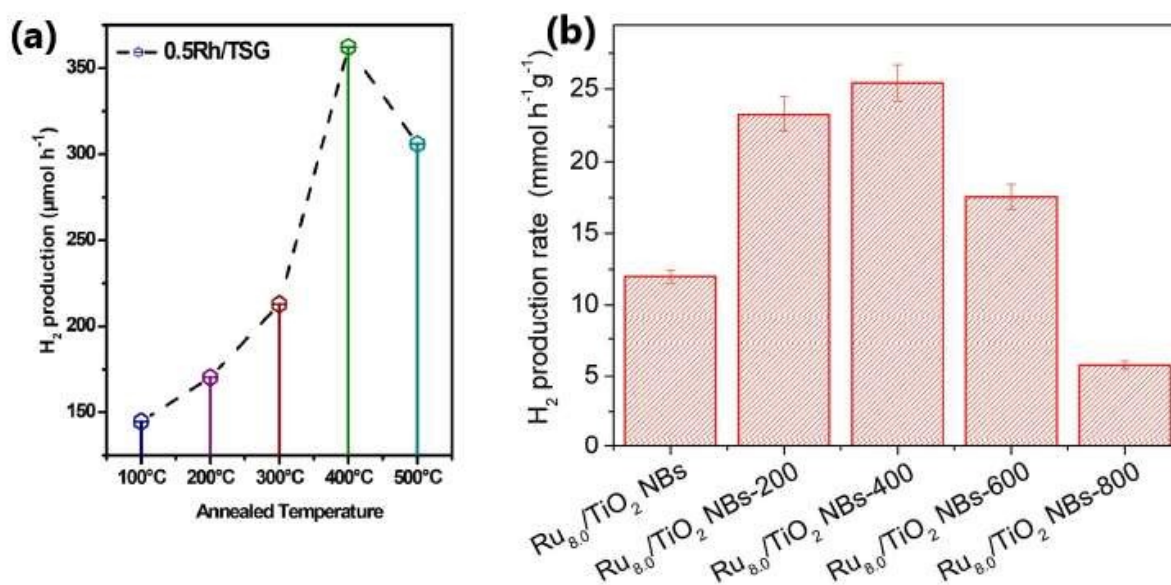


Figure 20. (a) The variation of rate of hydrogen production on 0.5Rh/TSG(TiO_2) as a function of calcination temperature (Reproduced with permission from ref.52. Copyright ©2018 Elsevier Ltd. (b) The variation of rate of hydrogen production as a function of calcination temperature for the photocatalyst Ru (wt%=8.0)/ TiO_2 NBs (Reproduced with permission from ref.48. Copyright ©2016, Wiley-VCH).

4.4. Effect of Morphology

Morphology of TiO_2 has a considerable role in deciding the photocatalytic hydrogen evolution activity by affecting the interaction between the dopant and TiO_2 ,¹⁸⁷ migration of photogenerated electrons,¹⁸⁰ and effectiveness of heterojunction.^{180,187} TiO_2 -based photocatalysts in specific morphologies, such as, nanosheet,¹⁸⁷ nanorod,¹⁸⁷ nanotetrahedrons,¹⁶⁸ etc. have been studied for understanding the influence of morphology in photocatalytic H_2 production. TiO_2 nanosheet with single-crystal structure and low density of defects was found highly effective in reducing the charge recombination and thereby enhancing the rate of hydrogen evolution.¹⁸⁷

Wang et al. fabricated a 2D/1D heterojunction of TiO_2/CdS composite with (001) facets of TiO_2 and CdS nano rod and it showed a photocatalytic hydrogen evolution rate of 128.3



mmol $g^{-1}h^{-1}$ with acetic acid-water mixture (20 ml acetic acid in 210 ml water) in visible light (300W Xe arc lamp; $\lambda > 400nm$); this is much higher than the conventionally prepared P25/CdS (35.3mmol $g^{-1}h^{-1}$).¹⁸⁰ The outstanding photocatalytic performance of 2D/1D TiO₂/CdS is attributed to the morphological features of TiO₂ and the formation of an optimized 2D/1D heterojunction leading to efficient charge separation and enhanced electron transport. The morphology of the cocatalyst also plays a vital role in enhancing the photocatalytic H₂ production rate. Thus, among TiO₂-Pd NSs (nanosheets) and TiO₂-Pd NTs (nanotetrahedrons), the photocatalytic hydrogen production rate is higher on TiO₂ integrated with ultrathin nanosheets of Pd due to the fast rate of hot electron generation and their transfer from Pd nanosheet.¹⁶⁸ Comparison of morphological features, optical properties and photocatalytic activities of TiO₂-Pd nanosheet and TiO₂-Pd nanotetrahedrons were shown in **Figure 21**.

The photocatalytic H₂ production activity of Pt@CuO/TiO₂ composite fabricated from TiO₂ nanosheet is higher than that of Pt@CuO/TiO₂ prepared from TiO₂ nanorod.¹⁸⁷ The relatively high activity of nanosheet-based photocatalyst is due to a variety of reasons including: (1) TiO₂ nanosheets are mainly exposed by relatively high surface energy (001) facets, whereas TiO₂ nanorods are dominated by comparatively less surface energy (101) facets, (2) CuO has strong interaction with TiO₂ nanosheet than with TiO₂ nanorod, (3) CuO can form a more stable p-n heterojunction with TiO₂ nanosheet, and (4) TiO₂ nanosheet has a low density of defects which reduce the charge recombination possibility. Compared to conventional Pd/P25 TiO₂, Pd/TiO₂ nanosheet showed relatively high photocatalytic H₂ production activity due to more exposed high surface energy (001) facets on nanosheets.¹⁷¹ Whereas for nanorod morphology, the aspect ratio is crucial for enhancing the photocatalytic water splitting as reported by Fuet et al. for the case of nanorods of rutile TiO₂.¹⁹³ The different works discussed above show that due to the larger surface area and more active sites, nanostructured TiO₂ materials such as nanotubes, nanorods, and nanospheres generally show improved photocatalytic activity when compared to bulk materials. Nevertheless, the production of these nanostructures frequently necessitates precise control of the synthesis parameters and more sophisticated and expensive techniques.

4.5. Crystallographic facet dependent activity

Certain exposed facets of TiO₂ can enhance the solar hydrogen generation to a large extent because of the effective electron-hole separation by way of enhancing the interfacial charge transfer, more exposed surface area, and high surface energy.^{137,171} The choice of TiO₂ with unique tailored facets ($\{001\}$ or $\{101\}$) in the composite has a significant influence on the performance of photocatalytic hydrogen evolution.^{137,171,193,194} Liu et al. studied the influence of (100), (001), and (101) crystal facets of TiO₂ on the photocatalytic hydrogen generation activity of TiO₂-graphene composite and observed that TiO₂-100-graphene composite exhibited the highest rate of hydrogen evolution.¹⁵³ The enhanced activity of Ti-100-G composite is due to the formation of Ti-C bonds, which increases the rate of charge



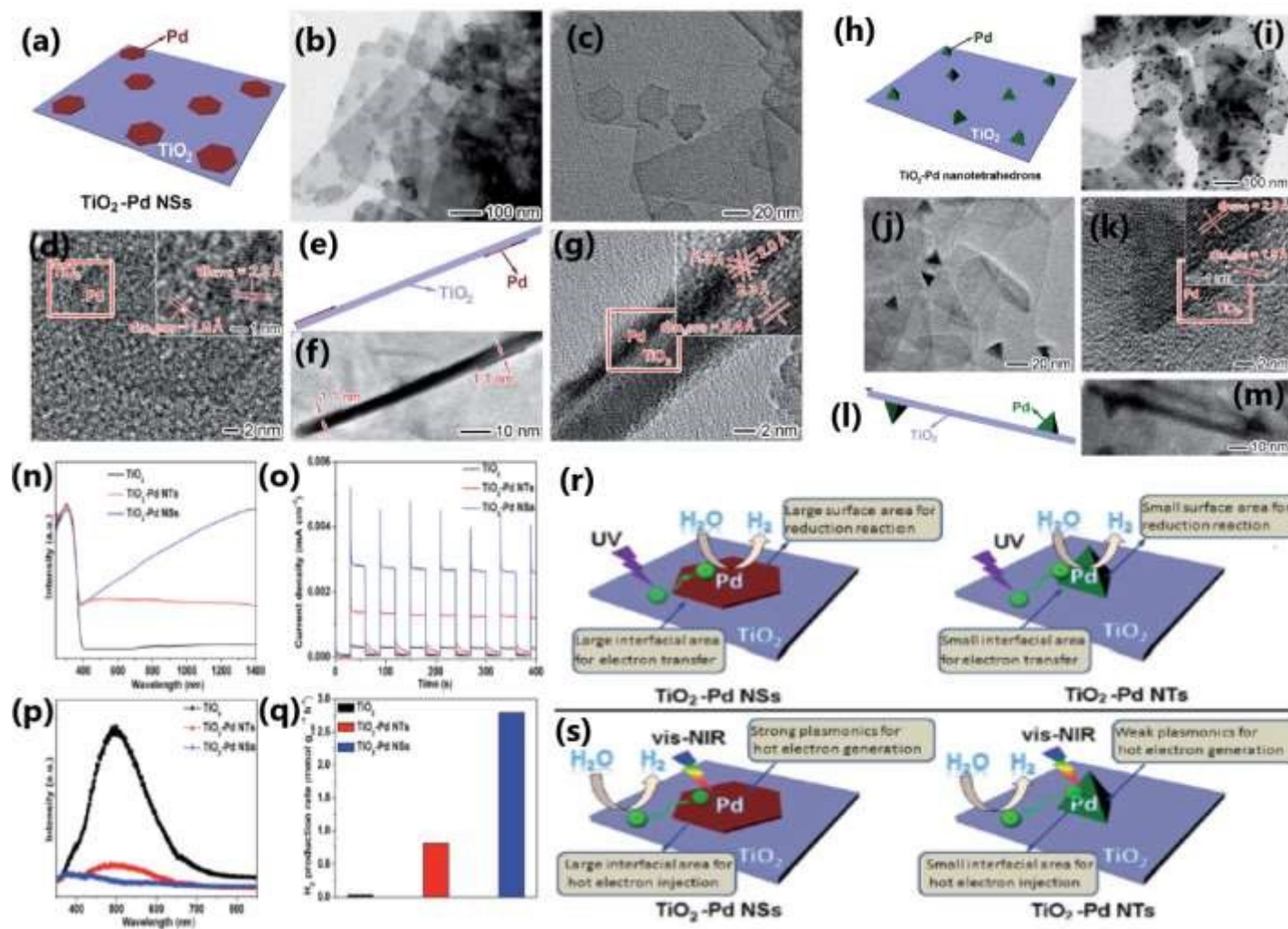


Figure 21. (a) Schematic illustration, TEM (b and c), and HRTEM (d) images of TiO₂-Pd NSs; (e) schematic diagram, TEM (f), and HRTEM (g) images of TiO₂-Pd NSs with TiO₂ nanosheet. (h) Schematic illustration, TEM (i and j), and HRTEM (k) images of TiO₂-Pd NTs; (l) schematic illustration and TEM (m) image of TiO₂-Pd NTs with TiO₂ nanosheet. UV-vis diffuse reflectance spectra (n), photocurrent response (o), PL spectra (p) and photocatalytic H₂ production performance (q) of bare TiO₂, TiO₂-Pd NTs and TiO₂-Pd NSs; Schematic illustrating the photocatalytic H₂ evolution reaction on the samples of TiO₂-Pd NSs and TiO₂-Pd NTs (r) under UV and (s) vis-NIR light irradiation, respectively. Reproduced with permission from ref.168. Copyright ©2016, Royal Society of Chemistry.



transfer and thereby improved hydrogen production activity. Whereas Ti-O-C bonds are formed in Ti-001-G and Ti-101-G composites, leading to a reduced charge transfer rate and lower hydrogen evolution activity. Due to very poor interfacial connections and unfavourable electronic structure, the Ti-001-G composite showed the lowest rate of hydrogen evolution.¹⁵³ The preparation of TiO₂-graphene nanocomposites, their physicochemical characteristics and a schematic illustration of the atomic structures of interfaces between graphene and different TiO₂ crystal facets and the photocatalytic process by them, and the photocatalytic H₂ production activities are provided in **Figure 22**.

Exposed facets of certain dopants can also influence the rate of hydrogen generation due to the formation of appropriate energy levels and reduced rate of electron-hole recombination by trapping the photogenerated electrons. For example, Pt/TiO₂ photocatalyst having (111) facets of Pt with higher Fermi level is highly effective for trapping the electron in the conduction band of TiO₂ than the (100) facets of Pt.¹⁸⁹ In yet another study, Qi et al. reported that CdS sensitized Pt/TiO₂ nano sheet photocatalyst with (001) exposed facets showed outstanding water splitting activity due to the special electronic and surface properties of (001) facets.¹⁹⁵ Compared to {101}-TiO₂/CdSe QDs, the relatively high photocatalytic production rate shown by {001}-TiO₂/CdSe QDs are due to an enhanced charge separation and efficient electron transfer from CdSe QDs to (001) facets of TiO₂.¹³⁷ Due to differences in surface energy, reactive site density, and charge carrier dynamics, different facets of TiO₂ exhibit different photocatalytic activities. Hence facet-controlled synthesis methods are required to maximise the photocatalytic performance. For example, nanocube and octahedron morphologies expose only (100) or (111) facets, respectively; while truncated octahedron exposes both (100) and (111) facets. By fine tuning such methods, it is possible to improve the performance of photocatalysts and well-defined synthetic methodologies are required.

4.6. Particle size

Particle size could significantly affect the performance of the photocatalyst by affecting the number of active sites, charge transfer and electron-hole recombination rates, and light penetration.^{137,138} Photocatalysts with smaller particle size provide a large number of active sites and accelerate the electron transfer process.¹¹⁸ Contrarily, the large sized catalyst particles not only reduce the number of active interfaces but also block the penetration of incident light.¹¹⁹ Particle size of metal dopants influence the energy separation between the Fermi level of metal and the conduction band of TiO₂, which directly affect the carrier separation ability of the photocatalyst.¹⁹⁶ In the case of SPR metals like Ag and Au, the wavelength of absorption varies with particle size and morphology.^{39,197} Dopants with small-sized particles facilitate high dispersion of particles on crystalline TiO₂. However, the metallic particles with very small size show poor stability due to high surface energy and easy detachment of particles from the TiO₂ surface when stirred intensely.¹⁹⁸ This suggests the material integration is of great significance for any sustainable operation for long period of reaction time.¹⁹⁹ Yang et al. reported that for a given amount of gold loading, Au@TNT with



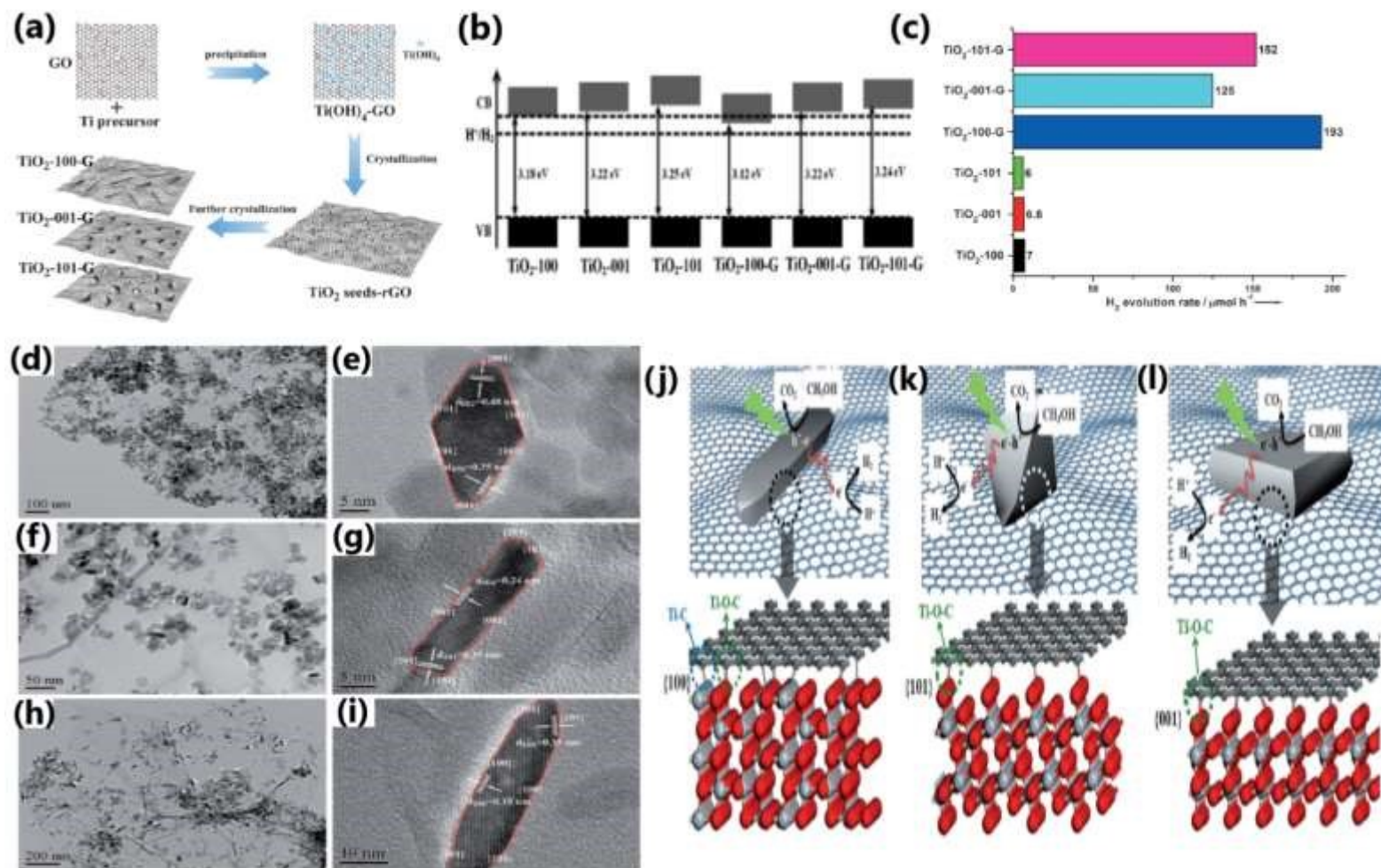


Figure 22. (a) Schematic illustration of the preparation of TiO₂-graphene nanocomposites with controllable TiO₂ crystal facets exposed. (b) Band structures of TiO₂ and TiO₂-graphene nanocomposites. (c) H₂ evolution rates from methanol solution catalyzed by TiO₂ and TiO₂-graphene nanocomposites. (d-i) TEM and HRTEM images: (d,e) TiO₂-101-G, (f,g) TiO₂-001-G, and (h,i) TiO₂-100-G. Schematic illustration of atomic structures of interfaces between graphene and different TiO₂ crystal facets and the photocatalytic process by TiO₂-Graphene nanocomposites: (j) TiO₂-100-G, (k) TiO₂-101-G, and (l) TiO₂-001-G. Reproduced with permission from ref. 153. Copyright ©2014, Wiley-VCH.



reduced particle size showed improved photocatalytic performance and is attributed to the high dispersion of Au particles on the surface of TiO₂ and its modified electronic properties.¹⁶⁹ Metal nanoparticles with small particle size produce an increased amount of highly energetic surface sites, which makes the catalyst highly effective for photo-injection and enhances the electron transfer process. The modified electronic state ought to have a positive effect by improving the charge transfer and electron-hole separation efficiency.¹⁶⁹ The superior photocatalytic H₂ production activity due to highly dispersed Cu⁰ nanoparticles in Cu-TiO₂ MS (Mesoporous microporous) photocatalyst,¹⁹⁸ small-sized Au nanoparticles in Au loaded mesoporous S, N-TiO₂(SNT),²⁰⁰ Pd and Pt nanoparticles in TiO₂,¹⁹⁶ substantiate the importance of controlling the metal particle size to achieve the desired properties and enhancing the photocatalytic efficiency.

Metal nanoparticles such as Au and Pt in the size range of 1-10 nm supported on TiO₂ leads to an increase of energy gap between the Fermi level of metal nano particle and the conduction band of TiO₂ resulting in an improved charge separation and enhanced hydrogen production activity.¹⁹⁶ Gold nanoparticle synthesized via a seeded growth method for sensitization of Pt/TiO₂ catalysts (**Figure 23a**) and it was evident from TEM images (**Figure 23b-e**) that narrow sized Au particles can be obtained through this method. Among the Au sensitized Pt/TiO₂ photocatalysts with different particle size of Au (10, 20, 30, and 50 nm) for photocatalytic hydrogen production, Au nanoparticle with a particle size of 20 nm showed the highest performance under visible light (**Figure 23g and h**).²⁰¹ The size of Au nanoparticles is clearly evident from TEM images as illustrated in **Figure 23** and the result show that the SPR effect and the electron injection into the CB of TiO₂ depends on the particle size of Au (**Figure 23h**).²⁰¹ Generally, smaller particles possess a large surface area and a greater number of reaction sites for unit weight of catalyst. Nonetheless, smaller particles can sometimes lead to a decline in photocatalytic activity in due course of time due to particle aggregation. If the size of the particles is smaller than twice the width of the space charge layer, the extent of band bending decreases, which eventually diminishes the potential to separate e⁻/h⁺ pairs. Alternatively, visible light absorbing small quantum dots could be grown inside the pores of a wide bandgap semiconductor; this approach is likely to bring higher activity, due to inherent and inevitable formation of heterojunctions.

4.7. Porosity

The porosity of a photocatalyst has significant influence on the photocatalytic hydrogen production rate by increasing the surface area, providing large number of exposed surface sites and enhances the absorption of a large number of reactant species, enhancing the light absorption performance and by increasing the mass transfer rate.^{15,88,202} A macroporous channel in a photocatalyst can increase the mass transfer within the macro-mesoporous framework and enhances the light absorption performance.¹⁵ The presence of meso-macroporous network in a TiO₂ photocatalyst improve the light-harvesting ability of it by



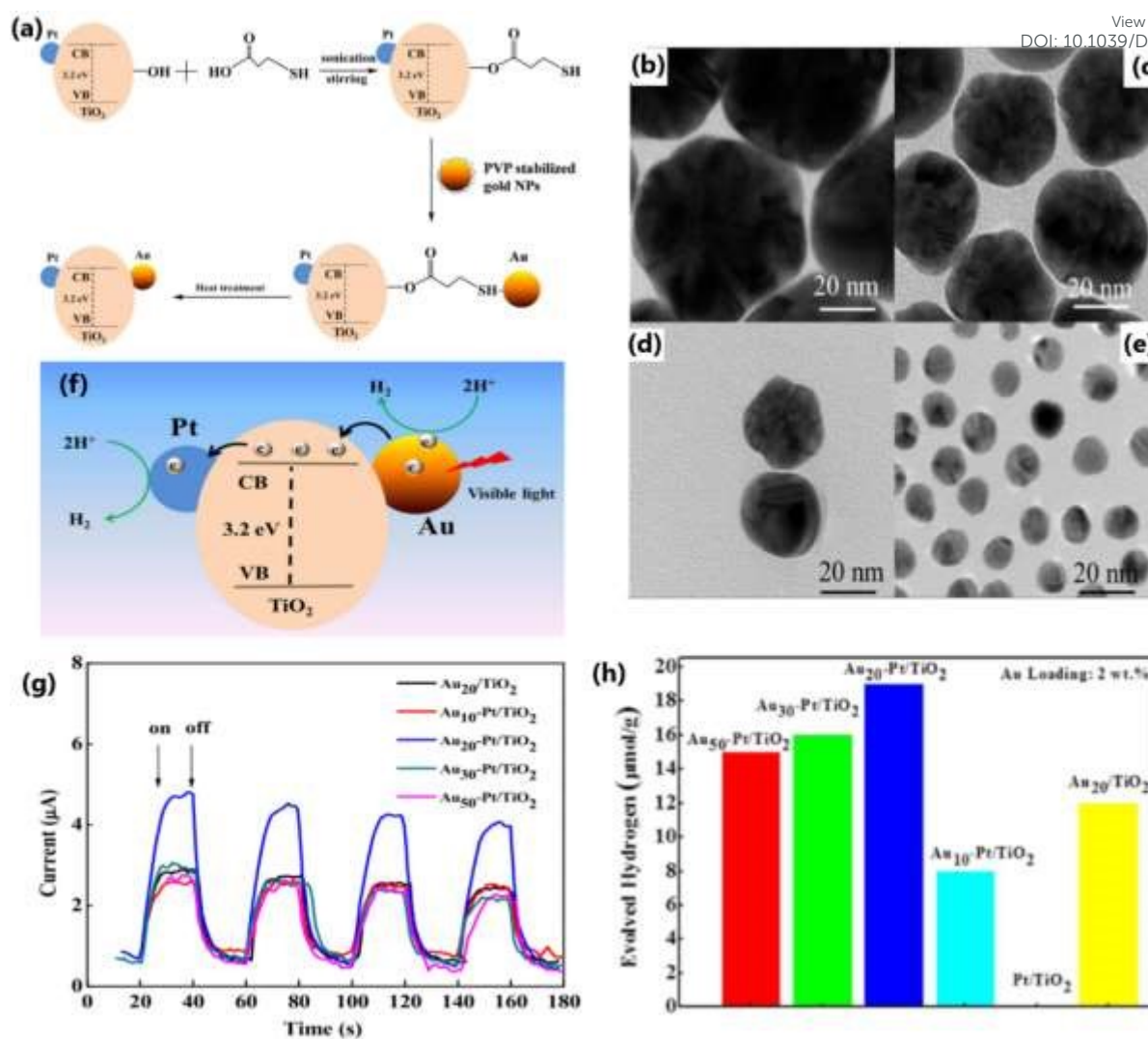


Figure 23. (a) Schematic diagram of synthesis of Au nanoparticles supported on Pt/TiO₂ composite catalysts. TEM images of the synthesized gold nanoparticles with size of approximately 50 nm (b), 30 nm (c), 20 nm (d), and 10 nm (e); TEM images of Pt/TiO₂. (f) The plausible photocatalytic mechanism of the Au sensitized Pt/TiO₂ under visible light. (g) Photocurrent response of Au nanoparticles with different sizes supported on Pt/TiO₂ nanocomposites under visible-light irradiation ($\lambda > 420$ nm). (h) Hydrogen-production activity of different catalysts under visible-light irradiation ($\lambda > 420$ nm) from water/methanol mixture. Reproduced with permission from ref.201. Copyright ©2017, American chemical Society.

transferring the incident photon flux into the internal surface of mesoporous TiO₂ through multiple internal reflections.¹⁵⁶ This type of macro-mesoporous architecture additionally supports easy channelization of photogenerated electrons via the mesoporous walls and facilitate the electron transportation to the surface of TiO₂ via the microporous channel and as a result the electron-hole recombination is suppressed and the photocatalytic activity is enhanced.¹⁸³ The 3D ordered macroporous Pt/TiO₂-ZrO₂ composite synthesized by using a combination of vacuum impregnation and photoreduction method, for example, exhibited high photocatalytic water splitting activity to H₂ due to the enhanced light absorption effected through multiple internal reflections in the pores of it.¹⁵⁶



A comparison of the H₂ evolution activity between Pt deposited mesoporous TiO₂ nonporous Pt/TiO₂-P25 revealed that mesoporous Pt/TiO₂-450 showed better activity than non porous Pt/TiO₂-P25 because the mesoporous network facilitates efficient charge transfer

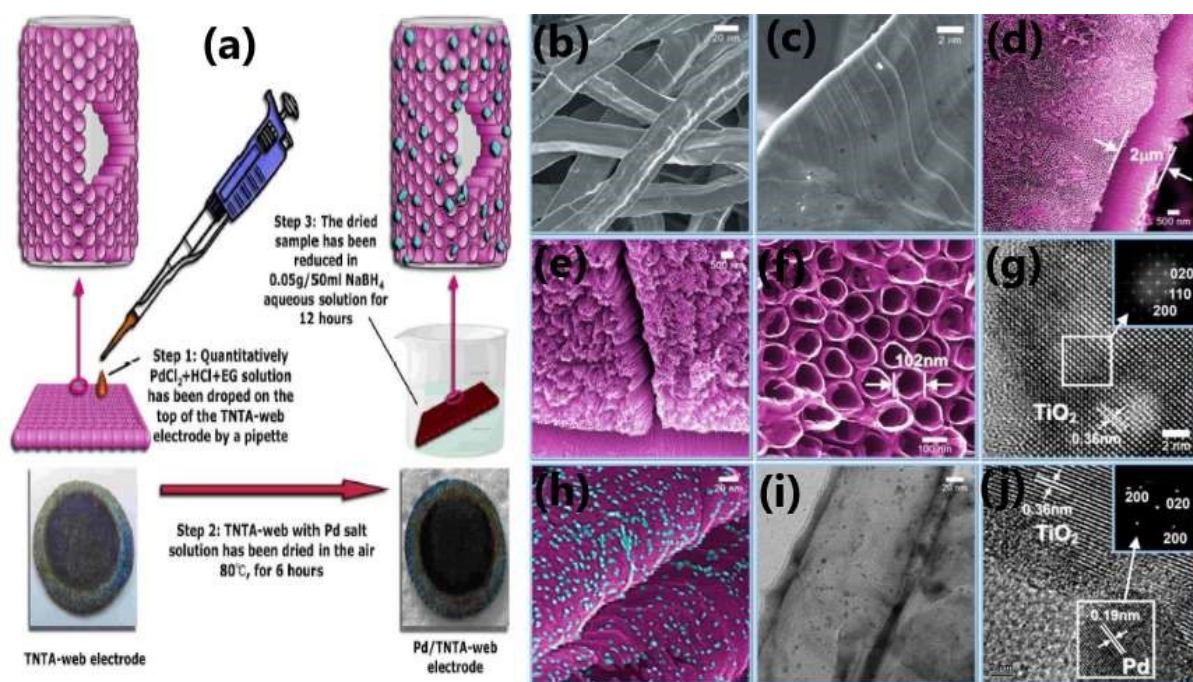


Figure 24. (a) Synthesis of Pd/TNTA-web (3D TiO₂ nanotube array). Scanning Electron Microscopy (SEM) of the pristine titanium-web substrate (b,c) and of the TiO₂ nanotubes arrays on the web (d,e, and f); HR-TEM of a nanotube (g) SEM image (h), TEM (i) and HRTEM (j) of the TNTA-web with 0.1mg cm⁻² Pd (0.26 wt.%). Reproduced with permission from ref.95. Copyright ©2018, Royal society of Chemistry.

by forming suitable interfaces and the reactants can easily diffuse through the pores.²⁰³ Li et al. reported that the CuO/TiO₂ photocatalyst prepared by chemical adsorption decomposition method (CAD) consists of a large number of small pores, which facilitates the absorption of a large number of reacting molecules on its surface due to the presence of more active sites and promote the hydrogen generation activity.¹⁸⁵ One of the reasons for the enhanced H₂ production rate displayed by Au deposited mesoporous S,N-TiO₂ (SNT) photocatalyst with pore diameter between 8 and 13 nm is due to its mesoporous nature, which enhances the light harvesting ability of the material.²⁰⁰ Further, using green leaf and highly porous architecture was proved to help for photocatalysis as well as light harvesting applications.^{204,205} For example, Devaraji et al. has demonstrated by using the green leaf as template to produce inorganic leaf to produce ZnO with nano-micro architecture and demonstrated the same for efficient oxidation of benzene to phenol in UV light. In another work, Chen and coworkers demonstrated the importance of porous architecture for enhanced photocatalytic H₂ production by fabricating TiO₂ nanotube arrays (TNTAs) grown on titanium fiber of a titanium web (TNTA-web) and titanium foil (TNTA-foil).⁹⁵ The TNTA-web generated 40 mmolh⁻¹m⁻² of hydrogen, while the TNTA-foil failed to produce hydrogen under similar conditions. Further, the addition of the same amount of Pd nanoparticles to the TNTA-web and TNTA-foil witnessed an increase in the production rate of 130 and 10 mmol/h.m², respectively. The enhanced photocatalytic H₂



production activity of TNTA-web material was attributed to its unique dual porosity. The synthesis procedure and morphological analysis of TNTA-web is depicted in **Figure 24**. Photocatalyst having dual porosity, such as hierarchical porous structured materials containing a combination of macroporosity and mesoporosity, is believed to be more advantageous than single porosity. However, more research in this direction is needed for proper control of porosity, which can be achieved by careful variation of the synthesis parameters and/or adopting novel synthesis strategies. Establishing a structure-activity relation is an interesting aspect in photocatalytic research, which deserves more attention.

4.8. Amount of catalyst

The rate of photocatalytic hydrogen evolution also relies on the quantity of catalyst to a large extent. In general, the catalyst shows maximum photocatalytic performance at an optimal amount of photocatalyst and with increasing amount of catalyst the photocatalytic H₂ evolution, generally, decreased and/or level off, which could be explained by the following reasons¹⁸³: (1) at higher concentrations of photocatalyst, there is a reduction in the light penetration depths into the suspension of catalyst; further, light scattering occurs more in suspension, rather than light absorption. (2) excess amount of catalyst may increase the electron-hole recombination rate, (3) the aggregation of catalyst particles is generally high in slurry form with uneven distribution of particles, resulting in vast differences in contact and reaction rate and hence the diffusion of reactants and photogenerated charges towards the reaction sites is less effective in the suspension form; and (4) the active site of the catalyst can be covered up by the presence of a large quantity of catalyst.⁴⁴

The photocatalytic performance of Ag/TiO₂ in water splitting reaction for different catalyst amounts revealed that the H₂ production rate increases initially with the catalyst concentration increases from 15 to 20 mg L⁻¹; with further increase in catalyst concentration, the activity declines (see **Figure 25a**).¹¹³ The catalyst in excess amount may hinder the absorption of radiation and in certain cases, it accelerates the electron-hole recombination possibility.¹¹³ The amount of catalyst needed for achieving optimum activity may vary as the nature of catalyst, catalyst composition and reaction conditions varies. For example, as illustrated in **Figure 25b**, the H₂ production rate on Ni/ γ -Al₂O₃/CNT-TiO₂ was maximum with 10 mg catalyst and the activity decreases with further increase of catalyst amount.¹⁰³ The excess amount of catalyst adversely affects the light penetration, which decreases the overall catalytic performance.¹⁰³ In fact, an earlier review,⁴³ lists out the very high activity associated with small amount of catalyst (1-3 mg in ~50-100 ml solution); same catalysts in larger quantity (10-200 mg in ~50-200 ml solution) shows a large drop in hydrogen production activity. The large difference in activity is attributed to the large light scattering with larger amount of catalyst quantity, and efficient light absorption with small quantity of the catalyst in large volumes of solution. Based on the available literature and above discussion, it can be concluded that careful optimisation of the amount of photocatalyst is necessary to extract the best catalytic performance from a photocatalytic material. Nonetheless, how the same can be scaled-up for large volume applications also needed to be addressed. Although it is an engineering issue, such thinking is likely to bring clarity and minimize the problems later on.



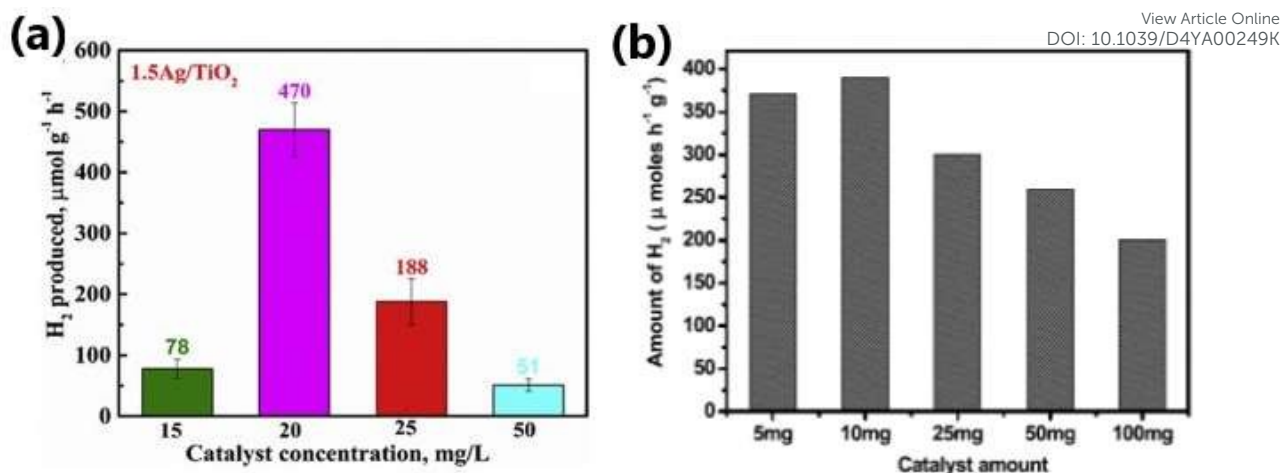


Figure 25. (a) Photocatalytic hydrogen evolution activity of Ag/TiO₂ by varying the amount of catalyst. Reproduced with permission from Ref.113. Copyright ©2019, Elsevier Ltd.(b)Variation of photocatalytic H₂ evolution rate with respect to the amount of Ni/γ-Al₂O₃/CNT-TiO₂ catalyst. Reproduced with permission from Ref.103. Copyright © 2017 Elsevier Ltd.

4.9 Amount of dopant

The photocatalytic activity of TiO₂ can be drastically improved by using various dopants. However, the amount of dopant is a critical factor in photocatalysis. It has been observed that the TiO₂-based composite for a given dopant shows maximum performance at an optimum concentration of it in the TiO₂ matrix and with further increase of dopant concentration the photocatalytic activity decreases.⁸⁵ High concentration of dopant in TiO₂ act as the recombination center for electron and hole,⁸⁵ and block the surface active sites. This reduces the light utilization ability of the catalyst and reaction rate and thereby the photocatalytic hydrogen production rate is decreased.¹³⁵ The increased loading of dopants may also cause agglomeration of particles and particle growth rather than uniform distribution of it.¹⁰⁵ However, an optimum amount of dopant can effectively separate the electron and hole, enhances the charge transfer through the interface between TiO₂ and the dopant and efficient utilization of it during the photocatalytic reaction. There are several reports available in the literature which illustrate the effect of dopant concentration on the photocatalytic H₂ production activity.

As illustrated in **Figure 26a**, the photocatalytic H₂ evolution activity of Cu decorated TiO₂ containing different wt% of Cu (1, 2, 3, 4, and 5wt%) revealed that the amount of hydrogen produced increases up to 3wt% of Cu (3.33 mmol g⁻¹ h⁻¹) and with further increase of Cu concentration the activity is reduced.¹⁰⁵ This study reveals that 3 wt% Cu is the optimum concentration to achieve maximum activity and at higher concentration of Cu (above 3 wt%) aggregation of Cu particles occurs on the surface of TiO₂ and these agglomerated Cu nanoparticles act as recombination centers for photogenerated electrons and holes. This



underlines that a suitable mass ratio of components is crucial to generate an efficient interface for excellent photocatalytic hydrogen evolution.

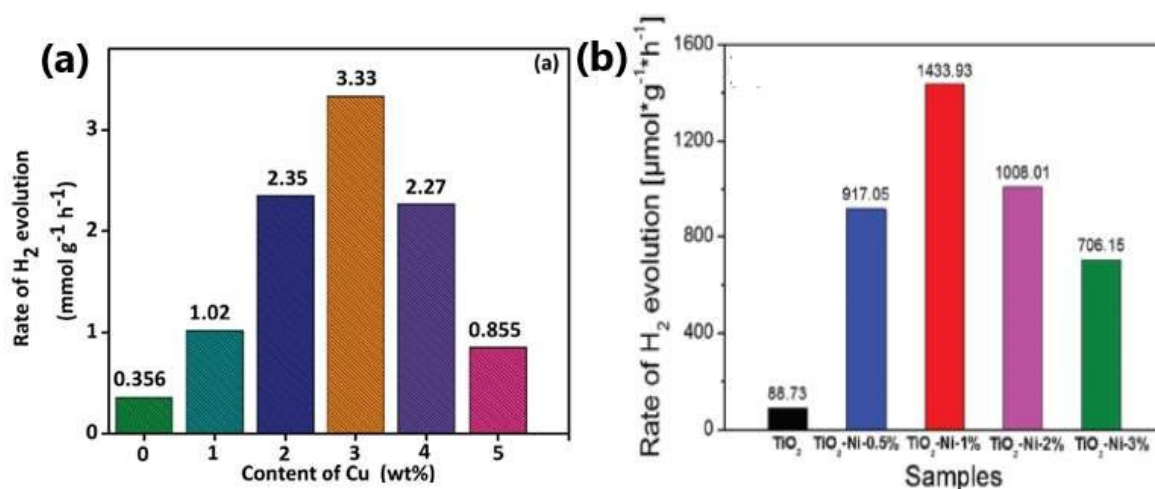


Figure 26. (a) Variation in the H₂ evolution activity of TiO₂ decorated with different wt% of Cu. Reproduced with permission from ref.105. Copyright ©2017, Royal Society of Chemistry. (b) The rate of hydrogen evolution of TiO₂ and TiNi samples with different loading amount of Ni. Reproduced with permission from ref.16. Copyright © 2018, Royal Society of Chemistry.

In yet another variation, the photocatalytic hydrogen production activity of Cu₂O-TiO₂/rGO revealed that TiO₂ with an optimum Cu loading of 1wt% and GO loading of 3wt% showed maximum performance because of the enhanced charge transfer and excellent light absorption capacity of the material. The highest photocatalytic H₂ production activity was observed with 3wt% Au loaded mesoporous S,N-TiO₂ when Au deposited mesoporous S,N-TiO₂ with different wt% of Au (0.5, 1, 2, 3, 4 and 5) were compared for the reaction.²⁰⁰ In this case, high gold content cause the blockage of active sites and obstruct the penetration of light to the catalyst surface. The high concentration of metal on the surface of TiO₂ may also act as electron-hole recombination centres, which reduces the rate of photocatalytic hydrogen production.⁸⁵ When a combination of metal nanoparticles are employed for the fabrication of TiO₂-based composites, the uniform distribution of all the metal nanoparticles in TiO₂ are crucial to achieve maximum photocatalytic performance.⁸⁵

Reddy et al. reported that the bimetallic Cu/Ag@TNT-2 (CAT-2) photocatalyst with an optimum amount of Ag and Cu prepared by using a mixture of 0.1 M Cu and 0.1 M Ag precursor showed the highest rate of photocatalytic hydrogen generation due to the uniform dispersion of Ag and Cu on TiO₂.¹⁰⁰ Less number of active sites are present at low concentration of Cu and Ag on the surface of TiO₂, whereas high concentration of metal nanoparticles leads to poor electron transfer.¹⁰⁰ Wei et al. reported that the TiO₂-Ni hybrid photocatalyst with an optimum Ni amount of 1 mol% showed the highest rate of hydrogen evolution during the photocatalytic water splitting reaction.¹⁶ Excess Ni loading limit the ability of light absorption and block the active sites of the catalyst, leading to decrease of activity (see **Figure 26b**).



The photocatalytic hydrogen evolution activity of Pd integrated TiO₂ nanosheets revealed that the photocatalyst showed the highest activity with an optimum amount of 0.1 mg/cm² Pd loading.⁹⁵ The H₂ evolution activity decreases when the amount of Pd is higher than the optimum value of loading due to the increase of Pd particle size and incorporation of Pd atoms in the bulk part rather than on the TiO₂ surface. Moreover, integration of large amount of Pd in TiO₂ limits the expansion of Pd-TiO₂ interface and reduces the number of charge carriers. Implantation of low amount of non metal dopants such as N into anatase TiO₂ nanotube creates defect centers while maintaining the anatase phase and strongly promotes the photocatalytic H₂ evolution performance of TiO₂ nanotube layers whereas high-dose N implantation leads to amorphization of the implanted region of TiO₂.¹¹⁵ To conclude, the effectiveness of TiO₂-based photocatalytic activity is highly sensitive to the amount of dopant used. Both insufficient and excessive dopant levels can significantly impair photocatalytic efficiency by either failing to adequately enhance charge separation or by introducing recombination centres, respectively.

4.12. Thin film approach

The photocatalysts in thin-film form shows distinctly high performance than the same catalyst in particulate form for hydrogen evolution.^{166,206,207} The catalyst nanoparticles assembled in thin film is nearly uniformly spread across the substrate and has a large exposed surface area to the reactants and irradiation, resulting in more efficient interactions between catalyst particles, light and reactants with relatively less mass transfer constraints. The possible reasons for the enhanced solar hydrogen evolution activity of photocatalysts fabricated in thin film form are:²⁰⁶(1) by optimizing the film thickness to around 10 microns, the light absorption achieved is the maximum with thin films, while the same material in suspension form scatters the light, rather than absorption; (2) exposure of maximum surface to solar radiation in thin film form is beneficial for enhancing light harvesting and light induced electron excitation processes and increases hydrogen production and apparent quantum yield (AQY); (3) maximum utilization of surface area and active sites is possible with thin film form, which is good for diffusion of charges toward reaction sites; (4) better contact of catalyst nanoparticles is possible in the film form, which enhance charge separation and charge utilization, whereas charge recombination is severe in powder form; (5) thin film form with some surface roughness helps for internal scattering of light within the depth of thin films and enhances charge carrier production/utilization. In powder form, additional energy in the form of electricity is needed for constant stirring to make the catalyst particles highly homogeneous in the reaction media.^{43,44,166,208} Unlike the case with solar cells, the charge carriers generated during the photocatalytic process were efficiently consumed within an ensemble of particles in a small area in thin film and hydrogen formation occurs from every part of the thin film. This underlines that the charge carriers need not diffuse for long distances of the order of microns.^{166,209}

A comparison of the solar H₂ production activity of titania (P25) and Pd/P25 fabricated in thin film form (4.69 cm²) on a glass plate and their powder form counterparts revealed that the Pd/P25 catalyst (1 mg) fabricated in thin film form resulted a H₂ production rate of 104 mmolh⁻¹g⁻¹, which is about 11-12 times higher than Pd/P25 catalyst (25 mg) in powder form.¹⁶⁶ The



digital photograph, FESEM images and photocatalytic performance of the prepared thin film was depicted in **Figure 27**a-d. The enhanced activity of Pd/P25 in thin film form is due to its maximum exposed surface area to the reactants and sunlight and other advantageous aspects of thin film as described above. A similar trend in photocatalytic H₂ production activity of thin film form of catalyst compared to its powder counter part was also observed with Ag/TiO₂ nanocomposites (**Figure 27**e).⁴⁴

The excellent catalytic performance of Pd/TiO₂,¹⁶⁶ Ag/TiO₂,⁴⁴ Cu–Ni/TiO₂,³ Cu/TiO₂,²⁰⁹ Cu–Ag/TiO₂²⁰⁶ and AuPd/C/TiO₂,⁴³ fabricated in thin-film form, compared to their powder counter parts are demonstrated in the literature. Tudu et al. reported that the thin film form of Cu–Ni/TiO₂ (1:1 = Cu:Ni) photocatalyst exhibited enhanced rate of hydrogen evolution (41.7 mmol h⁻¹g⁻¹) compared to its powder form (1.75 mmol h⁻¹g⁻¹) due to the efficient charge generation and its utilization of the film form of photocatalyst, which mimic the natural photosynthesis by green leaf.³ In another report, the film form of AuPd/rGO/TiO₂ photocatalyst displayed an enhanced hydrogen generation (21.5 mmol/h.g) performance compared to their powder form by a factor of 43 times. The higher activity of the film form of catalyst is attributed to its high light absorption capacity, efficient contact between the particles, remarkable charge generation and utilization.⁴³

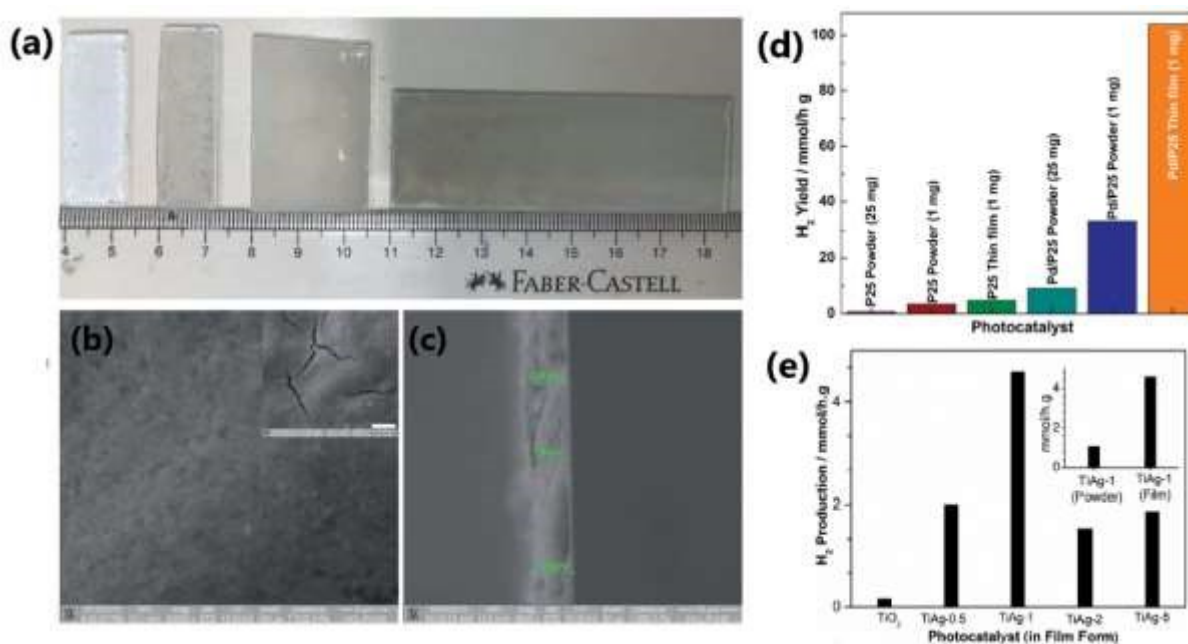


Figure 27. (a) Digital photographs of thin films of P25 and Pd/P25. FESEM images of Pd/P25 thin films over a glass plate at a scale bar of 2 μm (b) and (c) cross sectional view of a freshly cleaved thin film (scale bar:10 μm). Inset in (c) shows the cracks. (d) Photocatalytic H₂ evolution activity in the particulate and thin film form of different catalyst (Reproduced with permission from ref166. copyright©2019, Royal Society of Chemistry. (e) Photocatalytic H₂ production activity of mesoporous TiO₂ and Ag/TiO₂ nanocomposites, measured in thin-film form, in aqueous methanol solution under direct sunlight. Reproduced with permission from ref.44. Copyright ©2021, Wiley-VCH.



An important aspect of assembling and integrating thin film is to enhance the number of heterojunctions or Schottky junctions. A recent work on integrating BiVO₄ in the micro and mesopores of P25-TiO₂, showed a solar to fuel efficiency of 31 % under one sun condition for artificial photosynthesis to methanol and formaldehyde. One of the main reason attributed is the observation of 174 trillions of BiVO₄-TiO₂ heterojunctions in 1 mg of material.²¹⁰ Very likely, this is the first time that Salgaonkar et al. reported a number for heterojunctions, which is calculated from pore-size distribution, surface area by measuring them carefully before and after integrating BiVO₄ with TiO₂. This indeed opens up a new window to fabricate highly integrated materials for efficient charge separation as well as its diffusion to the redox sites. More such works may lead to enhancement in light to chemical conversion for a variety of reactions.

5. Co-production of H₂ and value added products (VAPs) from biomass components for concurrent utilisation of electrons and holes

In spite of utilizing the efficiency of sacrificial reagents as electron donors or hole scavengers to boost photocatalytic hydrogen production, their oxidized products were mostly ignored or unexplored. Recent studies indicated that some catalysts could produce oxidized products of sacrificial reagents along with H₂ due to the concurrent utilization of photogenerated electrons and holes.²¹¹ Most of the studies usually use comparatively costlier sacrificial reagents such as methanol; however, if methanol can be converted to value-added products (VAPs) such as formic acid, one could reduce the operating expenses of photocatalysis. Moreover, utilization of biodiesel byproduct, glycerol, as a sacrificial reagent could lead to the coproduction of H₂ fuel along with VAPs. Compared to pure water-splitting systems, these coupled photocatalytic H₂ production systems would be more reactive and economical in H₂ generation. However, some challenges, such as the removal of liquid products from the reaction system, low conversion efficiency, and product selectivity, need to be addressed. Appropriate chemical process design, coupled with efficient separation techniques, could solve the former issue. Currently, the coproduction of H₂ and the generation of VAPs from sacrificial reagents are still in their infancy stages, so some advanced research in this field is required to tackle the obstacles and explore the photocatalytic H₂ production coupled with the oxidation of sacrificial reagents with a wide range of sacrificial reagents, especially biomass-derived ones.⁵³

A bifunctional p-n heterojunction of NiO-TiO₂ photocatalysts could simultaneously produce H₂ and VAPs such as glyceraldehyde and dihydroxyacetone from glycerol-water solution (10 % v/v) under UV-visible light irradiation.²¹¹ The best performing catalyst (7.5 % Ni loaded TiO₂) produced 8000 μmol⁻¹g⁻¹ hydrogen and was able to achieve 20% of conversion of glycerol. Interestingly, in the beginning of the reaction the yield of glyceraldehyde was higher than that of DHA; however, after 24 h of reaction, almost same yields of both the products were obtained.

The reduction reaction occurs on the surface of TiO₂, while the glycerol oxidation occurs on NiO. The feasibility test revealed that glyceraldehyde contributes the highest share of annual earnings (89%), followed by dihydroxyacetone (11%) and H₂ (0.03%). The photocatalytic H₂ production performance, glycerol oxidation and corresponding reaction mechanism of NiO-



TiO₂ photocatalysts are provided in **Figure 28**. In another work, Bajpai et al. achieved an improved H₂ production rate of 18 mmol h⁻¹ g⁻¹ with the generation of three VAPs, glycolaldehyde, DHA, and formic acid from glycerol-water solution with Au integrated with

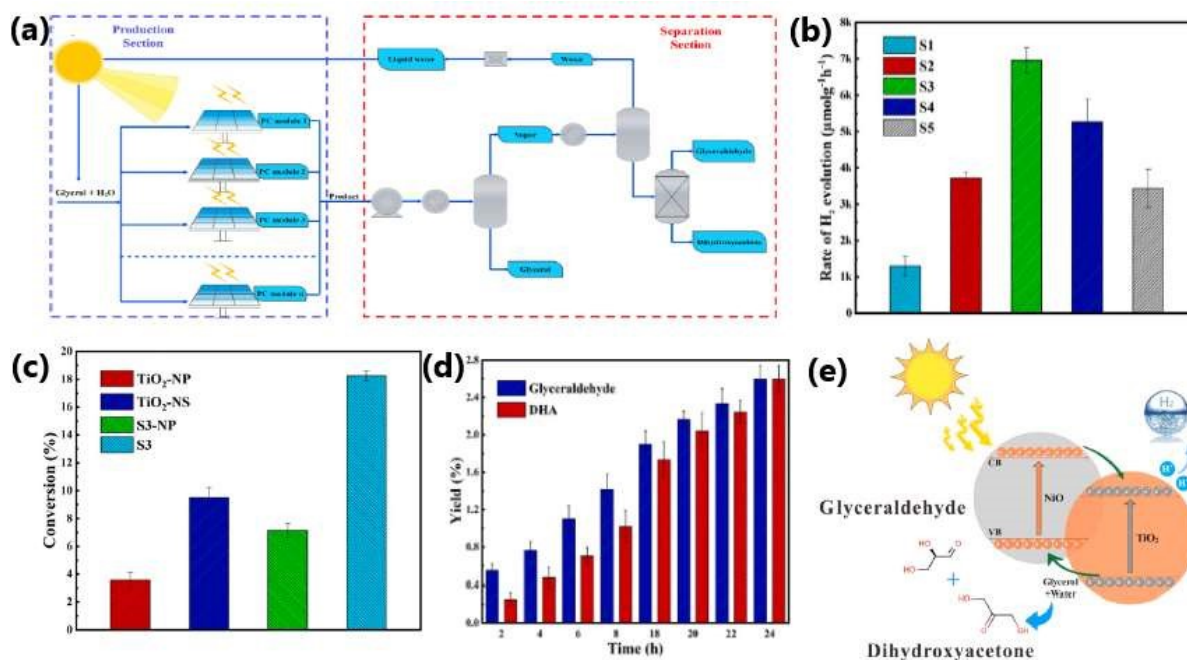


Figure 28. (a) Schematic illustration of the photocatalytic process. Comparison of H₂ production performance of samples with different nickel loading (b). (c) Glycerol conversion over different photocatalysts. Yield of liquid products obtained with best-performing catalyst (d) and (e) plausible reaction mechanism. Reproduced with permission from ref.211 copyright 2023 Elsevier.

P25–TiO₂ (Au@TiO₂).⁵³ The Au@TiO₂ catalyst system achieved a 4-10 % conversion of 0.05M glycerol to VAPs. The photocatalytic experiments were carried out under three different reaction conditions (aerobic, anaerobic and dry air) and under 2 different light sources (direct sunlight and one sun condition with 100 mW cm⁻²). The overall products yield was higher in aerobic conditions under sunlight irradiation compared to anaerobic and dry air conditions. However, 7.5 mmol g⁻¹ CO₂ was also observed under aerobic conditions due to the over oxidation of glycerol. The liquid and gaseous products were same when photocatalytic experiments were performed under one-sun conditions. However, the CO₂ production has declined (5.3 mmol g⁻¹) under one sun condition compared to direct sunlight. The dual functional ability of the catalyst was ascribed to improved charge transport and efficient separation of photogenerated charge carriers effected through the highly dispersed and electronically integrated Au with TiO₂. Photocatalytic systems that can selectively produce desired products with high yields from biomass components, without compromising the yield of H₂ is a real challenge in this area. It is also to be noted that similar concept in electrolysis of aqueous glycerol is growing rapidly in the last 3-4 years and few recent works are worth mentioning. Chauhan et al²¹² achieved a low-voltage pathway to water electrolysis while producing H₂ at cathode and value-added products at anode.



6. Simultaneous oxidation of organic contaminants and hydrogen evolution from waste water

View Article Online

DOI: 10.1039/C4EA00249K

Industrial and domestic areas produce a huge amount of waste water every day, and indeed it is a serious environmental issue. Treatment of wastewater is an energy consuming process, while the wastewater itself is a rich source of energy and it contains four to five times more energy than it needed for treatment. For example, wastewater is a potential source of bio hydrogen, a clean energy and a feedstock chemical.²¹³ The majority of research studies on hydrogen generation use pure water as the hydrogen source. Typically, holes oxidise water to make oxygen and photo generated electrons convert water into hydrogen. However, since the water oxidation process is a slow proces, molecules like alcohols, organic acids, triethanolamine etc. are frequently utilised as sacrificial agents to consume the photo-generated holes to increase the hydrogen production efficiency, thus making the overall process uneconomical.²¹³ Many studies have recently demonstrated that the construction of TiO₂-based photocatalytic system is thermodynamically advantageous for both the generation of hydrogen and the oxidation of organic contaminants from waste water.²¹³⁻²²⁰ Energy production and environmental cleanup are two advantages to use wastewater as a feedstock for photocatalytic hydrogen production. Waste water contains a variety of organic contaminants that can act as sacrificial agents, consuming photogenerated holes and lowering recombination rates to increase the efficiency of hydrogen generation. TiO₂ may oxidise common pollutants including dyes, pharmaceuticals, and industrial effluents, facilitating the breakdown process and facilitating the generation of hydrogen.²¹³⁻²¹⁶

Wu et al. developed a dual-functional photocatalyst system for the treatment of pharmaceutical-contaminated water using Co₃O₄-modified {001}/{101}-TiO₂(TC) nanosheets. The unique aspect of this photocatalytic system is that the p-type semiconductor Co₃O₄ creates a p-n junction with TiO₂ and the {001}/{101} facets of TiO₂ form an inherent surface heterojunction, which enhances the charge carrier separation. While the electrons on the surface of the TiO₂ nanosheet may convert water molecules into molecular hydrogen, the holes on the Co₃O₄ surface effectively oxidise pharmaceutical contaminants in the waste water.²¹³ An interesting idea of concurrent utilization of electrons and holes was employed by Salgaonkar for different isomers of butanol oxidation to corresponding butanal/butanone and hydrogen with TiO₂-Pd and Pd coated with half-a-monolayer of Pt in visible light.²¹⁶ This is a very generic procedure for the selective oxidation of alcohol to aldehyde/ketone with H₂ is worth pursuing for many different substrates. Mineralization of a serious endocrine disruptor, namely endosulphan, was tackled by Devaraji et al. with a solid solution of ZnO-ZnS in direct sunlight.²¹⁴ The a-TiO₂ (anatase TiO₂)/b-AC(biomass activated carbon) nanocomposite synthesized through the ultrasonication technique was very effective for the sulphide wastewater treatment along with excellent photocatalytic hydrogen production (400 ml/h).²¹⁷ The non-metal doped TiO₂ (NM_x-TiO₂, where x is the weight percentage of non-metal element) nanocomposites displayed high hydrogen production rate and COD elimination simultaneously when employed for waste water treatment.²¹⁵ In this case, by using a catalyst loading of 4g/L and a light intensity of 5.93 mW/cm², 7 wt % P- loaded TiO₂ (P7/TiO₂) could achieve a hydrogen production rate of 8.34 mmol/g and 50.6% COD elimination.



Simultaneous oxidation of organic waste and water reduction offer a viable solution to major environmental and energy problems. The goal of ongoing research and development is to remove financial and technological obstacles so that these technologies may be utilised in everyday life and made publicly available. The development of more sophisticated photocatalysts with increased efficiency has been the focus of recent research. Many organic wastes, such as plastic wastes, agricultural, and industrial pollutants, can be efficiently broken down by photocatalytic reactions. This helps in decreasing the environmental problems caused by waste accumulation. Photocatalytic breakdown of harmful organic compounds into less toxic chemicals may reduce the water and soil pollution.

7. Photoreactor setup

The amount of H₂ produced during a photocatalytic process not only depends on the efficiency of the catalyst system, but also on the photoreactor setup. The photoreactor set up plays an important role in the solar to hydrogen (STH) or solar to chemical (STC) conversion efficiency. An ideal photoreactor should facilitate to absorb maximum amount of incident photons on catalyst surface with minimal loss. The photoreactor should be designed in such a way that most of the incident irradiation must fall on the surface of the photocatalyst. The classification of photoreactors is based on the mode of operation, number of phases involved and the type of membrane used.²²¹ The commonly used photoreactors include slurry type, fixed bed and membrane photoreactors. Annular reactors are the most popular slurry type photoreactor.²²² Based on the relative positions of the reactor and the light source, the annular photoreactors are further classified into externally illuminated photoreactors and internally illuminated photoreactors. Among the fixed bed photoreactors, monolith, optical fiber, honeycomb, cylindrical and thin film photoreactors are commonly used. The annular reactor is a tubular reactor with a light source located only at its axis.²²² There are some technical and economic challenges for large-scale hydrogen production using photocatalytic reactor, and it could be made profitable in terms of energy only if energy output is greater than energy input. Hassan et al. fabricated an inner-irradiation quartz annular reactor illuminated with a 300 W Xe lamp with a vacuum and recirculation pumps, a gas collector and a water-cooled condenser.²²³ This photoreactor set up under photocatalytic water splitting reaction in presence of 0.1 g of TiO₂-CuO composite nanofiber photocatalyst suspended in 1 M KOH solution has resulted a H₂ production rate of 2116 and 2715 μmol g⁻¹ in oxygen and air atmosphere, respectively. In a different study, a photoreactor comprised of a flat cylindrical Plexiglas cell, equipped with an optical window made of Pyrex glass and connected to a closed stainless steel system and filled with a photocatalyst bed prepared from 14 mg of Pt/Cu/TiO₂ photocatalysts with different Cu/TiO₂ ratios 0.05 to 0.5 wt.% and 0.5 wt.% Pt on quartz beads was used for photocatalytic water splitting reaction using 20% v/v methanol- water mixture as hydrogen source and a xenon arc lamp having 40.0 mW·cm⁻² power density as the light source.²²⁴ Under these conditions Pt/Cu/TiO₂ photocatalyst containing 0.1 wt.% of Cu produced comparatively higher hydrogen production rate of 27.2 mmol h⁻¹ g⁻¹.²²⁴ In yet another variation by employing Photo-CREC Water-II (PCW- II) reactor and 0.25 wt.% Pd-TiO₂ photocatalyst, Rusinque and coworkers generated a H₂ volume of 113 and 29 cm³ STP, under UV and visible light irradiation, respectively, for 6 h.²²⁵ They used 6L of water and 0.15 g L⁻¹ of photocatalyst during the



reaction. The PCW- II is a slurry type batch reactor equipped with a storage tank to keep the photocatalyst, water and organic scavenger (ethanol). The tank also possesses two ports for gas and liquid phase sampling. The PCW- II reactor has several advantages such as uniform distribution of catalyst with well mixed suspension, a high surface to volume reactor ratio, negligible catalyst fouling, comparatively higher UV, with no internal/external diffusion transport and visible light transmittance (97 %), and higher resistance towards chemicals. Generally, most researchers use batch reactors; however, the low mass transfer and limited light penetration have constrained the light absorption and H₂ production efficiency of photocatalysts.²²⁶ The above drawbacks of batch reactors can be solved if a flow membrane reactor is employed. In this context, flow membrane reactor was employed for photocatalytic methanol dehydrogenation and reforming. The flow membrane reactor consists of three major parts including reactant vessel, reactor and product collector. The detailed schematic diagram and digital photograph of the flow membrane reactor is shown in **Figure 29**a-b. By employing this membrane reactor and using a 300W xenon lamp (T: 303 K, P: 1 atm), the optimized catalyst (1% Cu/PC50) fabricated in thin film form on a glass fibre membrane

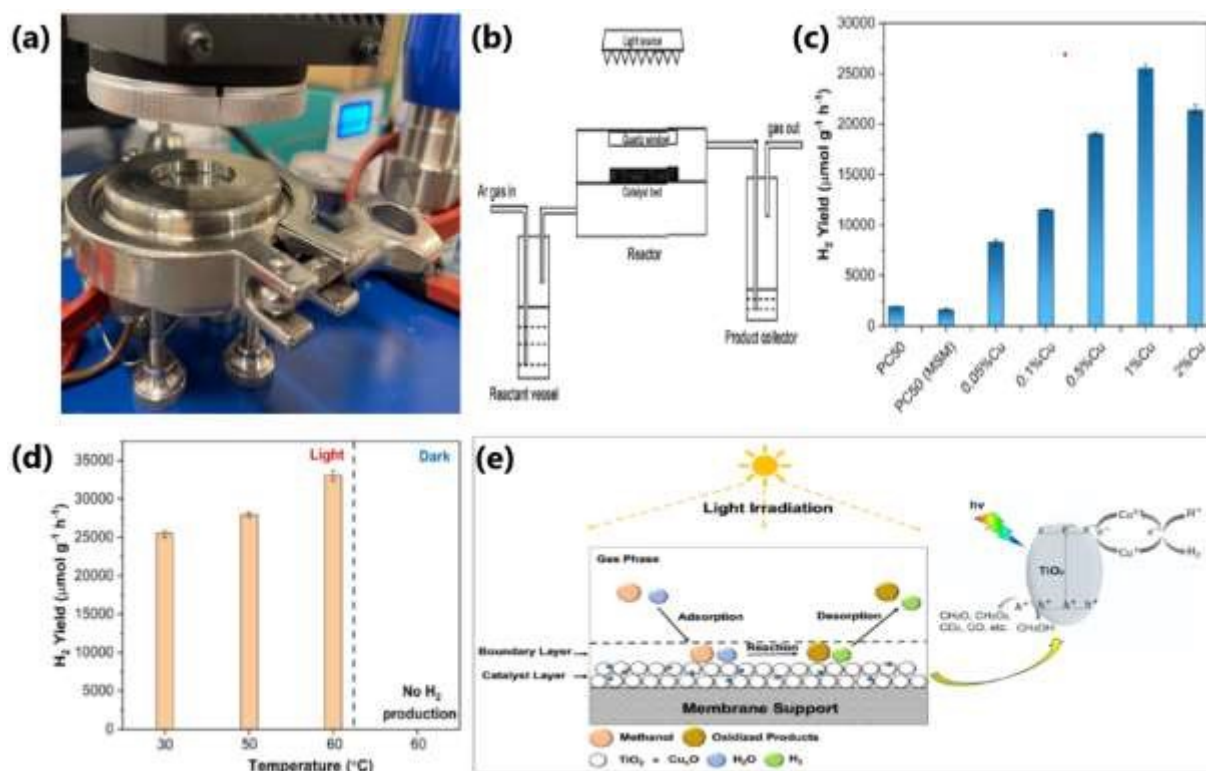


Figure 29. (a) Digital photograph and (b) schematic diagram of the flow membrane reactor used for photocatalytic methanol dehydrogenation and reforming. (c) H₂ yield obtained with different Cu wt% on PC50. (d) Amount of H₂ produced with 1% Cu/PC50 at different temperatures. (e) Schematic illustration of photocatalytic process on 1% Cu/PC50 in the flow membrane reactor. Reproduced with permission from Ref, 226. Copyright ©2022 Royal Society of Chemistry.

exhibits a hydrogen production rate of 25487 and 33702 μmolg⁻¹h⁻¹ at 303 and 333K, respectively.²²⁶ The photocatalytic performance and mechanism of Cu/PC50 photocatalysts are



shown in **Figure 29c-e**. The H₂ production rate observed with flow membrane reactor was 1.63 times higher than that obtained with conventional batch reactor. The enhanced H₂ production efficiency of 1% Cu/PC50 in the flow membrane reactor can be attributed to improved mass transfer, which subsequently advances the adsorption and desorption of reactants and products during photocatalysis. The implementation of membrane reactors, as compared to other conventional-type reactors for photocatalytic hydrogen production, is not only a cost-effective approach but also enhances the separation, sustainability, yield, and selectivity of H₂.

Conclusion and Perspectives

Solar hydrogen production with water as main hydrogen source by employing TiO₂-based semiconductor photocatalyst is a renewable process and an alternative to the steadily increasing demand for energy and the environmental issues pertaining to the increasing consumption of fossil fuels. In this regard, the present review attempts to enumerate the research work carried out in the last decade in the area of photocatalytic hydrogen evolution. In this review, we provide the recent progress in the material integration aspects by describing the integration of TiO₂ with different category of materials, and how the material integration helps in tailoring the electronic and optical properties for activity tuning in solar H₂ production with water as main source. The structure-activity correlation of TiO₂-based photocatalysts is given emphasis to understand the mechanistic aspects as well as how the entire photocatalytic hydrogen production area has been progressing. We also discussed the importance of fabrication of photocatalyst in thin form for enhanced photocatalytic activity and scalability, with the existing photocatalysts.

The TiO₂-based photocatalyst integrated with a second light absorbing component and/or co-catalyst could significantly influence the H₂ production rate. The metal nanoparticles in the form of single atoms and clusters reduce the amount of metal loading and improve the catalytic efficiency. The porosity of a photocatalyst influences solar hydrogen production rate by providing large number of surface exposed sites and enhances the light-harvesting ability of the photocatalyst by transferring the incident photon flux into the internal surface of mesoporous TiO₂ through multiple internal reflections and increasing the mass transfer rate. The photocatalysts fabricated in thin-film form shows distinctly high performance for solar hydrogen production than the same catalyst in particulate form because the catalyst nanoparticles fabricated in thin film is highly connected across the substrate and has a larger exposed surface area to the reactants and sunlight with relatively less mass transfer constraints. The efficient and concurrent utilization of both photogenerated holes and electrons is very important to improve the photocatalytic efficiency of the material as well as the overall energy efficiency of the process. We also discuss the importance of performing TiO₂-based photocatalytic water splitting reaction in different reactor set up for enhancing the photocatalytic performance of the material and its scalability.

Continuous and dedicated efforts are needed in the area of photocatalytic hydrogen generation to fabricate a commercially viable catalyst in scalable form, which is efficient to produce sufficient quanta of charge carriers and utilization. So far very less emphasis has been placed on scalability and long-term stability of the photocatalytic material. In fact, for real



wordl applications, photocatalysts that could deliver same performance for several months (or even a year) and its scalability are necessary, and hence focus may be placed on developing novel photocatalysts with exceptional stability along with scalability towards commercial applications. Despite significant advancements made in this field, the solar-to-hydrogen (STH) conversion efficiency is still need to be improved to implement it for practical applications. At least 10 % STH should be achieved, and the same is expected to attract industries attention. Overall water splitting leading to direct conversion of water into hydrogen without using any sacrificial reagent and by reducing greenhouse gas emission is a promising technique.^{227,228} Renewable H₂ production coupled with waste water treatment with a suitable photocatalyst is another way to compensate the energy loss at the expense of waste minimization. Renewable H₂ production and concurrent value added products formation by employing a waste biomass component, such as glycerol,^{53,212} is an attractive way to waste minimization with concurrent value addition. Oxidation of biomass component occurs at significantly lower potential than oxygen formation; in addition, electrons and holes are simultaneously used ensures the catalyst stability for longer period of time. Hence continous research in the above directions is needed to improve the energy efficiency of the process by optimising the photocatalyst and reaction conditions.

Conflicts of interest

The authors declare no conflict of interest.

Acknowledgements

S.S.M. and S.R gratefully acknowledges DST, New Delhi, for the facility support under DST-FIST programme in St. John's College, Anchal, Kerala, India. S.R also thank UGC for research fellowship. CSG thanks CSIR for funding through HCP-44 project.

References

- 1 N. S. Lewis and D. G. Nocera, *Acad. Sci. USA*, 2006, **103**, 15729–15736.
- 2 A. Kalair, N. Abas, M. S. Saleem, A. R. Kalair and N. Khan, *Energy Storage*, 2021, **3**, e135.
- 3 B. Tudu, N. Nalajala, P. Saikia and C. S. Gopinath, *Sol. RRL*, 2020, **4**, 1900557.
- 4 (a) X. Zong, H. Yan, G. Wu, G. Ma, F. Wen, L. Wang and C. Li, *J. Am. Chem. Soc.*, 2008, **130**, 7176–7177. (b) W. Siboo, B. Y. Guan, X. Wang, and X. W. David Lou. *J. Am. Chem. Soc.*, 2018, **140**, 15145–15148. (c) S. Wang, Y. Wang, S. L. Zhang, S. Q. Zang and X. W. Lou, *Adv. Mater.*, 2019, **31**, 1903404. (d) Z. Xiong, Y. Hou, R. Yuan, Z. Ding, W. J. Ong and S. Wang, *Acta Phys. - Chim. Sin.*, 2022, **38**, 2111021.
- 5 (a) Z. Xie, W. Wang, X. Ke, X. Cai, X. Chen, S. Wang, W. Lin and X. Wang, *Appl. Catal. B Environ.*, 2023, **325**, 122312. (b) Y. Zhang, Z. Yang, D. Zheng, S. Wang, Y. Hou, M. Anpo and G. Zhang, *Int. J. Hydrogen Energy*, 2024, **69**, 372–380. (c) M. Chang, Z. Pan, D. Zheng, S. Wang, G. Zhang, M. Anpo and X. Wang, *ChemSusChem*, 2023, **16**, e202202255.
- 6 (a) R. Guan, H. Zhai, J. Li, Y. Qi, M. Li, M. Song, Z. Zhao, J. Zhang, D. Wang and H. Tan, *Appl. Surf. Sci.*, 2020, **507**, 144772. (b) Z. Xi, C. Li, L. Zhang, M. Xing and J. Zhang, *Int. J. Hydrogen Energy*, 2014, **39**, 6345–6353.
- 7 (a) M. Wang, J. Iocozia, L. Sun and Z. Lin, *Energy Environ. Sci.*, 2014, **7**, 2182–2202. (b) M.



- Satish, R. P. Viswanath, and C. S. Gopinath, *Chem. Mater.*, 2005, **17**, 6349-6353. View Article Online
DOI: 10.1039/D4YA00249K
- 8 H. Tang, M. Xiong, D. Qu, D. Liu, Z. Zhang, Z. Xie, X. Wei, W. Tu and D. Qu, *Nano Energy*, 2015, **15**, 75–82.
- 9 W. Y. Cheng, T. H. Yu, K. J. Chao and S. Y. Lu, *ChemCatChem*, 2014, **6**, 293–300.
- 10 L. L. Tan, W. J. Ong, S. P. Chai and A. R. Mohamed, *Appl. Catal. B: Environ.*, 2015, **166–167**, 251–259.
- 11 J. Luo, X. Xia, Y. Luo, C. Guan, J. Liu, X. Qi, C. F. Ng, T. Yu, H. Zhang and H. J. Fan, *Adv. Energy Mater.*, 2013, **3**, 737–743.
- 12 M. Kulkarni, A. Mazare, P. Schmuki and A. Iglic, *Adv. Mater. Lett.*, 2016, **7**, 23–28.
- 13 M. Luna, M. J. Mosquera, H. Vidal and J. M. Gatica, *Build. Environ.*, 2019, **164**, 106347.
- 14 W. H. Hung, T. M. Chien and C. M. Tseng, *J. Phys. Chem. C*, 2014, **118**, 12676–12681.
- 15 S. Liu and H. Syu, *Int. J. Hydrogen Energy*, 2013, **38**, 13856–13865.
- 16 Y. Wei, J. Xiong, W. Li, R. H. Kollarigowda and G. Cheng, *Inorg. Chem. Front.*, 2018, **5**, 2709–2717.
- 17 Y. Chen, Z. Mou, S. Yin, H. Huang, P. Yang, X. Wang and Y. Du, *Mater. Lett.*, 2013, **107**, 31–34.
- 18 K. K. Patra and C. S. Gopinath, *ChemCatChem*, 2016, **8**, 3294–3311.
- 19 P. K. Sharma, M. A. L. R. M. Cortes, J. W. J. Hamilton, Y. Han, J. A. Byrne and M. Nolan, *Catal. Today*, 2019, **321**, 9–17.
- 20 (a) H. Gong, Q. Liu and C. Huang, *Int. J. Hydrogen Energy*, 2019, **44**, 4821–4831. (b) P. Devaraji, N. K. Sathu and C. S. Gopinath, *ACS Catal.* 2014, **4**, 2844-2853.
- 21 S. Rajaambal, K. Sivaranjani and C. S. Gopinath, *J. Chem. Sci.*, 2015, **127**, 33–47.
- 22 S. Martha, P. C. Sahoo, K. M. Parida, P. Chandra Sahoo and K. M. Parida, *RSC Adv.*, 2015, **5**, 61535–61553.
- 23 M. Z. Rahman, M. G. Kibria and C. B. Mullins, *Chem. Soc. Rev.*, 2020, **49**, 1887–1931.
- 24 J. Corredor, M. J. Rivero, C. M. Rangel, F. Gloaguen and I. Ortiz, *J. Chem. Technol. Biotechnol.*, 2019, **94**, 3049–3063.
- 25 A. Savateev and M. Antonietti, *ChemCatChem*, 2019, **11**, 6166–6176.
- 26 S. Patnaik, S. Martha and K. M. Parida, *RSC Adv.*, 2016, **6**, 46929–46951.
- 27 G. Zhang, Z. A. Lan and X. Wang, *Chem. Sci.*, 2017, **8**, 5261–5274.
- 28 X. Li, A. F. Masters and T. Maschmeyer, *Chem. Commun.*, 2017, **53**, 7438–7446.
- 29 P. Kumar, R. Boukherroub and K. Shankar, *J. Mater. Chem. A*, 2018, **6**, 12876–12931.
- 30 Y. J. Yuan, Z. T. Yu, D. Q. Chen and Z. G. Zou, *Chem. Soc. Rev.*, 2017, **46**, 603–631.
- 31 M. Gao, L. Zhu, W. L. Ong, J. Wang and G. W. Ho, *Catal. Sci. Technol.*, 2015, **5**, 4703–4726.
- 32 D. Zhao and C. F. Yang, *Renew. Sustain. Energy Rev.*, 2016, **54**, 1048–1059.
- 33 B. Gupta, A. A. Melvin, T. Matthews, S. Dash and A. K. Tyagi, *Renew. Sustain. Energy Rev.*, 2016, **58**, 1366–1375.
- 34 M. Ge, J. Cai, J. Iocozzia, C. Cao, J. Huang, X. Zhang, J. Shen, S. Wang, S. Zhang, K. Q. Zhang, Y. Lai and Z. Lin, *Int. J. Hydrogen Energy*, 2017, **42**, 8418–8449.
- 35 V. Kumaravel, S. Mathew, J. Bartlett and S. C. Pillai, *Appl. Catal. B: Environ.*, 2019, **244**, 1021–



- 1064.
- 36 R. Shwetharani, M. Sakar, C. A. N. Fernando, V. Binas and R. G. Balakrishna, *Catal. Sci. Technol.*, 2019, **9**, 12–46.
- 37 M. Ge, Q. Li, C. Cao, J. Huang, S. Li, S. Zhang, Z. Chen, K. Zhang, S. S. Al-Deyab and Y. Lai, *Adv. Sci.*, 2017, **4**, 1–31.
- 38 A. López Ortiz, M. Meléndez Zaragoza, J. Salinas Gutiérrez, M. Marques Da Silva Paula and V. Collins-Martínez, *Int. J. Hydrogen Energy*, 2015, **40**, 17308–17315.
- 39 F. Wu, X. Hu, J. Fan, E. Liu and T. Sun, *Plasmonics*, 2013, **8**, 501–508.
- 40 K. Wu, Y. Shang, H. Li, P. Wu, S. Li, H. Ye, F. Jian, J. Zhu, D. Yang, B. Li and X. Wang, *Molecules*, 2023, **28**, 4350.
- 41 M. Yasuda, T. Matsumoto and T. Yamashita, *Renew. Sustain. Energy Rev.*, 2018, **81**, 1627–1635.
- 42 C. S. Gopinath and N. Nalajala, *J. Mater. Chem. A*, 2021, **9**, 1353–1371.
- 43 B. Tudu, N. Nalajala, K. Reddy, P. Saikia and C. S. Gopinath, *ACS Appl. Mater. Interfaces*, 2019, **11**, 32869–32878.
- 44 S. S. Mani, S. Rajendran, N. Nalajala, T. Mathew and C. S. Gopinath, *Energy Tech.*, 2022, **10**, 2100356.
- 45 S. Y. Toledo Camacho, A. Rey, M. D. Hernández-Alonso, J. Llorca, F. Medina and S. Contreras, *Appl. Surf. Sci.*, 2018, **455**, 570–580.
- 46 G. Mishra, K. M. Parida and S. K. Singh, *ACS Sus. Chem. Eng.*, 2015, **3**, 245–253.
- 47 L. Peng, Y. Liu, Y. Li, F. Teng, A. Tang and Y. Yin, *Nanoscale*, 2019, **11**, 22575–22584.
- 48 Q. Gu, Z. Gao, S. Yu and C. Xue, *Adv. Mater. Interfaces*, 2016, **3**, 17–21.
- 49 M. A. Khan, M. Al-Oufi, A. Toseef, M. A. Nadeem and H. Idriss, *Catal. Letters*, 2018, **148**, 1–10.
- 50 G. Zhang, Z. Zhao, H. Tan, H. Zhao, D. Qu, M. Zheng, W. Yu and Z. Sun, *RSC Adv.*, 2015, **5**, 21237–21241.
- 51 C. Chen, L. Kuai, Y. Chen, Q. Wang, E. Kan and B. Geng, *RSC Adv.*, 2015, **5**, 98254–98259.
- 52 R. Camposeco, S. Castillo, V. Rodriguez-Gonzalez, M. Hinojosa-Reyes and I. Mejía-Centeno, *J. Photochem. Photobiol. A Chem.*, 2018, **356**, 92–101.
- 53 H. Bajpai, I. Chauhan, K. N. Salgaonkar, N. B. Mhamane and C. S. Gopinath, *RSC Sustain.*, 2023, **1**, 481–493.
- 54 B. Tudu, N. Nalajala, K. Prabhakar Reddy, P. Saikia and C. S. Gopinath, *ACS Sus. Chem. Eng.*, 2021, **9**, 13915–13925.
- 55 R. M. Mohamed, M. W. Kadi and A. A. Ismail, *Ceram. Int.*, 2020, **46**, 15604–15612.
- 56 M. Ameen Sha, P. Chandrasekharan Meenu, V. Sasidharan Sumi, T. Chithrajakumary Bhagya, B. Revamma Sreelekshmy and S. M. A. Shibli, *Mater. Sci. Semicond. Process.*, 2020, **105**, 104742.
- 57 S. A. Rawool, M. R. Pai, A. M. Banerjee, A. Arya, R. S. Ningthoujam, R. Tewari, R. Rao, B. Chalke, P. Ayyub, A. K. Tripathi and S. R. Bharadwaj, *Appl. Catal. B: Environ.*, 2018, **221**, 443–458.
- 58 G. Sadanandam, K. Lalitha, V. D. Kumari, M. V. Shankar and M. Subrahmanyam, *Int. J. Hydrogen Energy*, 2013, **38**, 9655–9664.
- 59 D. Pan, Z. Han, Y. Miao, D. Zhang and G. Li, *Appl. Catal. B: Environ.*, 2018, **229**, 130–138.



- 60 Q. Chen, R. Tong, X. Chen, Y. Xue, Z. Xie, Q. Kuang and L. Zheng, *Catal. Sci. Technol.*, 2018, **8**, 1296–1303. View Article Online
DOI: 10.1039/D4TA00249K
- 61 L. Clarizia, G. Vitiello, R. Bericat Vadell, J. Sá, R. Marotta, I. Di Somma, R. Andreozzi and G. Luciani, *Int. J. Mol. Sci.*, 2023, **24**, 2004
- 62 P. A. Bharad, A. V. Nikam, F. Thomas and C. S. Gopinath, *ChemistrySelect*, 2018, **3**, 12022–12030.
- 63 H. Bajpai, K. K. Patra, R. Ranjan, N. Nalajala, K. P. Reddy and C. S. Gopinath, *ACS Appl. Mater. Interfaces*, 2020, **12**, 30420–30430.
- 64 A. Gautam, Y. T. Prabhu and U. Pal, *New J. Chem.*, 2021, **45**, 10257–10267.
- 65 T. R. Kuo, H. J. Liao, Y. T. Chen, C. Y. Wei, C. C. Chang, Y. C. Chen, Y. H. Chang, J. C. Lin, Y. C. Lee, C. Y. Wen, S. S. Li, K. H. Lin and D. Y. Wang, *Green Chem.*, 2018, **20**, 1640–1647.
- 66 Z. Zhang, C. Shao, X. Li, Y. Sun, M. Zhang, J. Mu, P. Zhang, Z. Guo and Y. Liu, *Nanoscale*, 2013, **5**, 606–618.
- 67 M. M. Kumari, A. Priyanka, B. Mareenna and P. Haridoss, *RSC Adv.*, 2017, **7**, 7203–7209.
- 68 M. A. Alcudia-ramos, M. O. Fuentes-torres, F. Ortiz-chi and C. G. Espinosa-gonzález, *Ceram. Int.*, 2020, **46**, 38–45.
- 69 P. Devaraji and C. S. Gopinath, *Int. J. Hydrogen Energy*, 2018, **43**, 601–613.
- 70 P. A. Bharad, K. Sivaranjani and C. S. Gopinath, *Nanoscale*, 2015, **7**, 11206–11215.
- 71 A. A. Melvin, P. A. Bharad, K. Illath, M. P. Lawrence and C. S. Gopinath, *ChemistrySelect*, 2016, **1**, 917–923.
- 72 Q. Zhang, P. Chen, L. Chen, M. Wu, X. Dai, P. Xing, H. Lin, L. Zhao and Y. He, *J. Colloid Interface Sci.*, 2020, **568**, 117–129.
- 73 Y. Wang, M. Fiaz, J. Kim, N. Carl and Y. K. Kim, *ACS Appl. Energy Mater.*, 2023, **6**, 5197–5206.
- 74 X. Yao, X. Hu, Y. Cui, J. Huang, W. Zhang, X. Wang and D. Wang, *Chinese Chem. Lett.*, 2021, **32**, 750–754.
- 75 L. Zani, M. Melchionna, T. Montini and P. Fornasiero, *J. Phys. Energy*, 2021, **3**, 031001 .
- 76 A. A. Melvin, K. Illath, T. Das, T. Raja, S. Bhattacharyya and C. S. Gopinath, 2015, **7**, 13477–13488.
- 77 C. Beasley, M. Kumaran Gnanamani, E. Santillan-Jimenez, M. Martinelli, W. D. Shafer, S. D. Hopps, N. Wanninayake and D. Y. Kim, *ChemistrySelect*, 2020, **5**, 1013–1019.
- 78 M. J. Rivero, O. Iglesias, P. Ribao and I. Ortiz, *Int. J. Hydrogen Energy*, 2019, **44**, 101–109.
- 79 M. Ismael, *New J. Chem.*, 2019, **43**, 9596–9605.
- 80 S. Ida, K. Sato, T. Nagata, H. Hagiwara, M. Watanabe, N. Kim, Y. Shiota, M. Koinuma, S. Takenaka, T. Sakai, E. Ertekin and T. Ishihara, *Angew. Chem. Int. Ed.* 2018, **130**, 9211–9215.
- 81 Y. Ma, R. Chong, F. Zhang, Q. Xu, S. Shen, H. Han and C. Li, *Phys. Chem. Chem. Phys.*, 2014, **16**, 17734–17742.
- 82 J. B. Priebe, M. Karnahl, H. Junge, M. Beller, D. Hollmann and A. Brückner, *Angew. Chemie - Int. Ed.*, 2013, **52**, 11420–11424.
- 83 A. L. Luna, E. Novoseltceva, E. Louarn, P. Beaunier, E. Kowalska, B. Ohtani, M. A. Valenzuela, H. Remita and C. Colbeau-Justin, *Appl. Catal. B Environ.*, 2016, **191**, 18–28.
- 84 C. Ban, B. Li, J. Ma, Y. Feng, C. Lin, Y. Chen, Y. Wang, Y. Duan, K. Zhou, L. Gan, S. Wang and X.



- Zhou, *Ceram. Int.*, 2024, **50**, 15444–15451.
- 85 C. Zhao, A. Krall, H. Zhao, Q. Zhang and Y. Li, *Int. J. Hydrogen Energy*, 2012, **37**, 9967–9976.
- 86 R. A. Rather, S. Singh and B. Pal, *Sol. Energy Mater. Sol. Cells*, 2019, **160**, 463–469.
- 87 X. Hu, L. Xiao, X. Jian and W. Zhou, *J. Wuhan Univ. Technol. Mater. Sci. Ed.*, 2017, **32**, 67–75.
- 88 M. An, L. Li, Y. Tian, H. Yu and Q. Zhou, *RSC Adv.*, 2018, **8**, 18870–18879.
- 89 U. Kerketta, H. Kim, N. Denisov and P. Schmuki, *Adv. Energy Mater.*, 2024, **14**, 2302998.
- 90 M. Shahrezaei, S. M. H. Hejazi, H. Kmentova, V. Sedajova, R. Zboril, A. Naldoni and S. Kment, *ACS Appl. Mater. Interfaces*, 2023, **15**, 37976–37985.
- 91 I. Mondal, S. Gonuguntla and U. Pal, *J. Phys. Chem. C*, 2019, **123**, 26073–26081.
- 92 V. Jovic, K. E. Smith, H. Idriss and G. I. N. Waterhouse, *ChemSusChem*, 2015, **8**, 2551–2559.
- 93 M. Z. Ge, C. Y. Cao, S. H. Li, Y. X. Tang, L. N. Wang, N. Qi, J. Y. Huang, K. Q. Zhang, S. S. Al-Deyab and Y. K. Lai, *Nanoscale*, 2016, **8**, 5226–5234.
- 94 Choi, Y., Kim, H. I., Moon, G. H., Jo, S., & Choi, W. 2016. *Acs Catalysis*, 2016, **6**, 821–828
- 95 Y. X. Chen, V. Gombac, T. Montini, A. Lavacchi, J. Filippi, H. A. Miller, P. Fornasiero and F. Vizza, *Green Chem.*, 2018, **20**, 2299–2307.
- 96 J. Nie, A. O. T. Patrocínio, S. Hamid, F. Sieland, J. Sann, S. Xia, D. W. Bahnemann and J. Schneider, *Phys. Chem. Chem. Phys.*, 2018, **20**, 5264–5273.
- 97 P. Zhuang, H. Yue, H. Dong and X. Zhou, *New J. Chem.*, 2020, **44**, 5428–5437.
- 98 M. A. Eldoma, S. O. Alaswad, M. A. Mahmoud, I. Y. Qudsieh, M. Hassan, O. Y. Bakather, G. A. Elawadi, A. F. F. Abouatiaa, M. S. Alomar, M. S. Elhassan, I. G. Alhindawy and Z. M. Ahmed, *J. Photochem. Photobiol. A Chem.*, 2024, **446**, 115164.
- 99 L. Clarizia, G. Vitiello, G. Luciani, I. Di Somma, R. Andreozzi and R. Marotta, *Appl. Catal. A Gen.*, 2016, **518**, 142–149.
- 100 N. L. Reddy, S. Kumar, V. Krishnan, M. Sathish and M. V. Shankar, *J. Catal.*, 2017, **350**, 226–239.
- 101 L. S. Almazroai and R. E. El-Mekawy, *RSC Adv.*, 2019, **9**, 24670–24681.
- 102 W. T. Chen, A. Chan, D. Sun-Waterhouse, J. Llorca, H. Idriss and G. I. N. Waterhouse, *J. Catal.*, 2018, **367**, 27–42.
- 103 S. Gullapelli, M. S. Scurrell and D. K. Valluri, *Int. J. Hydrogen Energy*, 2017, **42**, 15031–15043.
- 104 H. Huang, J. Lin, L. Fan, X. Wang, X. Fu and J. Long, *J. Phys. Chem. C*, 2015, **119**, 10478–10492.
- 105 P. Zhang, T. Song, T. Wang and H. Zeng, *RSC Adv.*, 2017, **7**, 17873–17881.
- 106 W. T. Chen, A. Chan, D. Sun-Waterhouse, T. Moriga, H. Idriss and G. I. N. Waterhouse, *J. Catal.*, 2015, **326**, 43–53.
- 107 K. K. Patra, P. A. Bharad, V. Jain and C. S. Gopinath, *J. Mater. Chem. A*, 2019, **7**, 3179–3189.
- 108 M. Sathish, B. Viswanathan, R. P. Viswanath and C. S. Gopinath, *Chem. Mater.*, 2005, **17**, 6349–6353.
- 109 K. Liu, C. Su and T. Perng, *RSC Adv.*, 2015, **5**, 88367–88374.
- 110 M. Sun, Y. Jiang, M. Tian, H. Yan, R. Liu and L. Yang, *RSC Adv.*, 2019, **9**, 11443–11450.
- 111 S. K. Khore, N. V. Tellabati, S. K. Apte, S. D. Naik, P. Ojha, B. B. Kale and R. S. Sonawane, *RSC Adv.*, 2017, **7**, 33029–33042.



- 112 X. Zhou, V. Häublein, N. Liu, N. T. Nguyen, E. M. Zolnhofer, H. Tsuchiya, M. S. Killian, K. Meyer, L. Frey and P. Schmuki, *Angew. Chemie. Int. Ed.*, 2016, **55**, 3763–3767. View Article Online
DOI: 10.1039/D4YA00249K
- 113 D. Gogoi, A. Namdeo and A. Kumar, *Int. J. Hydrogen Energy*, 2020, **45**, 2729–2744
- 114 S. Rajaambal, M. Mapa and C. S. Gopinath, *Dalton Trans.*, 2014, **43**, 12546–12554.
- 115 (a) M. Mapa, K. Sivaranjani, D. S. Bhange, B. Saha, P. Chakraborty, A. K. Viswanath and C. S. Gopinath, *Chem. Mater.*, 2010, **22**, 565–578. (b) M. Mapa and C. S. Gopinath, *Chem. Mater.*, 2009, **21**, 351–359.
- 116 L. K. Preethi, R. P. Antony, T. Mathews, S. C. J. Loo, L. H. Wong, S. Dash and A. K. Tyagi, *Int. J. Hydrogen Energy*, 2016, **41**, 1–13.
- 117 C. Peng, W. Xu, P. Wei, M. C. Liu, L. Guo, P. Wu, K. Zhang, Y. Cao, H. Wang, H. Yu, F. Peng and X. Yan, *Int. J. Hydrogen Energy*, 2019, **44**, 29975–29985.
- 118 M. V. Dozzi, G. L. Chiarello, M. Pedroni, S. Livraghi, E. Giamello and E. Selli, *Appl. Catal. B Environ.*, 2017, **209**, 417–428.
- 119 S. S. Lee, H. Bai, Z. Liu and D. D. Sun, *Appl. Catal. B Environ.*, 2013, **140–141**, 68–81.
- 120 G. D. Moon, J. B. Joo, I. Lee and Y. Yin, *Nanoscale*, 2014, **6**, 12002–12008.
- 121 Y. J. Yuan, G. Fang, D. Chen, Y. Huang, L. X. Yang, D. P. Cao, J. Wang, Z. T. Yu and Z. G. Zou, *Dalt. Trans.*, 2018, **47**, 5652–5659.
- 122 R. Peng, C. Lin, J. Baltrusaitis, C. M. Wu, N. M. Dimitrijevic, T. Rajh, S. May and R. T. Koodali, *Phys. Chem. Chem. Phys.*, 2014, **16**, 2048–2061.
- 123 S. Shenoy, E. Jang, T. J. Park, C. S. Gopinath and K. Sridharan, *Appl. Surf. Sci.*, 2019, **483**, 696–705.
- 124 M. T. Uddin, Y. Nicolas, C. Olivier, W. Jaegermann, N. Rockstroh, H. Junge and T. Toupance, *Phys. Chem. Chem. Phys.*, 2017, **19**, 19279–19288.
- 125 T. N. Ravishankar, M. De Oliveira Vaz, S. Khan, T. Ramakrishnappa, S. R. Teixeira, G. R. Balakrishna, G. Nagaraju and J. Dupont, *New J. Chem.*, 2016, **40**, 3578–3587.
- 126 W. Wang, S. Zhu, Y. Cao, Y. Tao, X. Li, D. Pan, D. L. Phillips, D. Zhang, M. Chen, G. Li and H. Li, *Adv. Funct. Mater.*, 2019, **29**, 1901958.
- 127 M. Altomare, N. T. Nguyen, S. Hejazi and P. Schmuki, *Adv. Funct. Mater.*, 2018, **28**, 1704259.
- 128 M. N. Ha, F. Zhu, Z. Liu, L. Wang, L. Liu, G. Lu and Z. Zhao, *RSC Adv.*, 2016, **6**, 21111–21118.
- 129 J. D. Lin, S. Yan, Q. D. Huang, M. T. Fan, Y. Z. Yuan, T. T. Y. Tan and D. W. Liao, *Appl. Surf. Sci.*, 2014, **309**, 188–193.
- 130 H. Zhu, C. Zhen, X. Chen, S. Feng, B. Li, Y. Du, G. Liu and H. M. Cheng, *Sci. Bull.*, 2022, **67**, 2420–2427.
- 131 X. Wang, H. Dong, Z. Hu, Z. Qi and L. Li, *Mater. Sci. Eng. B*, 2017, **219**, 10–19.
- 132 C. Wang, X. Cai, Y. Chen, Z. Cheng, X. Luo, S. Mo, L. Jia, R. Shu, P. Lin, Z. Yang, S. Sun, E. Pu and Y. Shen, *Int. J. Hydrogen Energy*, 2017, **42**, 17063–17074.
- 133 A. Jakimińska, K. Spilarewicz and W. Macyk, *Nanoscale Adv.*, 2023, **5**, 1926–1935.
- 134 I. Tamiolakis, I. T. Papadas, K. C. Spyridopoulos and G. S. Armatas, *RSC Adv.*, 2016, **6**, 54848–54855.
- 135 T. N. Ravishankar, M. de O. Vaz, S. Khan, T. Ramakrishnappa, S. R. Teixeira, G. R. Balakrishna, G. Nagaraju and J. Dupont, *ChemistrySelect*, 2016, **1**, 2199–2206.



- 136 Y. Liu and C. Tang, *Russ. J. Phys. Chem. A*, 2016, **90**, 1042–1048. View Article Online
DOI: 10.1039/D4YA00249K
- 137 W. Chen, S. Yu, Y. Zhong, X. B. Fan, L. Z. Wu and Y. Zhou, *New J. Chem.*, 2018, **42**, 4811–4817.
- 138 Y. J. Yuan, Z. J. Ye, H. W. Lu, B. Hu, Y. H. Li, D. Q. Chen, J. S. Zhong, Z. T. Yu and Z. G. Zou, *ACS Catal.*, 2016, **6**, 532–541.
- 139 D. Zhao, Q. Wu, S. Wang, C. Zhao and C. Yang, *Res. Chem. Intermed.*, 2016, **42**, 5479–5493.
- 140 L. Guo, Z. Yang, K. Marcus, Z. Li, B. Luo, L. Zhou, X. Wang, Y. Du and Y. Yang, *Energy Environ. Sci.*, 2018, **11**, 106–114.
- 141 X. J. Lv, S. X. Zhou, C. Zhang, H. X. Chang, Y. Chen and W. F. Fu, *J. Mater. Chem.*, 2012, **22**, 18542–18549.
- 142 D. Xu, L. Li, R. He, L. Qi, L. Zhang and B. Cheng, *Appl. Surf. Sci.*, 2018, **434**, 620–625.
- 143 H. An, M. Li, W. Wang, Z. Lv, C. Deng, J. Huang and Z. Yin, *Ceram. Int.*, 2019, **45**, 14976–14982.
- 144 W. Liu, L. Wang, T. Chin, Y. Yen and T. Perng, 2018, **8**, 30642–30651.
- 145 J. Wang, J. Huang, H. Xie and A. Qu, *Int. J. Hydrogen Energy*, 2014, **39**, 6354–6363.
- 146 S. A. Hassanzadeh-Tabrizi, C. C. Nguyen and T. O. Do, *Appl. Surf. Sci.*, 2019, **489**, 741–754
- 147 S. Kamalakannan, N. Balasubramaniyan, N. Bernaurdshaw and G. Vattikondala, *Nanoscale Adv.*, 2023, **5**, 5907–5922.
- 148 Y. Tan, Z. Shu, J. Zhou, T. Li, W. Wang and Z. Zhao, *Appl. Catal. B Environ.*, 2018, **230**, 260–268.
- 149 I. Mondal, U. Pal, *New J. Chem.*, 2015, **39**, 6925–6934.
- 150 L. Kuang, W. Zhang, *RSC Adv.*, 2016, **6**, 2479–88.
- 151 S. Pany and K. M. Parida, *Phys. Chem. Chem. Phys.*, 2015, **17**, 8070–8077
- 152 Ma J, Tan X, Jiang F, Yu T., *Catal. Sci. Tech.*, 2017, **7**, 3275–82.
- 153 L. Liu, Z. Liu, A. Liu, X. Gu, C. Ge and F. Gao, *ChemSusChem*, 2014, **7**, 618–626.
- 154 M. Malizia, S. A. Scott, L. Torrente-Murciano, A. M. Boies, T. A. Aljohani and H. G. Baldovi, *Nanomaterials*, 2023, **13**, 2959.
- 155 A. Kumari, I. Mondal and U. Pal, *New J. Chem.*, 2015, **39**, 713–720.
- 156 Y. Sun, X. F. Wang, G. Chen, C. H. Zhan, O. Kitao, H. Tamiaki and S. ichi Sasaki, *Int. J. Hydrogen Energy*, 2017, **42**, 15731–15738.
- 157 S. Liu, X. Chen, C. Zhang, X. Liu and S. Xu, *Dye. Pigment.*, 2023, **212**, 111128.
- 158 C. Marchal, T. Cottineau, M. G. Méndez-Medrano, C. Colbeau-Justin, V. Caps and V. Keller, *Adv. Energy Mater.*, 2018, **8**, 1–12.
- 159 R. A. Rather, S. Singh and B. Pal, *Appl. Catal. B Environ.*, 2017, **213**, 9–17.
- 160 H. Shen, D. Ni, P. Niu, Y. Zhou, T. Zhai and Y. Ma, *Int. J. Hydrogen Energy*, 2017, **42**, 30559–30568.
- 161 S. B. Kokane, S. D. Sartale, C. A. Betty and R. Sasikala, *RSC Adv.*, 2014, **4**, 55539–55547.
- 162 K. Manjunath, V. S. Souza, G. Nagaraju, J. Marcos Leite Santos, J. Dupont and T. Ramakrishnappa, *New J. Chem.*, 2016, **40**, 10172–10180.
- 163 A. K. R. Police, S. V. P. Vattikuti, K. K. Mandari, M. Chennaiahgari, P. S. Phanikrishna, D. K. Valluri and C. Byon, *Ceram. Int.*, 2018, **44**, 11783–11791.
- 164 H Li, B Sun, F Yang, Z Wang, Y Xu, G Tian, K Pan, B Jiang, W Zhou *ChemCatChem*, 2017, **9**, 3752–



61. View Article Online
DOI: 10.1039/D4YA00249K
- 165 M. Shang, H. Hou, F. Gao, L. Wang and W. Yang, *RSC Adv.*, 2017, **7**, 30051–30059.
- 166 N. Nalajala, K. K. Patra, P. A. Bharad and C. S. Gopinath, *RSC Adv.*, 2019, **9**, 6094–6100.
- 167 S. K. Khore, S. R. Kadam, S. D. Naik, B. B. Kale and R. S. Sonawane, *New J. Chem.*, 2018, **42**, 10958–10968.
- 168 Y. Zhu, Z. Xu, W. Jiang, W. Yin, S. Zhong, P. Gong, R. Qiao, Z. Li and S. Bai, *RSC Adv.*, 2016, **6**, 56800–56806.
- 169 X. Yang, L. Wu, L. Du and X. Li, *Catal. Lett.*, 2015, **145**, 1771–1777.
- 170 H Li, B Sun, F Yang, Z Wang, Y Xu, G Tian, K Pan, B Jiang, W Zhou, *RSC Adv.*, 2019, **9**, 7870–7877.
- 171 J. Wu, S. Lu, D. Ge, L. Zhang, W. Chen and H. Gu, *RSC Adv.*, 2016, **6**, 67502–67508.
- 172 P. Gomathisankar, T. Noda, H. Katsumata, T. Suzuki and S. Kaneco, *Front. Chem. Sci. Eng.*, 2014, **8**, 197–202.
- 173 M. Xiao, L. Zhang, B. Luo, M. Lyu, Z. Wang, H. Huang, S. Wang, A. Du and L. Wang, *Angew. Chem. Int. Ed.*, 2020, **59**, 7230–7234.
- 174 Y. C. Huang, S. Y. Chang and J. M. Jehng, *J. Phys. Chem. C*, 2017, **121**, 19063–19068.
- 175 B. Yan, J. Zhou, X. Liang, K. Song and X. Su, *Appl. Surf. Sci.*, 2017, **392**, 889–896
- 176 I. Majeed, M. A. Nadeem, A. Badshah, F. K. Kanodarwala, H. Ali, M. A. Khan, J. A. Stride and M. A. Nadeem, *Catal. Sci. Technol.*, 2017, **7**, 677–686.
- 177 Y. Li, B. Wang, S. Liu, X. Duan and Z. Hu, *Appl. Surf. Sci.*, 2015, **324**, 736–744.
- 178 M. M. Hasan and N. K. Allam, *RSC Adv.*, 2018, **8**, 37219–37228.
- 179 G. Li, J. Huang, J. Chen, Z. Deng, Q. Huang, Z. Liu, W. Guo and R. Cao, *ACS Omega*, 2019, **4**, 3392–3397.
- 180 J. Wang, Z. Wang, P. Qu, Q. Xu, J. Zheng, S. Jia, J. Chen and Z. Zhu, *Int. J. Hydrogen Energy*, 2018, **43**, 7388–7396.
- 181 H. Zhang, F. Liu, H. Wu, X. Cao, J. Sun and W. Lei, *RSC Adv.*, 2017, **7**, 40327–40333.
- 182 Y. Yang, X. Li, C. Lu and W. Huang, *Catal. Letters*, 2019, **149**, 2930–2939
- 183 J. Xiao, Y. Luo, Z. Yang, Y. Xiang, X. Zhang and H. Chen, *Catal. Sci. Technol.*, 2018, **8**, 2477–2487.
- 184 W. Wei, X. Liu, S. Cui and J. Liu, *RSC Adv.*, 2017, **7**, 25650–25656.
- 185 Y. Li, Z. Hu, S. Liu, X. Duan and B. Wang, *React. Kinet. Mech. Catal.*, 2014, **112**, 559–572.
- 186 C. M. Wu, R. Peng, N. M. Dimitrijevic, T. Rajh and R. T. Koodali, *Int. J. Hydrogen Energy*, 2014, **39**, 127–136.
- 187 F. Teng, M. Chen, N. Li, X. Hua, K. Wang and T. Xu, *ChemCatChem*, 2014, **6**, 842–847.
- 188 M. S Park and M. Kang, *Mater. Lett.*, 2008, **62**, 183–187.
- 189 E. Cui and G. Lu, *J. Phys. Chem. C*, 2013, **117**, 26415–26425.
- 190 K. M. Parida, S. Pany and B. Naik, *Int. J. Hydrogen Energy*, 2013, **38**, 3545–3553.
- 191 N. Rungjaroentawon, S. Onsuratoom and S. Chavadej, *Int. J. Hydrogen Energy*, 2012, **37**, 11061–11071.
- 192 X. Sun, H. Liu, J. Dong, J. Wei and Y. Zhang, *Catal. Lett.*, 2010, **135**, 219–225.
- 193 B. Fu, Z. Wu, S. Cao, K. Guo and L. Piao, *Nanoscale*, 2020, **12**, 4895–4902.



- 194 Y. Chen, L. Soler, C. Cazorla, J. Oliveras, N. G. Bastús, V. F. Puentes and J. Llorca, *Nat. Commun.*, 2023, **14**, 6165. View Article Online
DOI: 10.1039/D4YA00249K
- 195 L. Qi, J. Yu and M. Jaroniec, *Phys. Chem. Chem. Phys.*, 2011, **13**, 8915–8923.
- 196 V. Jovic, Z. H. N. Al-Azri, W. T. Chen, D. Sun-Waterhouse, H. Idriss and G. I. N. Waterhouse, *Top. Catal.*, 2013, **56**, 1139–1151.
- 197 K. K. Patra and C. S. Gopinath, *J. Phys. Chem. C*, 2018, **122**, 1206–1214.
- 198 M. Xi, X. Guo, X. Feng, L. Qin, S. Z. Kang and X. Li, *Catal. Letters*, 2020, **150**, 1368–1372.
- 199 K. Sivaranjani, S. Rajaambal, T. Das and K. Roy, *ChemCatChem*, 2014, **6**, 522–530.
- 200 S. Pany, B. Naik, S. Martha and K. Parida, *ACS Appl. Mater. Interfaces*, 2014, **6**, 839–846.
- 201 F. Wang, R. J. Wong, J. H. Ho, Y. Jiang and R. Amal, *ACS Appl. Mater. Interfaces*, 2017, **9**, 30575–30582.
- 202 H. Zhang, C. Lin, T. Han, F. Du, Y. Zhao, X. Li and Y. Sun, *ACS Sus. Chem. Eng.*, 2016, **4**, 6277–6287.
- 203 T. A. Kandiell, A. A. Ismail and D. W. Bahnemann, *Phys. Chem. Chem. Phys.*, 2011, **13**, 20155–20161.
- 204 N. K. Sathu, P. Devaraji and C. S. Gopinath, *J. Nanosci. Nanotech.*, 2016, **16**, 9203–9208.
- 205 K. Sivaranjani, S. Agarkar, S. B. Ogale and C. S. Gopinath, *J. Phys. Chem. C*, 2012, **116**, 2581–2587.
- 206 S. S. Mani, S. Rajendran, P. S. Arun, A. Vijaykumar, T. Mathew and C. S. Gopinath, *Energy Adv.*, 2024, **3**, 829–840.
- 207 (a) N. Nalajala, K. N. Salgaonkar, I. Chauhan, S. P. Mekala and C. S. Gopinath, *ACS Appl. Energy Mater.*, 2021, **4**, 13347–13360. (b) , I. Chauhan, K. K. Patra, H. Bajpai, K. N. Salgaonkar, N. B. Mhamane, and C. S. Gopinath, *Dalton Tran.* 2023, **52**, 2051–2061.
- 208 A. Naldoni, M. Altomare, G. Zoppellaro, N. Liu, Š. Kment, R. Zbořil and P. Schmuki, *ACS Catal.*, 2019, **9**, 345–364.
- 209 S. Rajendran, S. S. Mani, T. R. Nivedhitha, A. K. Asoka, P. S. Arun, T. Mathew and C. S. Gopinath, *ACS Appl. Energy Mater.*, 2023, **7**, 104–116.
- 210 K. N. Salgaonkar, H. Bajpai, N. B. Mhamane, N. Nalajala, I. Chauhan, K. Thakkar, K. Joshi and C. S. Gopinath, *J Mater. Chem. A*, 2023, **28**, 15168–15182.
- 211 M. Eisapour, H. Zhao, J. Zhao, T. Roostaei, Z. Li, A. Omidkar, J. Hu and Z. Chen, *J. Colloid Interface Sci.*, 2023, **647**, 255–263.
- 212 (a) I. Chauhan, H. Bajpai, B. Ray, S. K. Kolekar, S. Datar, K. K. Patra and C. S. Gopinath, *ACS Appl. Mater. Interfaces*, 2024 (DOI:10.1021/acsami.4c02392). (b) I. Chauhan, P. M. Vijay, R. Ranjan, K.K. Patra, and C.S. Gopinath, *ACS Mater. Au*, 2024 (DOI: 10.1021/acsmaterialsau.4c00024). (c) A. Saha, M. Vasuntharadevi, R. Ranjan, I. Chauhan, K. K. Patra, H. Bajpai, A. Saha and C. S. Gopinath, *Sustainable Energy Fuels*, 2024 (DOI: 10.1039/D4SE00434E)
- 213 (a) Q. Wang, S. Zhu, S. Zhao, C. Li, R. Wang, D. Cao and G. Liu, *Fuel*, 2022, **322**, 124163. (b) Y. Wu, Y. Li, H. Hu, G. Zeng and C. Li, *ACS ES T Eng.*, 2021, **1**, 603–611.
- 214 P. Devaraji, M. Mapa, H. M. Abdul Hakeem, V. Sudhakar, K. Krishnamoorthy, and C. S. Gopinath, *ACS Omega*, 2017, **2**, 6768–6781.
- 215 N. Jandam, K. Serivalsatit, M. Hunsom and K. Pruksathorn, *ACS Omega*, 2021, **6**, 24709–24719.






- 216 K. N. Salgaonkar, S. R. Kale, N. Nalajala, S. Mansuri, and C. S. Gopinath, *Chem. Asia J.*, 2023, **18**, e202201239. View Article Online
DOI: 10.1039/D4YA00249K
- 217 (a) S. Sekar, V. Preethi, V. S. Srivishnu, S. Saravanan, S. Lee, *Int. J. Hydrogen Energy*, 2022, **47**, 40275-40285. (b) M. Anthony Raja, V. Preethi, Y. Pal, N. Nalajala, and C. S. Gopinath *J. Phys: Conf. Series*, **1495**, 012035 (2020).
- 218 A. Rioja-Cabanillas, D. Valdesueiro, P. Fernández-Ibáñez and J. A. Byrne, *J. Phys. Energy*, 2020, **3**, 012006.
- 219 J. Bharatvaj, V. Preethi, S. Kanmani, *Int.J. Hydrogen Energy*, 2018, **43**, 3935-3945.
- 220 H. A. Maitlo, B. Anand and K. H. Kim, *Appl. Energy*, 2024, **361**, 122932.
- 221 S. Tasleem and M. Tahir, *J. Environ. Chem. Eng.*, 2021, **9**, 105351.
- 222 S. Hu, F. Li, Z. Fan, J. Gui, *J. Power Sources*, 2014, **250**, 30-39.
- 223 M.M. Hasan and N.K. Allam, *RSC Adv.*, 2018, **8**, 37219-37228.
- 224 M.V. Dozzi, G.L. Chiarello, M. Pedroni, S. Livraghi, E. Giamello, E. Selli, *Appl. Catal. B: Environ.* 2017, **209**, 417-28.
- 225 B. Rusinque, S. Escobedo, H. D. Lasa, *Catalysts*. 2021, **11**, 405.
- 226 H. Jiao, J. Yang, X. Li, C. Wang, J. Tang, *Green Chem.*, 2022, **24**, 8345-8354.
- 227 W. Qian, G. Zhang, W. Xing, Z. Pan, D. Zheng, S. Wang, Y. Hou, and X. Wang., *Angew. Chem. Int. Ed.*, 2023, **135**, 202307930.
- 228 M. Liu, G. Zhang, X. Liang, Z. Pan, D. Zheng, S. Wang, Z. Yu, Y. Hou, X. Wang, *Angew. Chem. Int. Ed.*, 2023, **135**, 202304694.




Biosketch of all authors

View Article Online
DOI: 10.1039/D4YA00249K

	<p><i>Sunesh S Mani completed his Master's degree in chemistry from the University of Kerala, Trivandrum. He is currently working as a PhD student under the supervision of Dr. Thomas Mathew, Department of Chemistry, St. John's College, Anchal, affiliated to the University of Kerala, Trivandrum. His primary area of interest in research is the development of nanomaterials for photocatalytic applications</i></p>
	<p><i>Sivaraj Rajendran received his Bachelor's degree and Master's degree in chemistry from University of Kerala, Trivandrum. He is presently a PhD student at Department of Chemistry, St. John's College, Anchal, affiliated to University of Kerala, Trivandrum under the supervision of Dr. Thomas Mathew. His research interest mainly focuses on design of transition metal-based nanomaterials for photocatalytic and electrocatalytic applications.</i></p>
	<p><i>Thomas Mathew completed PhD at NCL, Pune and received degree from University of Pune on 2003. He gained Postdoctoral experience from AIST, Osaka, Japan (2003-2005), Academia Sinica, Taiwan (2005-2006) and as JSPS Fellow at the University of Tokyo, Japan (2006-2008), 3 years of industrial research experience as a visiting researcher at Toyota Central R&D Labs, Japan (2008-2011), 2 years teaching experience in B.Tech and M.Tech Nanotechnology at Noorul Islam University, India (2011-2013). He also received HRSMC Fellowship from The Netherlands to perform experiments on CO₂ utilization at University of Amsterdam, The Netherlands (02/2022 – 04/2022). He has been Assistant Professor since 2013 at St. John's College, India. He has published more than 30 research articles and 2 patents. He is actively involved in teaching chemistry and interdisciplinary topics at graduate and post-graduate level. His research interest includes heterogeneous catalysis, photocatalysis, electrocatalytic water splitting, steam</i></p>



	<p><i>reforming, CO₂ utilization and RWGS reaction, and development of novel functional materials.</i></p>	<p>View Article Online DOI: 10.1039/D4YA00249K</p>
	<p><i>Dr. Chinnakonda S. Gopinath (Gopi) completed PhD on 1993 at IIT, Madras. After two post-doc stints (AvH fellowship at Forschungszentrum Karlsruhe (1995-97), and PDF at University of California at Riverside (1997-2000), he joined CSIR - National Chemical Laboratory (CSIR-NCL), Pune on 2000 as Scientist. Currently he is an Outstanding Scientist at CSIR-NCL and also leading Hydrogen Technology program across CSIR laboratories. He is an elected fellow of the Indian Academy of Sciences from 2012. Gopi is a visiting CNRS Researcher in the University of Lille 1. Thus far, he has published 245 research articles with h-index of 60 and 10 patents. His research interests include heterogeneous catalysis, surface science under operando conditions, artificial photosynthesis, solar water splitting, electrocatalytic conversion of CO₂ and biomass, and development of novel materials. He is also interested in taking the artificial photosynthesis process from the laboratory level to the market.</i></p>	

